UNIVERSITY OF NAPLES
"FEDERICO II"

UNIVERSITY OF INSUBRIA
DEPARTMENT OF BIOLOGY AND LIFE SCIENCES

International Ph.D. School
"INSECT SCIENCE AND BIOTECHNOLOGY"
25th CYCLE

MOLECULAR AND MORPHO-FUNCTIONAL EFFECTS OF STARVATION ON *BOMBYX MORI* TISSUES

Coordinator
Prof. Francesco PENNACCHIO

Candidate
Barbara CASATI

Tutors
Prof. Magda DE EGUILEOR
Prof. Gianluca TETTAMANTI

Academic year 2013-2014

INDEX

Abstract	**page 1**
Introduction	**page 3**
Aim of the research	**page 15**
Materials and Methods	**page 16**
Results	**page 26**
Discussion	**page 37**
References	**page 45**
Figures and Tables	**page 59**

ABSTRACT

The silkworm, *Bombyx mori*, is a good model organism among Lepidoptera, a large order of holometabolous insects of valuable economic and agronomic interest. Thus a greater knowledge of morphological events, and their regulation at molecular level, occurring in the silkworm during metamorphosis and under stress conditions, such as complete food withdrawal, could boost studies on several biological areas.

Three main larval organs, the alimentary canal, the fat body, and the silk glands, undergo a drastic remodeling, or even disappear, during metamorphosis through programmed cell death (PCD) processes.

Autophagy is an evolutionarily conserved physiological process that can intervene in PCD during animal development, is activated during insect metamorphosis, and is rapidly induced when cells need to generate intracellular nutrients and energy, for example during starvation. During the autophagic process, a portion of cytoplasm and organelles, sequestered into autophagosomes, are degraded to small molecules, which are then recycled for macromolecular synthesis and/or used for generating energy. Autophagosome formation involves a series of Autophagy-related (Atg) proteins encoded by *ATG* genes; among these factors, Atg1, whose kinase activity is regulated by the nutrient status, plays a pivotal role. Even if it is known that, in *B. mori*, autophagy intervenes during metamorphosis, a clear evidence for the involvement of this process in silkworms subject to starvation, as well as a complete coding sequence for *ATG1*, are not yet available.

In order to evaluate the effects of starvation on tissues development, a morphological and functional characterization of midgut, fat body, and silk gland was carried out during last larval instar and spinning phase in larvae both fed and subjected to complete food withdrawal. In addition, the complete coding sequence for *BmATG1* was obtained and in silico analyses of its transcript and protein were performed. Moreover, *BmATG1* expression was evaluated, by quantitative real-time RT-PCR, in pre-spinning phase larvae, as well as in silkworms subjected to food deprivation during last larval instar, to gain insight into the involvement of this gene in the response to starvation.

According to our morphological and functional analyses, starvation induced anticipation in midgut development, and possibly delayed silk gland degeneration. Even if reduction in fat

body mass resulted in a total lipid content decrease, the rapid and massive consumption of glycogen indicated that this is a major energy source during food deprivation. Our morphological and histochemical data also confirmed the involvement of autophagic process in tissues remodelling during silkworm metamorphosis.

The complete coding sequence for *BmATG1* was obtained, revealing the existence of two transcripts variants differing by a 96 nucleotide-long insert in the variant B. Molecular analyses demonstrated that *BmATG1* is an evolutionarily conserved gene coding for a serine/threonine protein kinase whose N-terminus, containing the kinase domain and ATP- and Mg-binding sites, was the most conserved part of Atg1 proteins during evolution, thus confirming its fundamental role in function and regulation of this key autophagic protein. The *BmATG1* expression profiles confirmed the involvement of this gene in the starvation-induced autophagy, especially in an energy storing tissue such as fat body.

INTRODUCTION

Silkworm as lepidopteran model

Lepidoptera is a large order of holometabolous insects that includes moths and butterflies whose life cycle is composed of four stages: egg, larva, pupa, and adult or imago (Figure 1). Larvae feed actively and grow rapidly through a series of instars. At the end of last instar, larva stops feeding and spins a cocoon in which it undergoes metamorphosis, forming first the pupa or chrysalis, and then the adult. Once the adult insect emerges from the cocoon, it mates and lays eggs near or on the preferred plant, thus ensuring food supply for the next new larvae generation.

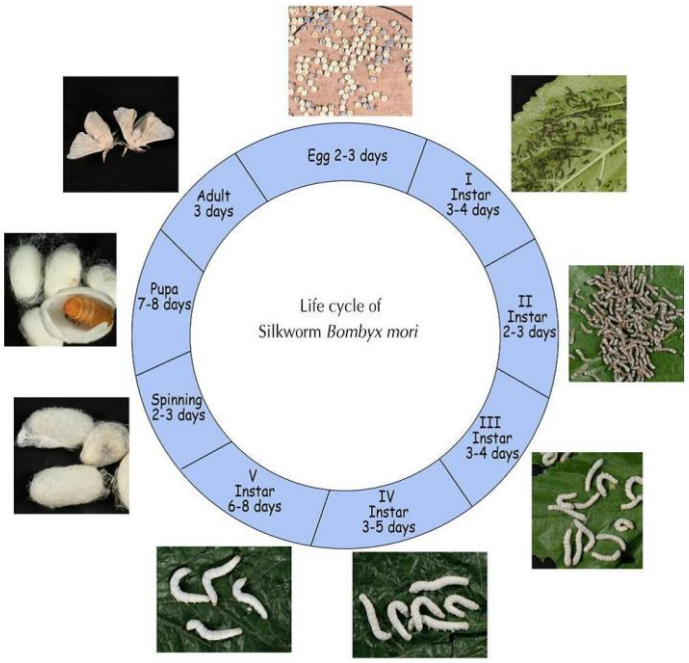

Figure 1. Life cycle of silkworm, *Bombyx mori* (Krishnan and König, 2011).

Beside species of valuable economic interest, such as the silkworm *Bombyx mori*, the larvae of many lepidopteran species are major pests in agriculture, such as armyworms and cotton bollworms belonging to the *Spodoptera* and *Helicoverpa* genus, respectively. For this reason, many studies are focused on methods for pest control using integrated strategies of management (Kogan, 1998; Tang et al., 2005, 2008; Zanuncio et al., 2006). In fact, the use of more effective techniques in the control of dangerous species could reduce, if not prevent,

the massive use of chemical pesticides, thus hindering the development of resistant strains and minimizing the environmental impact of pesticides themselves (Tang et al., 2005, 2008; Zanuncio et al., 2006). On the other hand, the possibility to acquire considerable knowledge about the species of agronomic and economic interest is very attractive. Therefore, a greater knowledge of morphological changes that occur during insect metamorphosis, and their regulation at molecular level, could lead to the development of new interesting applications.

The silkworm was domesticated over the last 5000 years from the wild progenitor *B. mandarina* and represents the basic livelihood for farmers engaged in silk production in many countries (Wang et al., 2005). Notably, thanks to the increasing amount of information available on its biology, physiology, and endocrinology, to the availability of numerous molecular tools, and to a completely sequenced genome, it has become an important lepidopteran model for genetic, genomic, and proteomic studies (for reviews see: Goldsmith et al., 2005; Zhou et al., 2008; Malagoli et al., 2010; Krishnan and König, 2011; Xia et al., 2014). Since many basic physiological processes in insects are conserved during evolution, studies carried out on the silkworm could help to increase the knowledge about the function of homologous genes as well as about morphogenesis, endocrinology, reproduction, behavior, and immunity (Wang et al., 2005). Hence, the increase of information about morphological events and molecular regulation of the developmental processes occurring during metamorphosis and under stress conditions, such as complete food withdrawal, could boost studies on several biological areas.

Main lepidopteran larval tissues: structure, physiology and development

The alimentary canal, the fat body, and the silk gland are three main organs recognizable in a lepidopteran larva during last instar, and all of them undergo a drastic remodeling, or even disappear, during metamorphosis from larva to pupa and adult.

Alimentary canal

The alimentary canal of Lepidoptera consists of three parts: the foregut, the midgut, and the hindgut (Figure 2; Wigglesworth, 1972; Dow, 1987). The foregut is considered a vestigial apparatus that leads to the midgut (Crowson, 1981), while the hindgut is subdivided in an anterior region (ileum), where excess fluids are removed, and in a posterior part (rectum),

where the undigested materials passes out through the anus (Dow, 1987). The larval midgut (MG) represents the middle part of the alimentary canal, it occupies most of the body cavity (Wigglesworth, 1972), and carries out digestive and absorptive functions (Dow, 1987).

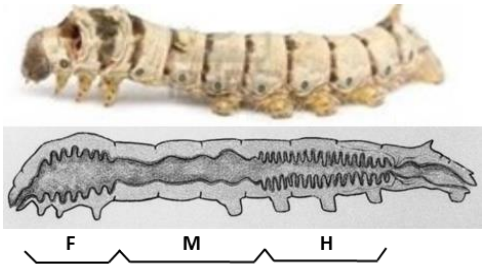

Figure 2. Alimentary canal of lepidopteran larvae. F, foregut; M, midgut; H, hindgut. (Giordana et al., 1998).

Midgut lumen is lined by a peritrophic membrane that protects the epithelium from mechanical damages, bacteria and parasites infections, creates a barrier against toxins and harmful insecticides (Terra, 2001), and is involved in the selective passage of nutrients (Tettamanti et al., 2011). Larval midgut consists of a simple epithelium supported by a basement membrane (Hakim et al., 2010) and composed of four morphologically and functionally distinct cell types (Figure 3; Dow, 1987).

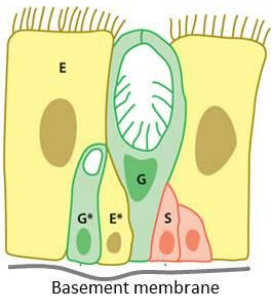

Figure 3. Structure of larval midgut epithelium. E, mature enterocyte; G, mature goblet cell; S, stem cell; E*, developing enterocyte; G*, developing goblet cell; YB, yellow body (Hakim et al., 2010).

Columnar cells are responsible for nutrients absorption (Giordana et al., 1998; Leonardi et al., 1998; Casartelli et al., 2001) and present a brush border at their apical surface and extensive invaginations of the basal cell membrane (Hakim et al., 2001; Nation, 2002). The nucleus is centrally located in the cell and the cytoplasm contains abundant rough endoplasmic reticulum and numerous mitochondria (Barbehenn and Kristensen, 2003). Goblet cells, responsible for ionic homeostasis of the midgut (Wieczorek et al., 2000), have a large intracellular cavity that communicate with the midgut lumen and is lined by microvilli (Nation, 2002). The apical membrane facing the goblet cavity houses a vacuolar-type proton

ATP-ase (v-ATPase) pump that establishes a voltage across the apical membrane that allows the alkalinisation of the lumen and the absorption of amino acids by columnar cells (Figure 4; Giordana et al., 1998; Wieczorek et al., 2000). Few scattered endocrine cells have been identified in the basal region of midgut epithelium (Endo and Nishiitsutsuji-Uwo, 1981). These cells play a role in the differentiation of stem cells and in the regulation of digestion enzyme synthesis and secretion (Wigglesworth, 1972). Interspersed near the base of mature cells, isolated or organized in clusters, there are small stem cells able to differentiate into columnar and goblet cells (Baldwin and Hakim, 1991; Nation, 2002; Tettamanti et al., 2007a; Hakim et al., 2010), as well as into endocrine cells (Rost-Roszkowska et al., 2008). Stem cells replace cells lost through age and wear, and actively proliferate during moults and pupation taking part into the larval midgut growth and pupa/adult midgut generation, respectively (Tettamanti et al., 2007a; Hakim et al., 2010).

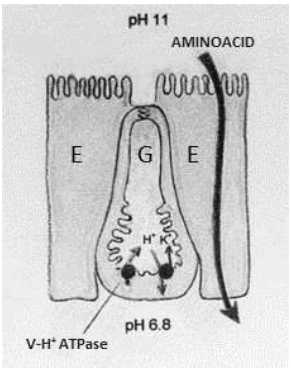

Figure 4. Schematic representation of a vacuolar-type proton ATP-ase and a $K^+/2H^+$ antiporter in the membrane lining the goblet cell cavity (Giordana et al., 1998).
E, columnar cell/enterocyte; G, goblet cell.

During insect metamorphosis midgut epithelium undergoes extensive remodeling; stem cells actively proliferate and give rise to the pupal/adult epithelium, a simple cuboidal epithelium that separates the remnant of larval one from the basement membrane (Figure 5) (Tettamanti et al., 2007a; Hakim et al., 2010). Once released into the lumen, the larval remnant, known as yellow body (Wigglesworth, 1972), undergoes autophagy and apoptosis, allowing the recycling of nutrients by the new epithelium (Uwo et al., 2002; Tettamanti et al., 2007a; Franzetti et al., 2012).

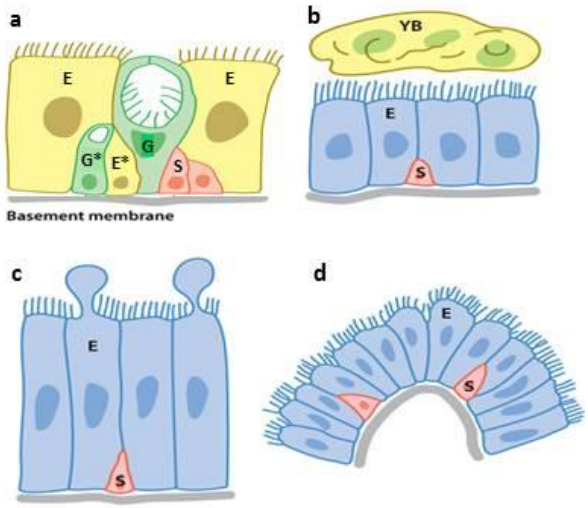

Figure 5. Structure and development of midgut epithelium during lepidopteran life cycle. (a) Larval epithelium. (b) Prepupal epithelium. The remnant larval epithelium is shed into the lumen, forming the yellow body (YB). (c) Pupal epithelium. (d) Adult epithelium.

Few enteroendocrine cells (not shown) are present at all stages. E, mature enterocyte; G, mature goblet cell; S, stem cell; E*, developing enterocyte; G*, developing goblet cell (modified from Hakim et al., 2010).

Fat body

Insect fat body (FB) is a major organ for nutrients storage and energy metabolism and is considered to be the central organ that integrates and coordinates different hormonal and nutritional signals for regulating insect development and metamorphosis (Arrese and Soulages, 2010). It synthesizes most of the hemolymph proteins and circulating metabolites, and is involved in innate immunity, producing antimicrobial peptides (AMP) and other molecules (Ferrandon et al., 2007; Arrese and Soulages, 2010). Moreover, the storage and release of various molecules from fat body modulates important aspects of the insect's life such as the rate of insect growth and the timing of metamorphosis (Mirth and Riddiford, 2007; Tian et al., 2010). Adipocytes are rounded or polygonal cells with a large irregular nucleus located at the periphery of the cell and containing many nucleoli, and characterized by the presence of lipid droplets (Arrese and Soulages, 2010; Roma et al., 2010). Triglycerides are the major component of the lipid droplets and, at the end of the feeding period, they occupy most of the cytoplasm along with glycogen and protein granules (Canavoso et al., 2001; Arrese and Soulages, 2010; Roma et al., 2010). Both triglycerides and glycogen are synthesized from dietary carbohydrates, fatty acids, or proteins (Arrese and Soulages, 2010). Fatty acids are used for many purposes, including the overall maintenance of tissues metabolic activity, and their mobilization has been observed during starvation (Arrese and Soulages, 2010). Glycogen is mobilized for maintenance of energy metabolism

during non-feeding periods, mainly by other tissues and mostly as threalose, the circulating sugar in the hemolymph (Thompson, 2003).

During metamorphosis fat body remodels and, at the end of the feeding period, fat body cells undergo programmed cell death (PCD) through both autophagy and apoptosis, as reported in *Manduca sexta* (Müller et al., 2004) and in *Bombyx mori* (Tian et al., 2012, 2013). In the silkworm, in particular, fat body PCD has been related to an increase of the ecdysteroid titer (Kaneko et al., 2011; Gui et al., 2006; Tian et al., 2013). A recent *in vitro* study has suggested that the 20-hydroxyecdysone (20E) peak might affect this process indirectly (Kaneko et al., 2011).

Silk gland

Bombyx mori silk glands (SG) are specialized structures able to synthesize the silk proteins. They are divided into three anatomically and physiologically distinct regions, the anterior (ASG), the middle (MSG), and the posterior (PSG) (Figure 6; Akai, 1983). Fibroin, the main silk component, is secreted by PSG and coated by sericin, produced by MSG. ASG is a mere duct through which silk is spun. Silk glands are constituted by a single layer of cells enwrapped by the tunica propria and separated from the lumen by the cuticula intima (Matsuura et al., 1968).

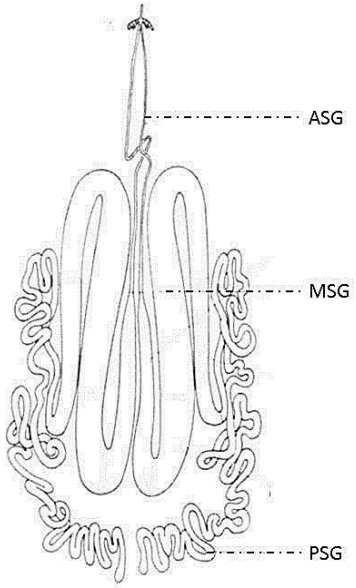

Figure 6. Structure of *B. mori* silk gland. ASG, anterior part; MSG, middle part; PSG, posterior part (Akai, 1983).

By the end of embryonic stage, silk glands are completely formed, the total number of cells is kept constant through larval development, and the growth of the gland is due to the enlargement of individual cells. At the beginning of the fifth instar, silk glands growth is triggered suddenly and DNA replication continues without concomitant cell or nuclear division, resulting in giant cells and in polyploidy and highly ramified nuclei (Perdrix-Gillot, 1979; Dhawan and Gopinathan, 2003). The whole process leads to an increase in the gene copy number per single cell, as well as to an increase in the synthesis of silk proteins (Patel and Gopinathan, 1991). Once the cocoon is spun, silk glands degenerate during the pupal stage through programmed cell death in response to the raise of 20E in the hemolymph (Chinzei, 1975; Terashima et al., 2000). During metamorphic process, from wandering to pupation, some specific features appear in silk gland cells (Matsuura et al., 1968). The cell diameter gradually decreases, the nucleus becomes more and more condensed and round-shaped, and, after spinning, the tunica propria invaginates into the cytoplasm and nucleus breaks up into dense globules (Matsuura et al., 1968; Goncu and Parlak, 2008). The first organelles which appear or increase in number in the cytoplasm at the beginning of the pre-pupal stage are lysosomes and autophagosomes (Matsuura et al., 1968; Goncu and Parlak, 2009). The degeneration process is also accompanied by increased levels of acid phosphatase activity and DNA fragmentation (Goncu and Parlak, 2008). Overall, these data indicate that PCD of silk gland cells is carried out by both autophagy and apoptosis (Goncu and Parlak, 2008, 2009).

Programmed cell death

As previously mentioned, larval organs undergo a drastic remodeling, or even disappearance, during metamorphosis from larva to pupa and adult. This remodeling is due to PCD events in response to an increase in 20E titer. 20E and juvenile hormone (JH), in fact, regulate insect molting and metamorphosis: 20E initiates and coordinates both events, while JH prevents the ecdysteroid-induced switching in gene expression necessary for metamorphosis (Riddiford et al., 1999, 2003). In particular, at the end of the last larval instar, a first pulse of 20E triggers the onset of pupal development, while a second pulse initiates pupation (Riddiford et al., 1999, 2003). At molecular level, the first pulse of 20E

induces the expression of some transcription factors that activate death of larval tissues and organs (Parthasarathy and Palli, 2007).

The Nomenclature Committee on Cell Death has defined three main types of PCD: apoptosis, autophagy, and necrosis (Kroemer et al., 2009; Galluzzi et al., 2012). Nevertheless, the most common forms of PCD observed during animal development are apoptosis and autophagy, which can be distinguished at the morphological and molecular levels (Baehrecke, 2002; Conradt, 2009).

Necrosis is characterized by a gain in cell volume swelling of organelles, plasma membrane rupture, and subsequent loss of intracellular contents (Kroemer et al., 2009). Even if it has been considered for a long time an uncontrolled form of cell death, it is now clear that necrosis can occur in a regulated manner not only in mammals, with a prominent role in many physiological and pathological contexts, but also in non-mammalian models (McCall, 2010; Galluzzi et al., 2012).

Apoptosis is characterized by cell shrinkage, plasma membrane blebbing, chromatin condensation, DNA fragmentation, and formation of apoptotic bodies, containing nuclear fragments and intracellular contents (Kerr et al., 1972; Cooper et al., 2009; Ulukaya et al., 2011), which are removed by neighboring cells or macrophages (Liu and Chejanovsky, 2006). The central component of the apoptosis machinery are caspases, a group of cysteine proteases that cleave proteins after aspartic acid residues. They can be divided into initiator and effector caspases: initiator caspases transmit the death signal generated by the apoptotic stimulus to the effector caspases, which in turn cleave the target proteins (Liu and Chejanovsky, 2006; Cooper et al., 2009; Ulukaya et al., 2011).

Autophagy is an evolutionarily conserved physiological process, important for maintaining cellular homeostasis (Tettamanti et al., 2011), that can be rapidly induced when the organism is undergoing structural remodeling, such as during metamorphosis, and when cells need to generate intracellular nutrients and energy, for example during starvation (Tsukada and Ohsumi 1993; Klionsky, 2007; Mizushima et al., 2002, 2008; Scott et al., 2004; Wang and Klionsky, 2003; Meléndez and Neufeld, 2008). In particular, the activation of autophagy following nutrient deprivation has been demonstrated from yeast to mammals. In budding yeast, autophagy is rapidly induced under nutrient-deficient conditions, as revealed by an extensive accumulation of so called “autophagic bodies” in which degradation of

cytosolic components occurs (Takeshige et al., 1992). The analysis of autophagy-deficient yeast mutants, then, demonstrated that this process is indispensable for protein degradation under starvation conditions (Tsukada and Ohsumi, 1993). In mammals, autophagy is induced by nutrient starvation in most tissues, even if it is differently regulated among organs (Mizushima et al., 2004). An increasing attention is being devoted to the activation and regulation of starvation-induced autophagy in holometabolous insects (Romanelli et al., 2014 in preparation). In Drosophila, for example, nutrient withdrawal rapidly induces autophagy in fat body cells (Scott et al., 2004) and a recent study on *Galleria mellonella* tissues suggested that starvation alone is sufficient to activate the autophagic process in the absence of 20E stimulation (Khoa and Takeda, 2012). In an *in vitro* study on *S. litura* and *B. mori* cell lines, both originated from ovaries, nutrient depletion rapidly induces autophagy that, after 48h, lead to cell death (Wu et al., 2011). Moreover, it has been recently demonstrated that, during metamorphosis, autophagy is set in motion once the larva stops feeding (Franzetti et al., 2012). The balance between growth and autophagy in response to changes in nutrient conditions, as well as in physiological conditions, is regulated by the protein kinase TOR (Target Of Rapamycin; Jung et al., 2010).

Three types of autophagy are known: micro-, macro-, and chaperone-mediated autophagy. Microautophagy refers to a direct sequestration of cytosolic components by lysosomes involved in selective organelles degradation. In chaperone-mediated autophagy unfolded proteins are translocated into the lysosome through a chaperone and its receptor. Macroautophagy, commonly referred to as “autophagy”, involves an active and controlled rearrangement of subcellular membranes that sequester a portion of cytoplasm and organelles (forming an autophagosome) to deliver the content to lysosomes (Mizushima et al., 2008). The sequestered cargo, within the newly formed autolysosome, is degraded by acidic lysosomal hydrolases (Kroemer et al., 2009) to small molecules which are then recycled for macromolecular synthesis and/or used for generating energy (Chang and Neufeld, 2010). Autophagosome formation requires a tightly controlled mechanism which involves a series of Autophagy-related (Atg) proteins encoded by *ATG* genes (Xie and Klionsky, 2007). Most of the molecular components of the autophagy pathway were initially characterized in *Saccharomyces cerevisiae*, but orthologs of many of these Atg proteins have

been found in other eukaryotes demonstrating their evolutionary conservation (Tsukada and Ohsumi 1993; Levine and Klionsky, 2004; Meijer et al., 2007; Meléndez and Neufeld, 2008).

In yeast, initiation of the autophagic process involves the formation of a pre-autophagosomal structure (PAS) on which a number of proteins are assembled and organized (Suzuki and Ohsumi, 2007). Among them, Atg1, Atg13, and Atg17 are particularly interesting since, under conditions of abundant nutrients, Atg13 is phosphorylated in a TOR-dependent manner, which disrupts its binding to Atg1 (Kamada et al., 2000, 2010). Under starvation condition, Atg13 is dephosphorylated, binds to Atg1 to promote its kinase function, and induces the association of Atg17 to Atg1/Atg13 (Kamada et al., 2000; Chan and Tooze, 2009). Atg1 then localizes to the PAS and helps recruit other essential factors, required for the autophagic process, such as Atg8, Atg14, Atg16, and Atg18 (Chan and Tooze, 2009). This Atg1/Atg13 regulatory mechanism in yeast shows both similarities and differences to that in Drosophila and mammalians (Chan and Tooze, 2009).

Ulk1, the mammalian Atg1 homolog (Kuroyanagi et al., 1998; Yan et al., 1998), enters into a large molecular complex containing mAtg13 and FIP200, counterparts of yeast Atg13 and Atg17, respectively (Hosokawa et al., 2009; Mizushima, 2010). While the Ulk1/FIP200/Atg13 complex forms independently of the nutrient status (Hosokawa et al., 2009; Chan and Tooze, 2009; Mizushima, 2010; Shang and Wang, 2011), nutrient-rich conditions promote the association of mTORC1 (mTOR-containing Complex) to this complex, as well as direct phosphorylation of Ulk1 and mAtg13 by mTOR (Hosokawa et al., 2009; Chan and Tooze, 2009; Shang and Wang, 2011; Kundu, 2011).

In insects, the insulin receptor/mTOR complex pathway plays a pivotal role in the regulation of autophagy and the activity of this pathway is influenced by both 20E and the nutritional status (Rusten et al., 2004; Scott et al., 2004; Malagoli et al., 2010). Under normal conditions, in fact, mTOR complex suppresses autophagy by inhibiting the activity of Atg1 and Atg13 (Chang and Neufeld, 2009). On the other hand, when nutrients concentration decreases, the activity of the mTOR complex decreases as well and the nucleation of the autophagosome membrane begins (Figure 7; Malagoli et al., 2010).

In Drosophila**,** in particular, Atg1 binds Atg13 under nutrient-rich conditions and their binding is strengthened by starvation. Under nutrient-rich conditions, in fact, both Atg1 and TOR contribute to Atg1 hyper-phosphorylation, whereas starvation promotes hyper-

phosphorylation of Atg13, thus strengthening its interaction with Atg1 (Chang and Neufeld, 2009; Chan and Tooze, 2009). Increased Atg1 levels down-regulate TOR kinase activity (Scott et al., 2007) and this event involves Atg13 by influencing in part TOR intracellular distribution and trafficking (Chang and Neufeld, 2009). Regardless of the mechanism, these results suggest that a self-reinforcing feedback loop exists, whereby increased Atg1 levels down-regulate TOR activity, which results in further activation of Atg1 (Scott et al., 2007).

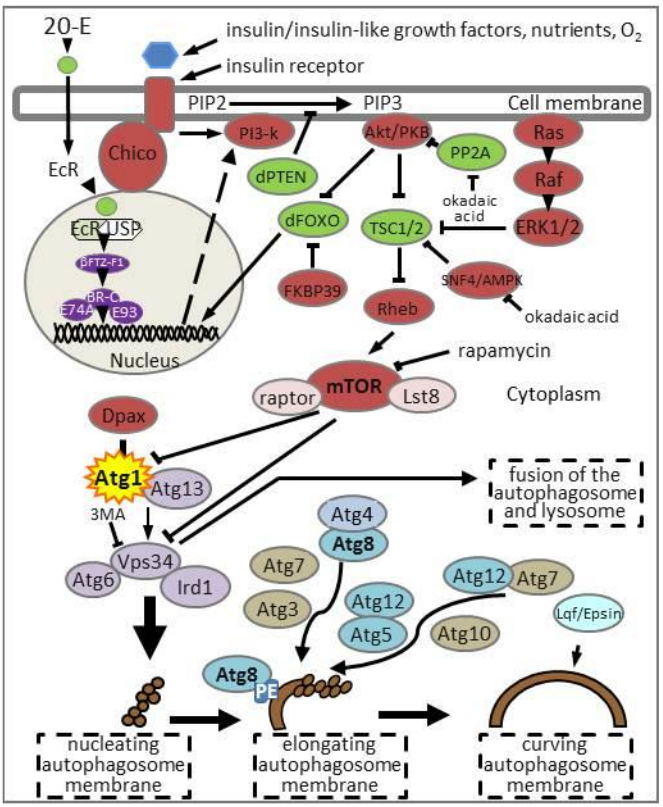

Figure 7. Schematic representation of molecular pathways leading to activation of autophagy in insects (from Malagoli et al., 2010). Codes: green activates autophagy; red inhibits autophagy; grey necessary for the membrane of the autophagosome; blue necessary for the elongation of the phagophore.

Atg1 itself is necessary and sufficient to induce the autophagic process in Drosophila. *ATG1* overexpression triggers downstream pathways and stimulates autophagy in a kinase-dependent manner (Scott et al., 2007), and null mutant flies for *ATG1* gene die during the

late pupal period, because mutation prevents starvation-induced autophagy (Scott et al., 2004).

Atg1 is a Serine/Threonine protein kinase that shows the characteristic structure of protein kinases: i) a catalytic domain localized in the N-terminal portion and composed of 12 conserved subdomain motifs (Hanks and Hunter, 1995); ii) a C-terminal domain showing a structural conservation among yeast, nematode, and human (Kuroyanagi et al., 1998); iii) an intervening region, rich in Proline and Serine residues (PS domain), that is less conserved among species (Matsuura et al., 1997; Kuroyanagi et al., 1998; Yan et al., 1998). The interaction site with Atg13 has been mapped to the C-terminal region of Atg1 both in yeast (Kijanska et al., 2010) and in mammals (Chan et al., 2009). It has been proposed that mTORC1 recruitment into the Ulk complex is mediated by the PS domain of Ulk1 and that this interaction is independent of mAtg13 (Mizushima, 2010).

In *Bombyx mori*, autophagy intervenes during metamorphosis and contributes to the degradation of larval tissues including midgut epithelium, fat body, and silk glands (Franzetti et al., 2012; Sumithra et al., 2010; Matsuura et al., 1968; Goncu and Parlak, 2009).

Eleven *ATG* genes have been identified in the silkworm genome, as well as other genes involved in the TOR signal transduction pathway (Owa et al., 2008; Zhang et al., 2009; Zhou et al., 2010), thus confirming the existence of a well-organized autophagy pathway in this insect, and many of these genes are actively transcribed in different larval tissues during development and metamorphosis (Zhang et al., 2009; Li et al., 2011; Franzetti et al., 2012; Tian et al., 2013). Nevertheless, clear evidence for the involvement of autophagy related genes in silkworms challenged by starvation is not available.

AIM OF THE RESERACH

The aims of the present research work on silkworm *B. mori* were:

- Morphological and functional characterization of midgut, fat body, and silk gland during last larval instar and spinning phase in larvae both fed and subjected to a complete food withdrawal.
- Molecular cloning and sequencing of *BmATG1* coding sequence followed by in silico analyses of its transcript and protein.
- Quantification, by quantitative real-time RT-PCR, of the *BmATG1* mRNA copy number in pre-spinning phase larvae, as well as in silkworms subjected to food deprivation during last larval instar, to gain insight into the involvement of this gene in the response to starvation.

MATERIALS AND METHODS

Animals and feeding protocol

Bombyx mori larvae (four-way polyhybrid strain (126×57)(70×90)) were provided by CRA-API (Padova, Italy), fed an artificial diet (Cappellozza et al., 2005) and reared at 25±0.5°C under a 12L:12D photoperiod and 70% relative humidity. After animals had ecdysed to the last larval stage (5^{th} instar), they were staged and synchronized according to Kiguchi and Agui (1981). Developmental stages used in this study are defined and described in Table 1. The daily amount of food supplemented to the fifth instar larvae is reported in Table 2. Starting from L5D3 (fifth larval instar, day 3), silkworm larvae were randomly divided into two groups. Larvae of the first group (control larvae) were normally fed, whereas larvae of the second group (starved larvae) were subjected to complete food withdrawal.

Table 1. Developmental stages of the silkworm, *Bombyx mori*, used in this study

Stage	Description
L5D3 - L5D4 - L5D5	Fifth larval instar, day 3 – day 4 – day 5
W(S)	Wandering stage (early spinning)
SD1 - SD2	Spinning phase, day 1 – day 2
PP	Pre-pupal stage

Table 2. Daily quantity of hydrated diet administered per larva

Day	I	II	III	IV	V	VI
Grams	1	1.5	2	2.5	3	2.5

Cell line

NIAS-Bm-aff3 cell line derived from *B. mori* fat body was maintained in IPL-41 insect cell culture medium (Invitrogen, Carlsbad, CA, USA) containing 10% FBS (Sigma-Aldrich, St. Louis, MO, USA) at 25°C.

Tissues sampling

Before dissection, animals were anesthetized with CO_2 and cut dorsally.

For morpho-functional analyses, midgut, fat body and silk glands (here referred as ASG, MSG, and PSG respectively; Akai, 1983) were collected from both control and starved larvae from L5D3 to SD2.

For molecular biology analyses, three larvae from each of the experimental groups were sampled at five time points, corresponding to L5D3, L5D4, L5D5, W(S), and SD1. Midgut, fat body, gonads, Malpighian tubules, and silk glands (ASG, MSG, and PSG) were dissected out from each larva and immediately frozen in liquid nitrogen and stored at −80°C until analysis. For the spatial distribution analysis of *BmATG1* transcripts, all tissue samples were collected from the control larvae at the end of fifth larval instar. For real-time RT-PCR quantification they were dissected out from both control and starved larvae at all-time points.

Samples preparation for light microscopy

After dissection, tissues were fixed in 4% glutaraldehyde (in 0.1 M Na cacodylate buffer, pH 7.4) overnight at 4°C. Specimens were then post-fixed in 1% osmium tetroxide for 1 h, dehydrated in an ethanol series, and embedded in an Epon/Araldite 812 mixture. Semi-thin sections (750 nm) for light microscopy were stained with crystal violet and basic fuchsine and observed by using an Olympus BH2 microscope (Olympus, Tokyo, Japan). Images were acquired with a DS-5M-L1 digital camera system (Nikon, Tokyo, Japan).

For paraffin embedding, midgut, fat body and silk glands were fixed in 4% paraformaldehyde in 0.1 M phosphate-buffered saline (PBS, pH 7.2) for 3 h at room temperature. Specimens were dehydrated in an ethanol series and embedded in paraffin. Sections (8-10 µm thick) were cut with a Jung Multicut 2045 microtome (Leica Microsystems, Wetzlar, Germany) and used for staining. Reference sections were stained with Mayer's haematoxylin (2% aqueous solution) and eosin (1% aqueous solution).

In order to obtain cryosections, dissected samples were embedded in polyfreeze cryostat embedding medium (Polyscience Europe, Eppelheim, Germany), frozen in liquid nitrogen and stored at -80°C until use. Cryosections (8 µm thick) were obtained on a Leica CM 1850 (Leica Microsystem) and slides were immediately used or stored at -20°C.

Enzymatic histochemistry

Periodic acid Schiff (P.A.S.)

Paraffin sections were dewaxed using xylene, rehydrated in an ethanol series, and processed for Periodic acid Schiff (PAS) staining (Bio-Optica, Milano, Italy) to evidence the presence of glycogen (Pearse, 1960), according to protocol. Sections were also stained with a solution of DAPI (Sigma-Aldrich) diluted 1:5000 in 1M PBS (pH 7.2) to evidence nuclei.

Oil Red O (O.R.O)

The Oil Red O (O.R.O) staining allows the identification of lipids on frozen sections. Cryosections were first incubated for 10 min with a Backer fixative (formaldehyde 5%, sucrose, sodium cacodylate, calcium chloride) then for 15 min with the O.R.O solution (Bio-Optica). Sections were also stained with a DAPI solution.

NADH diaphorase

To localize NADH-diaphorase (EC 1.9.3.1) activity associated to mitochondria in midgut, fat body, and silk glands (Pearse, 1960), cryosections were rehydrated and then processed with the Histopatological kit (Bio-Optica). According to the manufacturer's instructions, sections were incubated at 37°C for 30 min with the restored solution and then dehydrated in an acetone and ethanol series. Sections were also stained with a DAPI solution.

Acid phosphatase

To evaluate the distribution of acid phosphatase (EC 3.1.3.2) activity in *B. mori* tissues, rehydrated cryostatic sections were incubated with a 0.1N sodium acetate-acid acetic buffer pH 5.2, containing 0.01% naphtol phosphate AS-BI (Sigma-Aldrich), 2% N'-N'-dimethylformamide, 0.06% fast red violet LB (Sigma-Aldrich) and 0.5mM $MnCl_2$. Incubations were performed for 90 min at 37°C. Sections were also stained with a DAPI solution.

Alkaline phosphatase

To highlight alkaline phosphatase (EC 3.1.3.1) activity in *B. mori* tissues, paraffin sections were dewaxed using xylene, rehydrated in an ethanol series, and incubated with a *FAST*™ BCIP/NBT (5-Bromo-4-chloro-3-indolyl phosphate/Nitro blue tetrazolium) solution (Sigma-

Aldrich) at room temperature for 10 minutes (Horwitz et al., 1966; Blake et al., 1984). One SIGMA FAST™ BCIP/NBT tablet, dissolved in 10 ml of water, provides a ready-to-use buffered substrate solution containing BCIP (0.15 mg/ml), NBT (0.30 mg/ml), Tris buffer (100 mM), and $MgCl_2$ (5 mM), pH 9.25–9.75. Sections were also stained with a DAPI solution.

BmAtg8 immunohistochemistry

To assess the occurrence of autophagy in silkworm tissues, fat body from the control and starved larvae at L5D5 stage were isolated on ice, immediately embedded in polyfreeze cryostat embedding medium, and stored in liquid nitrogen until use. Cryosections were incubated for 30 min in a solution containing 2% BSA, 0.1% Tween 20 in PBS, and then for 1 h at 37 °C with an anti-BmAtg8 antibody, at a dilution of 1:200 (Franzetti et al., 2012). Incubation with an appropriate Goat anti-Rabbit IgG Cy3-conjugated antibody (diluted 1:200) was performed for 1 h. Antibodies were omitted in the negative controls. Sections were examined by using a TCS SP5 confocal microscope (Leica Microsystems).

Total RNA extraction and cDNA synthesis

Total RNA was extracted from tissue samples and NIAS-Bm-aff3 cells using the Maxwell 16 tissue LEV Total RNA Purification kit (Promega, Madison, WI, USA), following the manufacturers protocol. The quantity of RNA was calculated using absorbance at 260 nm, while the integrity and relative quantity of RNA were checked by gel electrophoresis in the presence of ethidium bromide. After extraction, 1 µg of total RNA was reverse transcribed into cDNA in a final volume of 20 µl containing 1 µl oligo$(dT)_{16}$ primers (50 pmol) as described in the M-MLV Reverse Transcriptase kit (Invitrogen).

Cloning and sequencing of *BmATG1*

To obtain the 3'-end of *BmATG1* coding sequence we performed 3'-RACE PCR. First-strand cDNA was synthesized from 4 µg of total RNA extracted from NIAS-Bm-aff3 cells using M-MLV Reverse Transcriptase kit (Invitrogen) and the Adapter Primer (AP; Table 3). The target cDNA was then amplified using 1 µl REDAccuTaq® LA DNA Polymerase (Sigma-Aldrich) in 50 µl of final volume containing 50 pmol of each of the designed *BmATG1* PCR primers. The resulting PCR products were run on a 1.5% agarose gel in 1X TAE buffer (Bio-Rad, Hercules,

CA, USA) and containing ethidium bromide, purified from gel using Wizard® SV Gel and PCR Clean-up System (Promega), cloned into the pGEM®-T Easy Cloning Vector System (Promega), and sequenced in both directions (T7 and SP6).

To perform PCR reactions, an aliquot of 3 µl of the cDNA was amplified with 1 µl GoTaq Polymerase (Promega) in 50 µl of final volume containing 50 pmol of each of the designed *ATG1* PCR primers (Table 3). A 30-cycle PCR amplification was performed for all primer sets, using an automated Thermal Cycler (Mycycler, Bio-Rad). The annealing temperatures depended on the melting temperatures of the primer set used. PCR products were extracted from the gel, cloned into the pGEM®-T Easy Vector and subsequently sequenced.

Quantitative real-time PCR

Generation of in vitro-transcribed ATG1 mRNAs for standard curves

The number of *ATG1* gene transcript copies in experimental samples could be absolutely quantified by comparing them with a standard graph constructed using the known copy number of mRNA of this gene in a reference sample. For this, a forward and a reverse primers were designed based on the mRNA sequence of *BmATG1* that we identified (GenBank ID: JN565288), flanking the region from 275 to 504 of the *ATG1* coding sequence (Table 3). This primer pair was used to create templates for the *in vitro* transcription of mRNAs for *ATG1* starting from total NIAS-Bm-aff3 RNA: the forward primer (fw2) was engineered to contain a T3 phage polymerase promoter gene sequence to its 5'-end (T3-fw2) and used together with the reverse primer (rv1) in a conventional RT-PCR. RT-PCR products were then checked on a 1.5% agarose gel stained with ethidium bromide, cloned using the pGEM®-T Cloning Vector System (Promega) and subsequently sequenced in the T7 and SP6 directions. *In vitro* transcription was performed using T3 RNA polymerase and other reagents supplied in the Riboprobe In Vitro Transcription System (Promega) kit according to the manufacturer's protocol. The molecular weight (MW) of the in vitro-transcribed RNA for *ATG1* was calculated according to the following formula: *ATG1* MW=[(129 (no. of A bases)×329.2)+(69 (no. of U bases)×306.2)+(66 (no. of C bases)×305.2)+(98 (no. of G bases)×345.2)]+159. The result was 73090.6.

Spectrophotometry at 260 nm gave a concentration of 367 ng/µl for *ATG1*. Therefore, the concentration of the final working solution was 3,02E+12 molecules/µl.

Generation of standard curves for BmATG1

The mRNA produced by *in vitro* transcription was used as a quantitative standard for analyzing the experimental samples. Defined amounts of mRNA at 10-fold dilutions were subjected to real-time PCR in 50 µl of final volume using one-step TaqMan EZ RT-PCR Core Reagents (Applied Biosystems, Carlsbad, CA, USA), according to the manufacturers protocol. Real-time PCR conditions were as follows: 2 min at 50 °C, 30 min at 60 °C, and 5 min at 95 °C, followed by 40 cycles consisting of 20 s at 92 °C and 1 min at 62 °C. The cycle threshold (Ct) values obtained by amplification were used to create standard curves for target genes.

Quantitation of ATG1 transcripts by one-step RT-PCR TaqMan system

A hundred nanograms of total RNA extracted from the experimental samples was subjected, in parallel to 10-fold-diluted defined amounts of standard mRNA, to real-time PCR under the same experimental conditions as used to establish the standard curves. Real-time Assays-by-Design^{SM} PCR primers and gene-specific fluorogenic probes were designed by Applied Biosystems (ABI). Primer sequences and TaqMan® probe of the obtained *ATG1* (GenBank ID: JN565288) target gene are reported in Table 3. TaqMan®PCR was performed on a StepOne™Real-Time PCR system (Applied Biosystems).

Sample quantification

Data from TaqMan® PCR runs were collected with ABI's Sequence Detector Program. Ct values corresponded to the number of cycles at which the fluorescence emission monitored in real-time exceeded the threshold limit. The Ct values were used to create standard curves to serve as a basis for calculating the absolute amounts of mRNA in total RNA. Real-time PCR data were statistically compared using one-way ANOVA (ANalysis Of VAriance) and the level of statistical significance of the post-ANOVA Student–Newman–Keuls test was set at $p<0.05$.

Table 3. Sequence of primers used in this work

Primer	Sequence 5'–3'	Purpose
ATG1-fw1	GAATCATGTCCGTGGTTAAGGG	Cloning
ATG1-rv1	ATCTGATGGGTGTGGAGTACG	Cloning
ATG1-fw2	CCCCGCCTATGTCTATGTTG	Cloning
ATG1-rv2	AGTTCTGGACTCGTTCCTGG	Cloning
ATG1-fw3	GTCTACCAGTGCCTTACCGG	Cloning
ATG1-rv3	CGCGGTAGGTGTGCAAGG	Cloning
ATG1-fw4	GGACTTTGTGTTGGTGGAGG	Cloning
ATG1-rv4	CATCAGGGATACAACGCTGC	Cloning
ATG1-fw5-3'RACE	GATGGATACGTCCGATGAGC	Cloning
ATG1-rv5	GCATTATGAGATCCCGGCTTC	Cloning
AP	GGCCACGCGTCGACTAGTACTTTTTTTTTTTTTTTT	3'-RACE
ATG1-fw5-3'RACE	GATGGATACGTCCGATGAGC	3'-RACE
UAP (rv)	CUACUACUACUAGGCCACGCGTCGACTAGTAC	3'-RACE
ATG1-T3-fw2	gtaatacgactcactatagggCCCCGCCTATGTCTATGTTG	Standard curve
ATG1-rv1	ATCTGATGGGTGTGGAGTACG	Standard curve
qPCR_fw	AGACCACGATCCAGTTGTT	Real-time
qPCR_rv	GCGTGGATGGCGCTCAT	Real-time
TaqMan® probe	CTGCAAGCTGCGCTAAG	Real-time

In silico analyses

Phylogenetic analysis

A phylogenetic tree was constructed based on the complete *ATG1* coding sequences of *B. mori* and those of other invertebrate and vertebrate species. The phylogenetic reconstruction was generated by the neighbor-joining method (Saitou and Nei, 1987), as implemented in MEGA 4.0 (Tamura et al., 2007). GenBank accession numbers for cDNA sequence comparisons are reported in Table 4.

Table 4. *ATG1* coding sequences used in the phylogenetic analysis

GenBank accession numbers	Scientific name	Common name
NM_003565.2	*Homo sapiens*	human
XM_001148902.2	*Pan troglodytes*	chimpanzee
XM_003276127.1	*Nomascus leucogenys*	Northern white-cheeked gibbon
XM_002824003.1	*Pongo abelii*	Sumatran orangutan
XM_001105326.2	*Macaca mulatta*	Rhesus monkey
XM_002753165.1	*Callithrix jacchus*	white-tufted-ear marmoset
XM_002724094.1	*Oryctolagus cuniculus*	rabbit
XM_001928551. 2	*Sus scrofa*	pig
XM_002694455.1	*Bos taurus*	cattle
XM_001493927.3	*Equus caballus*	horse
XM_534635.2	*Canis familiaris*	dog
XM_002923190.1	*Ailuropoda melanoleuca*	giant panda
BC059835.1	*Mus musculus*	mouse
NM_001108341. 1	*Rattus norvegicus*	rat
NM_001112917	*Xenopus tropicalis*	western clawed frog
XM_003226274.1	*Anolis carolinensis*	green anole
XM_415091.2	*Gallus gallus*	red jungle fowl
XM_003210879.1	*Meleagris gallopavo*	turkey
NM_001130631.1	*Danio rerio*	zebrafish
NM_140344.2	*Drosophila melanogaster*	fruit fly
JN565288	*Bombyx mori*	silkworm
XM_001944479.2	*Acyrthosiphon pisum*	pea aphid
XM_624947.3	*Apis mellifera*	honey bee
Z38016.1	*Caenorhabditis elegans*	nematode
XM_003105126.1	*Caenorhabditis remanei*	nematode
XM_002648339.1	*Caenorhabditis briggsae*	nematode
XM_001187166.1	*Strongylocentrotus purpuratus*	sea urchin

Analysis of conserved domains

The amino acid sequence of BmAtg1 was obtained using the open reading frame (ORF) finder program which is available at NCBI (Table 5) and compared, through ClustalW (Table 5), to sequences from Drosophila, yeast, nematode, mouse, and human by searching for conserved single residues and domains which are reported in literature.

Protein annotation

We performed an analysis of the primary sequences of the two isoforms of BmAtg1 for annotation at the MemPype server (Pierleoni et al., 2011). The presence of signal peptides was searched at the SignalP 3.0 server (Petersen et al., 2011) for secretory proteins, and at the TMHMM server, v. 2.0 (Krogh et al., 2001) for transmembrane domains. Other functional conserved domains were searched at the PROSITE (Sigrist et al., 2002, 2010) and at InterPro Scan (Hunter et al., 2009).

Sites for post-translational modifications

- Phosphorylation and SUMOylation. The NetPhos 2.0 server (Blom et al., 1999; Table 5) predicted the sites of phosphorylation of Serine, Threonine, and Tyrosine; sites for SUMOylation were found by the SUMOsp 2.0 program (Ren et al., 2009; Table 5).
- Glycosylation. The mucin-type mannosyl-O-glycosylation and the N-glycosylation are two post-translational modifications of proteins phylogenetically conserved and documented in insects (Gutternigg et al., 2007; Lommel and Strahl, 2009; Vandenborre et al., 2011). The motifs associated with them were searched in our isomers at the CBS prediction server (Table 5), using the Net-O-glyc 3.1 (Julenius et al., 2005) and the Net-N-glyc 1.0 (Blom et al., 1999, 2004) tools. This latter is optimized for proteins in mammals; however, the same consensus sequence was found in insects, and the tool was successfully used in *B. mori* and other insects (Vandenborre et al., 2011). A description of accessible N-glycosylation sites in the protein tertiary structure was obtained with the GlyProt application at the Glycosciences server (Table 5). Finally, C-mannosylation (NetCGlyc 1.0; Julenius, 2007; Table 5) and epsilon-glycosylation of Lysine residues were checked (NetGlycate 1.0; Johansen et al., 2006; Table 5).

Tertiary structure

Because of the lack of a template for Atg1 protein in the Protein Data Bank (PDB), a "de novo" prediction of the tertiary structures of the putative proteins was obtained at the I-Tasser server (Table 5). The four stages of the method implement a threading procedure, followed by structural assembly, refinement of the model, and structural-based functional annotation. The output consists of five models, the first of which is the most accurate (Roy et al., 2010; Zhang, 2007, 2008). We used the UCSF Chimera software, release 1.5.3 (Pettersen et al., 2004) to visualize, analyze, and compare the structural models.

Table 5. Web sites used in this study for in silico analyses

Web site name	Web address
CBS prediction server	http://www.cbs.dtu.dk/services
ClustalW	http://www.ebi.ac.uk/Tools/msa/clustalw2
Glycosciences server	http://www.glycosciences.de/modeling
I-Tasser	http://zhang.bioinformatics.ku.edu/I-TASSER
NCBI	http://www.ncbi.nlm.nih.gov
NetCGlyc 1.0	http://www.cbs.dtu.dk/services/ NetCGlyc
NetGlycate 1.0	http://www.cbs.dtu.dk/services/NetGlycate
NetPhos 2.0 server	http://www.cbs.dtu.dk/services/NetPhos
SUMOsp 2.0 program	http://sumosp.biocuckoo.org

RESULTS

➢ Morphological and metabolic characterization of silkworm tissues during last larval instar and spinning phase, in both fed and starved larvae

Aim of this part of the present work was the morphological and metabolic characterization of midgut, fat body, and silk gland during last larval instar, both in physiological conditions and during starvation to evaluate to effects of complete food withdrawal on these tissues.

Midgut

- *Morphological characterization*

Light microscopy observations revealed that, in larvae subjected to complete food withdrawal, an anticipation in midgut development occurred and that the larval epithelium was removed since the early spinning phase. Under physiological conditions, in fact, midgut epithelium consisted of a monolayered epithelium in which columnar and goblet cells were prevalent (Figure 1A). During spinning phase, stem cells proliferated and gave rise to a new cell layer which progressively separated larval epithelium from basal membrane (Figures 1B, C). At SD1 (day 1 of spinning phase), larval epithelial cells were still in close contact with the new cell layer (Figure 1B) but, at SD2 (day 2 of spinning phase), the remnant of larval epithelium was visible in the gut lumen as yellow body (Figure 1C). In larvae subjected to complete food withdrawal, larval midgut epithelium retained its structure up to the end of larval instar (Figure 1D). At SD1, stem cells actively proliferated producing a continuous cell layer and larval epithelium detached from the new pupal one (Figure 1E). At SD2, a new pupal epithelium was formed and yellow body is clearly visible in the gut lumen (Figure 1F).

- *Histochemical characterization*

P.A.S. During fifth instar, glycogen granules were present in the cytoplasm of epithelial cells (Figures 2A, B), while during spinning phase the positivity was confined in the new epithelium (Figures 2C, D). Under starvation, glycogen granules disappeared as soon as 6 hours after food deprivation (Figure 2E) and were not present in the new epithelial layer (Figures 2F-H). No reactivity was detectable inside the yellow body (data not shown).

O.R.O Complete food deprivation seemed to have no effects on lipids contents of midgut epithelial cells (Figure 3). The positivity associated with the presence of fatty acids, in fact, was detected in larval epithelial cells of both control (Figure 3A) and starved larvae (Figure 3C). At the end of spinning phase, O.R.O positivity was detected in the yellow body as well as in the new pupal epithelium of control (Figure 3B) and unfed (Figure 3D) animals.

NADH diaphorase Midgut epithelial cells retained a good mitochondrial activity for the whole period in both control and starved larvae (Figure 4). During larval development, the positivity for NADH diaphorase activity was detected in epithelial cells of both fed (Figure 4A) and starved (Figure 4C) larvae. During the spinning phase, the positivity was present in the new epithelial layer in both control (Figure 4B) and unfed (Figure 4D) animals.

Acid phosphatase The distribution of histochemical staining for acid phosphatase (Figure 5) showed a similar trend in both control (Figures 5A-C) and starved (Figures 5D-F) larvae. The enzymatic activity, in fact, was present in the apical region of epithelial cells in larval samples (Figures 5A, D) and became more intense and widespread from wandering (W) stage (Figures 5B, E). The positivity associated with acid phosphatase was then restricted to the yellow body cells and absent in the new pupal midgut epithelium (Figures 5C, F).

Alkaline phosphatase In control larvae, the positivity associated with the activity of alkaline phosphatase (Figure 6) was observed on both the brush borders and the goblet cell cavities during the feeding period (Figure 6A). From the wandering stage, brush borders gradually lost the positivity (Figure 6B) and, at SD1, the signal was present only in goblet cell cavities (Figure 6C). After the new epithelium was formed, active enzyme was present in the yellow body, but not in the new epithelial layer (Figure 6D). In larvae subjected to complete food deprivation, enzyme reactivity was observed on both brush borders and cell cavities up to L5D5 (Figure 6E), while at wandering it was limited to the goblet cavities (Figure 6F). Finally, at SD1 and SD2, the histochemical staining was observed only in the yellow body, while the pupal epithelium was negative (Figures 6G, H).

Fat body

- *Morphological characterization*

According to light microscopy observations, complete food deprivation induced a significant reduction of fat body mass from wandering stage (72 hours of starvation) (Figure 7), in association with an overall reduction in silkworm body size (data not shown). Moreover, fat body filaments were thinner and cell shapes less defined in starved larvae with respect to control ones. In fat body of fed silkworms (Figures 7A-D), cell morphology was well defined, cell volume increased at wandering (Figure 7B) and SD1 (Figure 7C), and lipids were identifiable as white droplets in the cytoplasm. In starved animals (Figures 7E-H), fat body cells were less clearly identifiable, even if lipid droplets were still present.

- *Histochemical characterization*

P.A.S. During feeding period as well the spinning phase, larvae accumulated glycogen in fat body cells as granules (Figures 8A, B). In starved larvae, the presence of glycogen stores decreased as early as 6 hours after food deprivation (Figure 8C). Interestingly, PAS positivity was present in fat body cells of starved spinning larvae (Figure 8D). Moreover, peripheral and perivisceral fat body behaved differently: while the PAS positivity in the two districts was roughly comparable in fed animals (Figure 8B), a dramatic decrease in glycogen stores was observed, under starvation, mainly in the perivisceral fat body (Figure 8D).

O.R.O The positivity associated with the presence of fatty acids in fat body cells was strong in both fed (Figure 9A) and unfed (Figure 9B) larvae for the whole period under examination.

NADH diaphorase According to the histochemical staining for NADH diaphorase enzyme, fat body cells retained a good mitochondrial activity for the whole period under examination, in both control (Figure 9C) and starved (Figure 9D) larvae.

Acid phosphatase An intense lysosomal activity was observed in fed larvae at the end of feeding period (Figure 10A) and at wandering stage (Figure 10B), while the decrease in the signal intensity observed during the spinning phase (Figure 10C) was followed by an intense positivity in pre-pupal samples (Figure 10D). On the other hand, in starved larvae (Figures

10D-H), acid phosphatase activity intensified from the end of spinning phase (Figure 10G) and at pre-pupal stage (Figure 10H).

Silk gland

During metamorphosis, silk gland degenerate and completely disappear (Matsuura et al., 1968; Goncu and Parlak, 2008). In the present work, we analyzed the three silk gland compartments, anterior (ASG), medium (MSG), and posterior (PSG), focusing on the changes that occur during last larval instar and up to the pre-pupal stage, in both control and starved larvae.

- *Morphological characterization*

During last larval instar, silk gland appeared as a lumen organ filled by silk proteins and the diameter of three compartments was very different; irregular nuclei were visible in the gland wall and a thick cuticula intima was present in both MSG and ASG (Figure 11A).

The diameter of ASG and PSG was comparable between control and starved larvae for the whole period (Figures 11B-E, J-M), with a reduction registered only in PP starved PSG (Figure 11M), while MSG from fed larvae experienced a significant size reduction from SD2 (Figures 11F, G) compared to unfed (Figures 11H, I).

In control silkworms, clear morphological features of silk gland degeneration were observed from late spinning phase (Figure 12). Invagination of tunica propria, nuclear condensation, and appearance of cytoplasmic vacuoles, in fact, were observed from SD2 in both MSG (Figures 12C, D) and PSG (Figures 12E, F). From PP stage ASG showed nuclear condensation and cytoplasmic vacuolization while invaginations of tunica propria were not seen (Figure 12B). In conditions of complete food withdrawal, these degeneration features appeared from SD2 in PSG (Figures 12K, L) and at PP in ASG (Figure 12H). MSG did show any degeneration features during spinning phase (Figure 12I); nuclear condensation and cytoplasmic vacuolization, but not tunica propria invaginations, were observed in pre-pupal samples (Figure 12J).

- *Histochemical characterization*

P.A.S. Strong positivity for P.A.S. staining was present in all silk gland compartments during the feeding period (data not shown), and reduced from W in all compartments at different extent (Figures 13A-F). In particular, intense and widespread P.A.S. positivity was observed in ASG up to the end of spinning phase (Figure 13A) and, partially, in PP samples (Figure 13B). In MSG, glycogen content dramatically decreased at W (Figure 13C) and disappeared from SD1 (Figure 13D), while in PSG glycogen granules, which were present up to SD2 (Figure 13E), further reduced at PP (Figure 13F). A similar trend was registered in silk glands from starved larvae (Figures 13G-L). In these animals, in fact, intense P.A.S. staining was widespread in ASG (Figure 13G) and locally reduced in PSG (Figure 13K) up to SD2, while it completely disappeared from SD1 in MSG (Figure 13J). Pre-pupal ASG (Figure 13H) and PSG (Figure 13L) samples presented only few glycogen granules.

NADH diaphorase According to NADH diaphorase staining (Figure 14), silk gland cells retained a good mitochondrial activity through the whole period under examination, in all the compartments and in both control (Figures 14A-C) and starved (Figures 14D-F) larvae. Strong staining for this enzyme, in fact, was observed in ASG, MSG, and PSG during the feeding period and up to PP of fed larvae as well as in the corresponding samples from animals subjected to food deprivation.

Acid phosphatase Histochemical staining for acid phosphatase was registered in silk gland compartments during fifth larval instar, independently from the nutritional status of larvae (Figures 15A, C, E controls, Figures 15G, I, K starved), and the intensity of this staining increased from the end of feeding period (Figures 15B, D, F controls, Figures 15H, J, L starved). In fed silkworm, in particular, intensity and distribution of signal associated with the activity of this enzyme increased from SD1 in MSG (Figure 15D), and markedly from wandering in ASG (Figure 15B) and from SD2 in PSG (Figure 15F). Under starvation, the positivity for the lysosomal enzyme clearly increased from SD1 in ASG (Figure 15H) and from SD2 in PSG (Figure 15L), while it was less pronounced from SD1 in MSG (Figure 15J).

➢ **Molecular cloning, characterization, and expression of *BmATG1***

Aim of this part of the present work was the molecular cloning and sequencing of *BmATG1* coding sequence and the evaluation of its expression in larvae both fed and subjected to food deprivation during last instar, to gain insight into the involvement of this gene in the response to starvation.

***BmATG1* coding sequence**

ATG1 is a key player in the autophagic process (Scott et al., 2004, 2007) and its kinase activity is regulated by nutrient status through a phosphorylation mechanism involving TOR (Scott et al., 2007; Chang and Neufeld, 2009; Chan and Tooze, 2009). Nevertheless, the complete coding sequence for silkworm *ATG1* was not available in public databases.

- *Preliminary in silico analysis*

Starting from three EST (Expressed Sequence Tag) sequences identified (Owa et al., 2008) as sharing significant sequence identity with Drosophila *ATG1* gene (GenBank ID: NM_140344.2), a BLAST (Basic Local Alignment Search Tool) search was carried out at the Silkworm Genome Database (SilkDB) and two highly similar sequences were identified (Table 6). A multiple nucleotide sequence alignment was then carried out on the five silkworm sequences, and a preliminary sequence for *BmATG1* gene of about 2000 nucleotides (nt) was obtained. According to these data, we assumed that all the fragments available in the two databases belonged to a single sequence.

Table 6. *ATG1* sequences for nucleic acid in silico analysis.

Species	Accession number	Database
B. mori	CK550585.1	GenBank
B. mori	BY923290.1	GenBank
B. mori	BP125878.1	GenBank
B. mori	BGIBMGA005492-TA	SilkDB
B. mori	BGIBMGA005491-TA	SilkDB
D. melanogaster	NM_140344.2	GenBank

- *BmATG1 cloning and sequencing*

A primers pair (ATG1-fw2 and ATG1-rv1; Table 3) was designed on the above ESTs and the resulting PCR product cloned and sequenced, thus confirming that the sequences were correctly aligned.

To obtain the complete open reading frame, a gene-specific primer (ATG1-fw5-3'RACE; Table 3) was designed and the 3'-end of the partial sequence and used in a Rapid Amplification of cDNA Ends (3'-RACE-PCR). The PCR product of this amplification was then cloned and sequenced. The 3'-end sequence of the partial *BmATG1* cDNA was thus extended by about 500 nucleotides, including a stop codon TAA, and a putative coding sequence (cds) of 1938 base pairs (bp) was identified. To confirm that the cds was correct, five primer pairs were designed on it (Table 3) and used in a standard PCR amplification, obtaining five partially overlapping amplification products (Figure 16). Then, by connecting in silico the resulting PCR products, two cds for *B. mori ATG1* were determined, which differed in 96 nucleotides from each other. Notably, this 96 bp insert did not alter the frame of the sequences that were deposited in GenBank under the accession no. JN565288 and JN565289 (Casati et al., 2012). *B. mori ATG1* transcript variant A (GenBank ID: JN565288) consisted of 2183 bp, comprising an open reading frame (ORF) of 2175 bp, while *B. mori ATG1* transcript variant B (GenBank ID: JN565289) consisted of 2279 bp, comprising an ORF of 2271 bp. The conceptual translation showed that *B. mori* Atg1 transcript variant A coded a 724 amino acid (aa) long protein with a calculated molecular mass of approximately 78.6 kDa, whereas Atg1 transcript variant B coded a 756 aa long protein with a calculated molecular mass of approximately 82.2 kDa.

- *Phylogenetic analysis*

To analyze the evolutionary relationship of silkworm *ATG1* gene with respect to other publicly available related genes in nematodes, insects, amphibians, reptiles, avian, and mammalian/primate species, a phylogenetic tree was reconstructed (Casati et al., 2012). According to clustering pattern, *B. mori ATG1* grouped in the lineage of other insects (fruit fly, pea aphid, and honey bee) and nematodes with a good bootstrap value, whereas avians (red jungle fowl, turkey), amphibians (western clawed frog), reptiles (green anole), teleosts (zebrafish), echinoderms (sea urchin), and mammals (human, rhesus monkey, dog, rat,

mouse, cattle, pig, marmoset, chimpanzee, gibbon, rabbit, and orangutan) grouped into distinct lineages (Figure 17).

- *Analysis of conserved domains*

Independent studies carried out on yeast and nematode reported nine subdomains, as well as specific phosphorylation or ATP-binding sites within the catalytic domain of Atg1 protein (Kijanska et al., 2010; Matsuura et al., 1997; Ogura et al., 1994; Yeh et al., 2010). For this reason, BmAtg1 sequence was aligned with Atg1 sequences available for yeast, nematode, Drosophila, mouse, and human searching for the conserved domains and residues reported in literature (Casati et al., 2012). The alignment confirmed the presence of seven out of nine subdomains within the kinase domain of BmAtg1, but it shifted in comparison with those of other organisms (Figure 18). It was also possible to identify specific residues reported as phosphorylation sites or ATP-binding sites as well as an Mg-binding domain (DFG). In addition, two sequence motifs for Serine/Threonine kinase substrate specificity (DLKPQN and GSPMYM) were highly conserved in the orthologs, including the silkworm. The only exception was S34, which was present only in yeast and mutated into Alanine in all other organisms.

In silico characterization of BmAtg1 proteins

A set of bioinformatics analyses was performed to characterize the two putative Atg1 isoforms (Atg1 IsoA, shorter, and Atg1 IsoB, longer) isolated in *B. mori*. The two proteins differed in an insert of 33 amino acid residues present between positions 298 and 299, and for the mutation K289E (Casati et al., 2012).

- *Protein annotation*

Using specific servers (Table 5), an analysis of primary BmAtg1 sequences was performed, looking for signal peptides and other functional domains (Casati et al., 2012). The two BmAtg1 isoforms were classified as globular proteins, localized in the cytosol, and pre-autophagosomal structures; they did not show neither features associated with organelle or membrane localization, nor N-terminal signal peptide or transmembrane domains. Only a short transmembrane peptide, extending between positions 60 and 78 in both proteins, was

found. The segment 21-288 of the two Atg1 isoforms aligned with the protein kinase profile, where both signature patterns of the profile were present: the ATP-binding region (27IGHGAFAMVT35) with an additional Lysine residue at position 51, and the active catalytic site, centered on the residue 146D. A further Serine/Threonine kinase domain near the C-terminus (position in IsoA: 575–709, shifted by 33 positions in IsoB: 607–741) was identified. A schematic representation of BmAtg1 isoform structures is reported in Figure 19. The insert in the long isoform (33 aa) followed this domain, starting from position 298.

- *Sites of post-translational modifications*

Sites of phosphorylation, SUMOylation (Table 7) and glycosylation (Table 8) (cut off=0.5) were present, and Table 9 reports the accessible N-glycosylation sites in the tertiary structure and their spatial coordinates (Casati et al., 2012).

- *Protein tertiary structure*

The predicted tertiary structures of the two *B. mori* Atg1 isoforms revealed a prevalence of alpha helices, with a tubular-like complex of 6–8 aligned alpha helices extending from the end of the protein kinase functional (PK) domain, described below, to the C-terminus of the two isoforms (superimposed in Figure 20). The PK functional domain near the N-terminus folded as a structure composed of six alpha helices and two pairs of beta sheets. The transmembrane domain found by MEMSAT occupied the alpha helix nearer the N-terminus of the protein (not shown).

BmATG1 mRNA expression

Even if *ATG1* plays a pivotal role in the autophagic process (Scott et al., 2004, 2007), clear evidence about an involvement of this gene in starvation-induced autophagy was missing in silkworm. For this reason, *BmATG1* gene expression was evaluated in midgut and fat body samples from both fed and starved larvae. *BmATG1* gene expression was also evaluated in seven different tissues at the end of fifth larval instar to gain insight into its expression pattern under physiological conditions.

The number of *BmATG1* gene transcript copies in experimental samples could be absolutely quantified by comparing them with a standard graph constructed using the known copy

number of mRNA of this gene in a reference sample. For this reason, a standard curve was created for *ATG1* based on the linear relationship between the cycle threshold (Ct) value and the logarithm of the starting amount in a reference sample (Casati et al., 2012).

- *BmATG1 mRNA expression in silkworm tissues*

Total RNA from different silkworm tissues (midgut, fat body, Malpighian tubules, gonads, ASG, MSG and PSG) was subjected to real-time RT-PCR, using the standard curve established for the *in vitro* transcribed *BmATG1* mRNA, to determine absolute amounts of *BmATG1* mRNA in the experimental samples (Casati et al., 2012). This analysis revealed the following spatial distribution of *BmATG1* mRNA in silkworm: high levels of expression in the gonads, lower levels in ASG, followed in a decreasing way by Malpighian tubules, fat body, MSG, midgut, and PSG (Figure 21A). The three regions of silk gland showed different *BmATG1* transcript abundance: in fact, *BmATG1* mRNA copy number found in ASG was twice that of MSG, and the latter was twice that of PSG.

- *BmATG1 mRNA expression in silkworm midgut and fat body samples in response to food deprivation*

To evaluate the effects of food withdrawal of *BmATG1* gene expression, quantitative real-time PCR on midgut and fat body from both fed and starved silkworms was performed during last larval instar (Casati et al., 2012). Total RNA from *B. mori* tissues was subjected to real-time PCR using the standard curve established for *BmATG1* mRNA to determine absolute amounts of *BmATG1* mRNA in the experimental samples. The expression level of *BmATG1* mRNA in midgut was comparable between control and starved animals from L5D3 up to W, with a daily slight increase. Subsequently, at the end of the fifth day of starvation, corresponding to SD1, a marked increase occurred, when the levels became significantly higher from all the previous days of observation in both groups. Moreover, this rise was significantly higher in starved in comparison to that of the control larvae (Figure 21B). In fat body of fed animals, *BmATG1* was nearly constantly expressed up to W and significantly increased at SD1 only, by three times. On the other hand, starvation during the fifth larval instar significantly influenced *BmATG1* mRNA copy number in silkworm fat body, inducing an up-regulation which started from L5D4, 24 hours after food withdrawal, up to the spinning

stage ($p \leq 0.05$). The differences among the two groups of treatment were significant over the entire period, from L5D4 to SD1 (Figure 21B).

BmAtg8 immunohistochemistry

To investigate the occurrence of autophagy in control and starved larvae, an antibody specific for BmAtg8 was used on fat body samples since it showed the most significant changes in *BmATG1* expression after starvation (Figure 22). This allowed us to assess the presence of puncta, an indisputable marker of autophagy (Klionsky et al., 2012). Moreover, BmAtg8 immunostaining was performed on samples from late fifth instar, when developmentally-programmed autophagy has not started yet in this organ (Sumithra et al., 2010). At L5D5 stage, only few Atg8 puncta were visible in the fat body of the control larvae (Figure 22a), while the amount of autophagic compartments massively increased in the starved larvae (Figure 22b).

DISCUSSION

During insect metamorphosis, larval tissues and organs undergo dramatic remodelling or even disappearance to adapt to adult form. This metamorphic process is accomplished by programmed cell death events that, besides apoptosis and necrosis, include autophagy, an evolutionarily conserved physiological process that can be rapidly induced during both metamorphosis and starvation (for reviews see: Mizushima et al., 2002, 2008; Levine and Klionsky, 2004; Wang and Klionsky, 2003; Klionsky, 2007; Meléndez and Neufeld, 2008; Berry and Baehrecke, 2008).

- **Morphological and metabolic characterization of silkworm tissues**

The first part of the work focused on morphological and metabolic effects of starvation on the development of three main larval organs, midgut, fat body, and silk gland, during last larval instar and spinning phase. Larvae were subjected to complete food deprivation from 3th day of fifth instar (L5D3) because, according to the literature, most of larvae starved from L5D1 or L5D2 died after 4-6 days, while when starvation began on L5D3 all larvae underwent metamorphosis (Chen and Gu, 2006).

Midgut and fat body

Morphological observations revealed that starvation induces anticipation in midgut epithelium development with a consequent advance in yellow body formation, which may represent a way to overcome the increased nutrients demand. During larva–pupa transition, in fact, larval epithelium is completely replaced by pupal epithelium (Hakim et al., 2010) and degraded into gut lumen providing nutrients for the pupal period (Franzetti et al., 2012; Tettamanti et al., 2007a, 2007b). Food deprivation also induces a significant reduction of fat body mass and, considering that it plays an essential role in storing and utilizing energy (Arrese and Soulages, 2010), this reduction may reflect the lack of nutrient intake.

Glycogen stores appear to be the main energy source during midgut and fat body remodelling. In both tissues, in fact, the positivity associated with P.A.S. staining dramatically decreases as soon as 6 hours after food withdrawal. These results are consistent with previous studies on *B. mori* in which the rapid decrease in fat body glycogen content was

correlated with a decrease in hemolymph glucose concentration, which in turn induced glycogen phosphorylase activity (Horie, 1960; Satake et al., 2000). Similar results are reported in both *M. sexta* larvae, where a rapid decrease in haemolymph glucose levels was accompanied with a slight increase in trehalose concentration (Gies et al., 1988), and in *M. sexta* adults, in which carbohydrate reserves rapidly decreased in both fat body and hemolymph and inversely correlated with glycogen phosphorylase activity (Ziegler, 1991). In addition, these authors reported a decrease in fat body lipid content but an increase of hemolymph lipid concentration, suggesting that *M. sexta* adults utilize lipids to save carbohydrates during starvation. Nevertheless, a comparison of the effects of starvation between larvae and adults of different species should be done carefully: *M. sexta* larvae, for example, are constantly feeding, while adults are irregular feeders (Gies et al., 1998). According to our results, both midgut and fat body from starved larvae present lipid stores up to the end of spinning phase, but the reduced size of fat body mass does not exclude the hypothesis that a rapid consumption, as well as a lower accumulation, of fatty acids occurrs. Moreover, different distribution of glycogen in peripheral and perivisceral fat body, observed during spinning phase, may reflect their different roles in proteins biosynthesis and storage: peripheral fat body is predominantly responsible for biosynthetic activity, while perivisceral fat body is specialized as storage organ (Vanishree et al., 2005). Storage proteins serve as amino acids source and their uptake from hemolymph occurs during spinning phase (Haunerland, 1996; Vanishree et al., 2005). Thus the usage of amino acids from storage proteins for glycogen (and lipids) biosynthesis (Arrese and Soulages, 2010) might explain P.A.S. positivity observed during spinning phase in fat body of starved larvae.

Acid phosphatase was chosen as a marker for lysosomal activity during tissues degeneration because, during autophagic process, formation of autolysosomes requires the recruitment of lysosomes and their fusion to autophagosomes (Mizushima et al., 2008; Klionsky et al., 2012). Thus lysosomal activity is often used as an indirect marker of autophagy (Klionsky et al., 2012; Franzetti et al., 2012; Tian et al., 2013). The distribution of the signal associated with acid phosphatase activity confirms the increase of lysosomal activity in larval midgut epithelium that is degenerating (Franzetti et al., 2012). Complete food deprivation does not alter signal distribution, excluding the possibility of an increased rate of autophagy induced by starvation (Scott et al., 2004).

Alkaline phosphatase (ALP) is a digestive enzyme involved in hydrolase/transferase reactions and connected with absorption and transport mechanisms (Eguchi, 1995; Terra and Ferreira, 2005; Terra et al., 2006). In silkworm, two forms of this enzyme exist: the membrane bound type (m-ALP) is present on the brush border membrane of the columnar cells and is the most similar to mammalian ALPs in its localization and properties; the soluble type (s-ALP) is found in the cavity of the goblet cells in a soluble form and is considered to be unique and involved in alkalinisation of midgut lumen (Eguchi, 1995). In our samples, alkaline phosphatase localization is similar in both control and starved samples, still reflecting the starvation-induced anticipation in midgut development, thus suggesting that complete food deprivation does not affect the absorption capacity of midgut larval epithelium. m-ALP, in fact, completely disappears at SD1 in controls and at wandering in starved larvae, when larvae physiologically stop feeding.

Finally, positivity for NADH diaphorase activity confirm that both midgut and fat body are metabolically active tissues during the whole period under examination, in both fed and starved larvae.

Silk gland

According to morphological observations, silk gland degeneration process proceeds, in control samples, from the posterior to the anterior portion: features typical of this degenerative process, in fact, are observed from late spinning phase in both PSG and MSG and, partially, from PP in ASG. Under food deprivation, the process is less regular, with a clear delay in the appearance of the typical morphological features in MSG. Histochemical staining for acid phosphatase, whose activity is correlated with PCD events occurring in the tissue during late spinning phase (Matsuura et al., 1968, 1976; Goncu and Parlak, 2008), suggested that, in absence of food supply, a delay in activation of the lysosomal enzyme occurrs in all compartments.

Overall, these data shows that autophagy, while inducing an advance in midgut development, delays silk gland degeneration, thus suggesting that in silkworm, as in mouse, the regulation of starvation-induced autophagy is organ-dependent (Mizushima et al., 2004).

Food withdrawal does not affect spatial and temporal distribution of glycogen stores in the three compartments. In both fed and starved larvae, in fact, high glycogen content is

observed in silk gland during last larval instar, especially in ASG, with a general reduction during the spinning phase, suggesting that glycogen stores are used as energy source during larval-pupa transition, regardless of the nutritional status.

Similarly to midgut and fat body, positivity for NADH diaphorase activity indicates that silk gland is a metabolically active tissue during the whole period under examination, in both fed and starved larvae.

Noteworthy, this is the first study concerning a comparative (morphological and histochemical) analysis of the three silk gland compartments. The possibility of a correlation between different roles in silk production and different timing in degenerative process among silk gland compartments will require further investigations.

- **Molecular cloning, characterization, and expression analysis of *BmATG1***

The second part of this project was focused on *ATG1*, a key player in the autophagic process (Scott et al., 2004, 2007), whose complete coding sequence for *B. mori* was not available in public databases. To evaluate the effects of food deprivation in two tissues with a pivotal role in the metabolism of silkworm during larva–pupa transition, *BmATG1* expression was analyzed in midgut and fat body from larvae both fed or undergoing starvation.

Cloning of BmATG1 coding sequence

First of all, the complete coding sequence of *BmATG1* gene was obtained, revealing the presence of two transcript variants differing by a 96 nucleotide-long insert in the variant B. Specific roles of these transcript variants should be assessed by further investigations.

In silico characterization of BmAtg1 protein

The BmAtg1 amino acid sequence was used to predict the tridimensional structure of the protein and to identify functional domains by using bioinformatics tools. The two isoforms differ by an insertion of 32 amino acids in length, and have great similarities in all functional and structural features; however, the biological or functional significance of these features requires further study. They are defined as cytoplasmic, non-secretory, non-transmembrane Serine/Threonine protein kinases with enzymatic properties localized, with the highest probability, within the 288 amino acid-long domain near the N-terminus, that contains one

site for the ATP-binding and one catalytic domain in the expected positions. This is consistent with the findings for Atg1 proteins in nematode, yeast, and mammals (Kuroyanagi et al., 1998; Matsuura et al., 1997; Ogura et al., 1994; Yan et al., 1998). Our bioinformatics analyses identify a short transmembrane peptide extending between positions 60 and 78 in both isoforms that could be interpreted as a possible region for anchoring to not conventional membranes, due to the absence of other features for anchoring to classical intracellular systems. In addition, BmAtg1 isoforms show localization in pre-autophagosomal site (PAS). This result is comparable to that found for yeast Atg proteins, including Atg1, that localize on the PAS near the vacuole membrane (Suzuki et al., 2001). Similarly, mammalian Ulk1 was found on or near the endoplasmic reticulum, indicating that early autophagic structures may be associated with this organelle (Itakura and Mizushima, 2010). It is possible to hypothesize that the short transmembrane peptide may help BmAtg1 in anchoring to PAS, making it possible to recruit other Atg proteins in forming autophagosomes. The catalytic N-terminal region is identical in both isoforms and, despite a difference in a few predicted sites for Threonine phosphorylation, they can be phosphorylated at Serine, Threonine, and Tyrosine residues. Accordingly, it has been widely demonstrated that phosphorylation events regulate Atg1 kinase activity in response to nutrient availability, from yeast to mammals (Chan and Tooze, 2009; Chang and Neufeld, 2009; Kundu, 2011; Scott et al., 2007). Glycosylation appears to be important for regulating protein biological properties and activity in different classes of organisms (Gutternigg et al., 2007; Lommel and Strahl, 2009) and it has been documented in a large number of proteins in insects, including *B. mori* (Vandenborre et al., 2011). Sites for possible glycosylation are present in the C-terminal region of BmAtg1 but our results remain highly hypothetical in the absence of experimental evidences for glycosylation in this protein. Finally, BmAtg1 isomers could be also substrates for SUMOylation on equivalent residues along the molecule. Although SUMOylation has emerged as a key regulatory cellular mechanism involved in a variety of processes, including cell cycle regulation, transcription, nuclear architecture, chromosome stability, and subcellular transport (Lomelí and Vázquez, 2011), the involvement of this post-translational modification in Atg1 activity regulation has not yet been reported. Our analyses reveal the presence of a second kinase domain near the C-terminal region of BmAtg1, not reported in other Atg1 proteins. Notably, the Atg13 interaction site was mapped to this region in yeast

(Kijanska et al., 2010) and mammals (Chan et al., 2009; Hosokawa et al., 2009), but unfortunately this interaction can not be verified in silkworm due to a lack of the BmAtg13 sequence. In addition, Atg13 phosphorylation requires Atg1 kinase activity in Drosophila (Chang and Neufeld, 2009) and Ulk1 directly phosphorylated Atg13 in mammals (Chan et al., 2009; Hosokawa et al., 2009). Although the function of this additional kinase domain requires further investigations, our data suggest that, in silkworm, this domain may be involved in Atg13 phosphorylation in Atg1/Atg13 interaction. Additionally, many phosphorylation sites as well as ATP- and Mg-binding sites and Serine/Threonine substrate specificity motifs have been characterized within the catalytic domain of Atg1 from yeast to mammals (Egan et al., 2011; Kijanska et al., 2010; Ogura et al., 1994; Scott et al., 2007; Shang and Wang, 2011; Yan et al., 1998; Yeh et al., 2010, 2011). These residues were also present in BmAtg1 sequences confirming their evolutionary importance in Atg1 function and regulation.

Phylogenetic analysis of BmATG1

Phylogenetic analysis demonstrate that *BmATG1* and other insect *ATG1* coding sequences cluster in a node that is distinct from vertebrates; interestingly, nematodes also belong to this node. This result supports the existence of a close relationship between arthropods and nematodes, belonging to a single clade named Ecdysozoa (Aguinaldo et al., 1997) in which all members undergo ecdysis during at least part of their life cycle. Performing a phylogenetic analysis of 18S ribosomal DNA sequences, in fact, the authors found a close relationship among arthropods, nematodes, and all other moulting phyla such as crustaceans, myriapods, and chelicerates. Similarly to 18S, *ATG1* may thus be viewed as an evolutionarily conserved gene.

BmATG1 gene expression

BmATG1 gene expression was evaluated in seven tissues of silkworm at the end of last larval instar through quantitative real-time PCR. This analysis reveals that expression levels of *BmATG1* in the midgut, fat body, and Malpighian tubules are not significantly different, whereas a great difference is found in *BmATG1* mRNA copy number between the anterior, middle and posterior portion of the silk gland. Moreover, the gonads show high levels of

expression of *BmATG1*. Midgut (Franzetti et al.,2012), fat body (Sumithra et al., 2010), silk glands (Li et al., 2010,2011), and Malpighian tubules (Ryerse, 1979) are structurally rearranged or degraded during the pupal stage, and similar *BmATG1* expression levels in these tissues at the end of the feeding period is consistent with a physiological role of autophagy in the maintenance of basal cellular homeostasis (Mizushima et al., 2008). Strong evidence collected over the years (Goncu and Parlak, 2008; Zhang et al., 2009; Li et al., 2010, 2011) supports the intervention of autophagy in silk gland compartments, and the results of the present study seem to corroborate this evidence and suggests that the three silk gland regions behave differently during metamorphosis. It has been demonstrated that autophagy is essential for oogenesis in Drosophila and it is controlled by the insulin/TOR pathway (Barth et al., 2011; Bass et al., 2009; Hou et al., 2008; Nezis et al., 2009, 2010). Although the occurrence of autophagy during oogenesis in silkworm pupae has been reported (Mpakou et al., 2008), the high expression levels of *BmATG1* that we detect in the gonads at the end of last larval instar could represent an early involvement of the autophagic mechanism in this process, since the initial development of gonads in silkworm occurs during larval life (Sakaguchi, 1978).

To evaluate the effects of food deprivation in two tissues that have pivotal role in the metabolism of silkworm during larva–pupa transition (Arrese and Soulages, 2010; Franzetti et al., 2012; Hakim et al.,2010; Tettamanti et al., 2007a), *BmATG1* expression was analyzed in the midgut and fat body dissected out from larvae both fed and undergoing starvation. According to real-time PCR data, *BmATG1* mRNA copy number in the midgut fluctuates until SD1, when a significant increase is registered in both control and starved larvae with respect to the expression levels of the previous stages. On the other hand, the effects of starvation in the fat body are detected 24 h after food deprivation, while in the control larvae an increase in *BmATG1* expression is detected later. These findings suggest that starvation has only a slight effect on *BmATG1* expression in the midgut, while its effects are more evident in fat body, thus confirming this organ to be a highly responsive tissue following nutrient deprivation (Colombani et al., 2003).

BmAtg8 immunostaining

BmAtg8 immunostaining shows a massive accumulation of Atg8 puncta in the fat body from the starved larvae at L5D5, concomitant with a significant increase in *BmATG1* transcription. Although further studies are necessary and a more detailed characterization of this phenomenon by using multiple autophagic markers (Klionsky et al., 2012) is needed, this result suggests a correlation between increased *BmATG1* transcription and occurrence of autophagy.

- **Conclusions**

In conclusion, according to our morphological and functional analyses, complete food deprivation induces anticipation in midgut epithelium development, and delays silk gland degeneration. Even if reduction in fat body mass results in a total lipid content decrease, the rapid and robust consumption of glycogen stores indicates that this organ could be a major energy source during food deprivation. Our morphological and histochemical data also confirms the involvement of autophagy in tissues remodelling during silkworm metamorphosis.

Moreover, our molecular data demonstrate that *BmATG1* has been conserved through evolution and is likely involved in starvation-induced autophagy, especially in an energy storing tissue such as the fat body. This gene encodes for a Serine/Threonine protein kinase whose N-terminus, containing the kinase domain and ATP- and Mg-binding sites, represents the most conserved part of Atg1 proteins during evolution, thus confirming its fundamental role in function and regulation of this key autophagic protein. These results set the stage for additional investigations to shed light on different aspects such as BmAtg1 regulation at post translational level, e.g. clarifying the role of phosphorylation, glycosylation, and SUMOylation at specific residues, the role of a second kinase domain near the C-terminus, and the biological or functional significance of two protein isoforms.

REFERENCES

- Aguinaldo AM, Turbeville JM, Linford LS, Rivera MC, Garey JR, Raff RA, Lake JA. *Evidence for a clade of nematodes, arthropods and other moulting animals*. Nature. 1997; 387(6632): 489-493.
- Akai H. *The structure and ultrastructure of the silk gland*. Experientia. 1983; 39: 443-449.
- Arrese EL, Soulages JL. *Insect fat body: energy, metabolism, and regulation*. Annu Rev Entomol. 2010; 55: 207-225. Review.
- Baehrecke EH. *How death shapes life during development*. Nat Rev Mol Cell Biol. 2002; 3(10): 779-787. Review.
- Baldwin KM, Hakim RS. Grow*th and differentiation of the larval midgut epithelium during molting in the moth, Manduca sexta.* Tissue Cell. 1991; 23(3): 411-422.
- Barbehenn RV, Kristensen NP. *Digestive and escretory systems*. In: Kristensen N.P. (ed.) *Lepidoptera, moths and butterflies*. Vol. 2: Morphology, Physiology, and Development. Handbuch der Zoologie/Handbook of Zoology IV/36. Walter de Gruyter, Berlin and New York, 2003; 165-187.
- Barth JM, Szabad J, Hafen E, Köhler K. *Autophagy in Drosophila ovaries is induced by starvation and is required for oogenesis*. Cell Death Differ. 2011; 18(6): 915-924.
- Bass BP, Tanner EA, Mateos San Martín D, Blute T, Kinser RD, Dolph PJ, McCall K. *Cell-autonomous requirement for DNaseII in nonapoptotic cell death*. Cell Death Differ. 2009; 16(10): 1362-1371.
- Blake MS, Johnston KH, Russell-Jones GJ, Gotschlich EC. *A rapid, sensitive method for detection of alkaline phosphatase-conjugated anti-antibody on Western blots*. Anal Biochem. 1984; 136(1): 175-179.
- Blom N, Gammeltoft S, Brunak S. *Sequence and structure-based prediction of eukaryotic protein phosphorylation sites*. J Mol Biol. 1999; 294(5): 1351-1362.
- Blom N, Sicheritz-Pontén T, Gupta R, Gammeltoft S, Brunak S. *Prediction of post-translational glycosylation and phosphorylation of proteins from the amino acid sequence*. Proteomics. 2004; 4(6): 1633-1649. Review.
- Cağlayan SH. Ch*anges in the chemical composition of fat body during the last larval instar of Manduca sexta*. Acta Biol Hung. 1990; 41(4): 363-372.

- Canavoso LE, Jouni ZE, Karnas KJ, Pennington JE, Wells MA. *Fat metabolism in insects*. Annu Rev Nutr. 2001; 21: 23–46. Review.
- Cappellozza L, Cappellozza S, Saviane A, Sbrenna G. *Artificial diet rearing system for the silkworm Bombyx mori (Lepidoptera: Bombycidae): effect of vitamin C deprivation on larval growth and cocoon production*. Appl. Entomol. Zool. 2005; 40: 405–412.
- Casartelli M, Leonardi MG, Fiandra L, Parenti P, Giordana B. *Multiple transport pathways for dibasic amino acids in the larval midgut of the silkworm Bombyx mori*. Insect Biochem Mol Biol. 2001; 31(6-7): 621-632.
- Casati B, Terova G, Cattaneo AG, Rimoldi S, Franzetti E, de Eguileor M, Tettamanti G. *Molecular cloning, characterization and expression analysis of ATG1 in the silkworm*, *Bombyx mori*. Gene. 2012; 511(2): 326-337.
- Chan EY, Longatti A, McKnight NC, Tooze SA. *Kinase-inactivated ULK proteins inhibit autophagy via their conserved C-terminal domains using an Atg13-independent mechanism*. Mol Cell Biol. 2009; 29(1): 157-171.
- Chan EY, Tooze SA. *Evolution of Atg1 function and regulation*. Autophagy. 2009; 5(6): 758-765. Review.
- Chang YY, Neufeld TP. *An Atg1/Atg13 complex with multiple roles in TOR-mediated autophagy regulation*. Mol Biol Cell. 2009; 20(7): 2004-2014.
- Chang YY, Neufeld TP. *Autophagy takes flight in Drosophila*. FEBS Lett. 2010; 584(7): 1342-1349. Review.
- Chen CH, Gu SH. *Stage-dependent effects of starvation on the growth, metamorphosis, and ecdysteroidogenesis by the prothoracic glands during the last larval instar of the silkworm, Bombyx mori*. J Insect Physiol. 2006; 52(9): 968-974.
- Chinzei Y. *Induction of histolysis by ecdysterone in vitro: Breakdown of anterior silk gland in silkworm, Bombyx mori (Lepidoptera: Bombycidae*). Appl. Ent. Zool. 1975; 10(2): 136-138.
- Colombani J, Raisin S, Pantalacci S, Radimerski T, Montagne J, Léopold P. *A nutrient sensor mechanism controls Drosophila growth*. Cell. 2003; 114(6): 739-749.
- Conradt B. *Genetic control of programmed cell death during animal development*. Annu Rev Genet. 2009; 43: 493-523. Review.
- Cooper DM, Granville DJ, Lowenberger C. *The insect caspases*. Apoptosis. 2009; 14(3): 247-256. Review.

- Crowson RA. *The biology of the Coleoptera*. Academic (London). 1981; 43.
- Dhawan S, Gopinathan KP. *Cell cycle events during the development of the silk glands in the mulberry silkworm Bombyx mori*. Dev. Genes Evol. 2003; 213(9): 435-444.
- Dow JAT. *Insect midgut function*. In: P.D. Evans and V.B. Wigglesworth, Editor(s), Advances in Insect Physiology, Academic Press. 1987; 19: 187-328.
- Egan D, Kim J, Shaw RJ, Guan KL. *The autophagy initiating kinase ULK1 is regulated via opposing phosphorylation by AMPK and mTOR*. Autophagy. 2011; 7(6): 643–644.
- Eguchi M. *Alkaline phosphatase isozymes in insects and comparison with mammalian enzyme*. Comp Biochem Physiol B Biochem Mol Biol. 1995; 111(2): 151-162. Review.
- Endo Y, Nishiitsutsuji-Uwo J. *Gut endocrine cells in insects: the ultrastructure of the gut endocrine cells of the lepidopterous species*. Biomed Res. 1981; 2(3): 270-280.
- Ferrandon D, Imler JL, Hetru C, Hoffmann JA: *The Drosophila systemic immune response: sensing and signaling during bacterial and fungal infections*. Nat Rev Immunol. 2007; 7(11): 862-874. Review
- Franzetti E, Huang ZJ, Shi YX, Xie K, Deng XJ, Li JP, Li QR, Yang WY, Zeng WN, Casartelli M, Deng HM, Cappellozza S, Grimaldi A, Xia Q, Feng Q, Cao Y, Tettamanti G. *Autophagy precedes apoptosis during the remodeling of silkworm larval midgut*. Apoptosis. 2012; 17(3): 305-324.
- Galluzzi L, Vitale I, Abrams JM, Alnemri ES, Baehrecke EH, Blagosklonny MV, Dawson TM, et al. *Molecular definitions of cell death subroutines: recommendations of the Nomenclature Committee on Cell Death 2012*. Cell Death Differ. 2012; 19(1): 107-120. Review.
- Gies A, Fromm T, Ziegler R. *Energy metabolism in starving larvae of Manduca sexta*. Comp. Biochem. Physiol. 1988; 91A(3): 549-555.
- Giordana B, Leonardi MG, Casartelli M, Consonni P, Parenti P. *K(+)-neutral amino acid symport of Bombyx mori larval midgut: a system operative in extreme conditions.* Am J Physiol. 1998; 274(5 Pt 2): R1361-R1371.
- Goldsmith MR, Shimada T, Abe H. *The genetics and genomics of the silkworm*, *Bombyx mori*. Annu Rev Entomol. 2005; 50: 71-100. Review.
- Goncu E, Parlak O. *Some autophagic and apoptotic features of programmed cell death in the anterior silk glands of the silkworm, Bombyx mori*. Autophagy. 2008; 4(8): 1069-1072.

- Goncu E, Parlak O. *Morphological changes and patterns of ecdysone receptor B1 immunolocalization in the anterior silk gland undergoing programmed cell death in the silkworm, Bombyx mori*. Acta Histochem. 2009; 111(1): 25-34.
- Gui ZZ, Lee KS, Kim BY, Choi YS, Wei YD, Choo YM, Kang PD, Yoon HJ, Kim I, Je YH, Seo SJ, Lee SM, Guo X, Sohn HD, Jin BR. *Functional role of aspartic proteinase cathepsin D in insect metamorphosis*. BMC Dev Biol. 2006; 6: 49.
- Gutternigg M, Kretschmer-Lubich D, Paschinger K, Rendić D, Hader J, Geier P, Ranftl R, Jantsch V, Lochnit G, Wilson IB. *Biosynthesis of truncated N-linked oligosaccharides results from non-orthologous hexosaminidase-mediated mechanisms in nematodes, plants, and insects.* J Biol Chem. 2007; 282(38): 27825-27840.
- Hakim RS, Baldwin KM, Loeb M. *The role of stem cells in midgut growth and regeneration*. In Vitro Cell Dev Biol Anim. 2001; 37(6): 338-342. Review.
- Hakim RS, Baldwin K, Smagghe G. *Regulation of midgut growth, development, and metamorphosis*. Annu Rev Entomol. 2010; 55: 593-608. Review.
- Hanks SK, Hunter T. Protein kinases 6. *The eukaryotic protein kinase superfamily: kinase (catalytic) domain structure and classification*. FASEB J. 1995; 9(8): 576-596. Review.
- Haunerland NH. *Insect storage proteins: gene families and receptors*. Insect Biochem Mol Biol. 1996; 26(8-9): 755-765. Review.
- Horie Y. *Blood trehalose and fat-body glycogen in the silkworm, Bombyx mori*. Nature. 1960; 188(4750): 583-584.
- Horwitz JP, Chua J, Noel M, Donatti JT, Freisler J. *Substrates for Cytochemical Demonstration of Enzyme Activity. II. Some Dihalo-3-indolyl Phosphates and Sulfates1*. J. Med. Chem. 1966; 9(3): 447.
- Hosokawa N, Hara T, Kaizuka T, Kishi C, Takamura A, Miura Y, Iemura S, Natsume T, Takehana K, Yamada N, Guan JL, Oshiro N, Mizushima N. *Nutrient-dependent mTORC1 association with the ULK1-Atg13-FIP200 complex required for autophagy*. Mol Biol Cell. 2009; 20(7): 1981-1991.
- Hou YC, Chittaranjan S, Barbosa SG, McCall K, Gorski SM. *Effector caspase Dcp-1 and IAP protein Bruce regulate starvation-induced autophagy during Drosophila melanogaster oogenesis*. J Cell Biol. 2008; 182(6): 1127-1139.

- Hunter S, Apweiler R, Attwood TK, Bairoch A, Bateman A, Binns D, Bork P, et al. *InterPro: the integrative protein signature database*. Nucleic Acids Res. 2009; 37(Database issue): D211-D215.
- Itakura E, Mizushima N. *Characterization of autophagosome formation site by a hierarchical analysis of mammalian Atg proteins*. Autophagy. 2010; 6(6): 764–776.
- Johansen MB, Kiemer L, Brunak S. *Analysis and prediction of mammalian protein glycation.* Glycobiology. 2006; 16(9): 844-853.
- Julenius K, Mølgaard A, Gupta R, Brunak S. *Prediction, conservation analysis, and structural characterization of mammalian mucin-type O-glycosylation sites*. Glycobiology. 2005; 15(2): 153-164.
- Julenius K. *NetCGlyc 1.0: prediction of mammalian C-mannosylation sites*. Glycobiology. 2007; 17(8): 868-876.
- Jung CH, Ro SH, Cao J, Otto NM, Kim DH. *mTOR regulation of autophagy*. FEBS Lett. 2010; 584(7): 1287-1295. Review.
- Kakei M, Iwami M, Sakurai S. *Death commitment in the anterior silk gland of the silkworm, Bombyx mori*. J. Insect physiol. 2005; 51(1): 17-25.
- Kamada Y, Funakoshi T, Shintani T, Nagano K, Ohsumi M, Ohsumi Y. *Tor-mediated induction of autophagy via an Apg1 protein kinase complex*. J Cell Biol. 2000; 150(6): 1507-1513.
- Kamada Y, Yoshino K, Kondo C, Kawamata T, Oshiro N, Yonezawa K, Ohsumi Y. *Tor directly controls the Atg1 kinase complex to regulate autophagy*. Mol Cell Biol. 2010; 30(4): 1049-1058.
- Kaneko Y, Yasanga T, Suzuki M, Sakurai S. *Larval fat body cells die during the early pupal stage in the frame of metamorphosis remodelation in Bombyx mori*. J Insect Physiol. 2011; 57(12): 1715-1722.
- Kerr JF, Wyllie AH, Currie AR. *Apoptosis: a basic biological phenomenon with wide-ranging implications in tissue kinetics*. Br J Cancer. 1972; 26(4): 239-257. Review.
- Khoa DB, Takeda M. *Expression of autophagy 8 (Atg8) and its role in the midgut and other organs of the greater wax moth, Galleria mellonella, during metamorphic remodelling and under starvation*. Insect Mol Biol. 2012; 21(5): 473-487.

- Kiguchi K, Agui N.. *Ecdysteroid levels and developmental events during larval moulting in the silkworm, Bombyx mori*. J. Insect Physiol. 1981; 27: 805–812.
- Kijanska M, Dohnal I, Reiter W, Kaspar S, Stoffel I, Ammerer G, Kraft C, Peter M. *Activation of Atg1 kinase in autophagy by regulated phosphorylation*. Autophagy. 2010; 6(8): 1168-1178.
- Klionsky DJ. *Autophagy: from phenomenology to molecular understanding in less than a decade.* Nat. Rev. Mol. Cell Biol. 2007; 8, 931–937. Review
- Klionsky DJ, Abdalla FC, Abeliovich H, Abraham RT, Acevedo-Arozena A, Adeli K, Agholme L, et al. *Guidelines for the use and interpretation of assays for monitoring autophagy. Autophagy*. 2012; 8(4): 445-544.
- Kogan M. *Integrated pest management: historical perspectives and contemporary developments*. Annu Rev Entomol. 1998; 43: 243-270. Review.
- Krishnan M, König S. *Progress of proteomic analysis in silkworm Bombyx mori*. Biomacromolecular Spectrometry. 2011; 2(3): 179-188.
- Kroemer G, Galluzzi L, Vandenabeele P, Abrams J, Alnemri ES, Baehrecke EH, Blagosklonny MV, El-Deiry WS, Golstein P, Green DR, Hengartner M, Knight RA, Kumar S, Lipton SA, Malorni W, Nuñez G, Peter ME, Tschopp J, Yuan J, Piacentini M, Zhivotovsky B, Melino G; Nomenclature Committee on Cell Death 2009. *Classification of cell death: recommendations of the Nomenclature Committee on Cell Death 2009*. Cell Death Differ. 2009; 16(1): 3-11.
- Krogh A, Larsson B, von Heijne G, Sonnhammer EL. *Predicting transmembrane protein topology with a hidden Markov model: application to complete genomes*. J Mol Biol. 2001; 305(3): 567-580.
- Kundu M. *ULK1, mammalian target of rapamycin, and mitochondria: linking nutrient availability and autophagy*. Antioxid Redox Signal. 2011; 14(10): 1953-1958. Review.
- Kuroyanagi H, Yan J, Seki N, Yamanouchi Y, Suzuki Y, Takano T, Muramatsu M, Shirasawa T. *Human ULK1, a novel serine/threonine kinase related to UNC-51 kinase of Caenorhabditis elegans: cDNA cloning, expression, and chromosomal assignment*. Genomics. 1998; 51(1): 76-85.
- Leonardi MG, Casartelli M, Parenti P, Giordana B. *Evidence for a low-affinity, high-capacity uniport for amino acids in Bombyx mori larval midgut*. Am J Physiol. 1998; 274(5 Pt 2): R1372-R1375.

- Levine B, Klionsky DJ. *Development by self-digestion: molecular mechanisms and biological functions of autophagy*. Dev Cell. 2004; 6(4): 463-477. Review.
- Li Q, Zheng S, Liu L, Tettamanti G, Cao Y, Feng Q. *Expression of autophagy related genes in the anterior silk gland of Bombyx mori during metamorphosis*. Can. J. Zool. 2011; 89: 1019–1026.
- Li Q, Deng X, Yang W, Huang Z, Tettamanti G, Cao Y, Feng Q. *Autophagy, apoptosis and ecdysis-related gene expression in the silk gland of the silkworm (Bombyx mori) during metamorphosis*. Can. J. Zool. 2010; 88: 1169–1178.
- Liu Q, Chejanovsky N. *Activation pathways and signal-mediated upregulation of the insect Spodoptera frugiperda caspase-1*. Apoptosis. 2006; 11(4): 487- 96.
- Lomelí H, Vázquez M. *Emerging roles of the SUMO pathway in development*. Cell Mol. Life Sci. 2011; 68: 4045–4064.
- Lommel M, Strahl S. *Protein O-mannosylation: conserved from bacteria to humans*. Glycobiology. 2009; 19(8): 816-828. Review.
- Malagoli D, Abdalla FC, Cao Y, Feng Q, Fujisaki K, Gregorc A, Matsuo T, Nezis IP, Papassideri IS, Sass M, Silva-Zacarin EC, Tettamanti G, Umemiya-Shirafuji R. *Autophagy and its physiological relevance in arthropods: current knowledge and perspectives*. Autophagy. 2010; 6(5): 575-588. Review.
- Manaboon M, Iga M, Sakurai S. *Nongenomic and genomic actions of an insect steroid coordinately regulate programmed cell death of anterior silk glands of Bombyx mori*. ISJ 2008; 5: 1-11. Review.
- Matsuura S, Morimoto T, Nagata S, Tashiro Y. *Studies on the posterior silk gland of the silkworm, Bombyx mori. II. Cytolytic processes in posterior silk gland cells during metamorphosis from larva to pupa*. J Cell Biol. 1968; 38(3): 589-603.
- Matsuura S, Shimadzu T, Tashiro Y. *Lysosomes and Related Structures in the Posterior Silk Gland Cells of Bombyx mori. II. In Prepupal and Early Pupal Stadium*. Cell structure and Function. 1976; 1: 223-235.
- Matsuura A, Tsukada M, Wada Y, Ohsumi Y. *Apg1p, a novel protein kinase required for the autophagic process in Saccharomyces cerevisiae*. Gene. 1997; 192(2): 245-250.
- McCall K. *Genetic control of necrosis - another type of programmed cell death*. Curr Opin Cell Biol. 2010; 22(6): 882-888. Review.

- Meijer WH, van der Klei IJ, Veenhuis M, Kiel JA. *ATG genes involved in non-selective autophagy are conserved from yeast to man, but the selective Cvt and pexophagy pathways also require organism-specific genes*. Autophagy. 2007; 3(2): 106-116.
- Meléndez A, Neufeld TP. *The cell biology of autophagy in metazoans: a developing story*. Development. 2008; 135(14): 2347-2360. Review.
- Mirth CK, Riddiford LM. *Size assessment and growth control: how adult size is determined in insects*. Bioessays. 2007; 29(4): 344-355. Review.
- Mizushima N, Ohsumi Y, Yoshimori T. *Autophagosome formation in mammalian cells*. Cell Struct Funct. 2002; 27(6): 421-429. Review.
- Mizushima N, Yamamoto A, Matsui M, Yoshimori T, Ohsumi Y. *In vivo analysis of autophagy in response to nutrient starvation using transgenic mice expressing a fluorescent autophagosome marker*. Mol Biol Cell. 2004; 15(3): 1101-1111.
- Mizushima N, Levine B, Cuervo AM, Klionsky DJ. *Autophagy fights disease through cellular self-digestion*. Nature. 2008; 451(7182): 1069–1075. Review.
- Mizushima N. *The role of the Atg1/ULK1 complex in autophagy regulation*. Curr Opin Cell Biol. 2010; 22(2): 132-139. Review.
- Mpakou VE, Nezis IP, Stravopodis DJ, Margaritis LH, Papassideri IS. *Different modes of programmed cell death during oogenesis of the silkmoth Bombyx mori*. Autophagy. 2008; 4(1): 97-100.
- Müller F, Adori C, Sass M. *Autophagic and apoptotic features during programmed cell death in the fat body of the tobacco hornworm* (*Manduca sexta*). Eur J Cell Biol. 2004; 83(2): 67-78.
- Nation JL. *Insect physiology and biochemistry*. CRC Press. 2002; chapter 2: 28.
- Nezis IP, Lamark T, Velentzas AD, Rusten TE, Bjørkøy G, Johansen T, Papassideri IS, Stravopodis DJ, Margaritis LH, Stenmark H, Brech A. *Cell death during Drosophila melanogaster early oogenesis is mediated through autophagy*. Autophagy. 2009; 5(3): 298-302.
- Nezis IP, Shravage BV, Sagona AP, Lamark T, Bjørkøy G, Johansen T, Rusten TE, Brech A, Baehrecke EH, Stenmark H. *Autophagic degradation of dBruce controls DNA fragmentation in nurse cells during late Drosophila melanogaster oogenesis*. J Cell Biol. 2010; 190(4): 523-531.

- Ogura K, Wicky C, Magnenat L, Tobler H, Mori I, Müller F, Ohshima Y. *Caenorhabditis elegans unc-51 gene required for axonal elongation encodes a novel serine/threonine kinase*. Genes Dev. 1994; 8(20): 2389-2400.
- Owa C, Aoki F, Nagata M. *Gene expression and lysosomal content of silkworm peritracheal athrocytes*. J Insect Physiol. 2008; 54(8): 1286-12892.
- Parthasarathy R, Palli SR. *Developmental and hormonal regulation of midgut remodeling in a lepidopteran insect, Heliothis virescens*. Mech Dev. 2007; 124(1): 23-34.
- Patel CV, Gopinathan KP. *Development stage-specific expression of fibroin in the silk worm Bombyx mori is regulated translationally*. Indian J Biochem Biophys. 1991; 28(5-6): 521-530.
- Pearse EAG. *Histochemistry, theoretical and applied*. Little, Brown and Company, Boston. 1960.
- Perdrix-Gillot S. *DNA synthesis and endomitoses in the giant nuclei of the silkgland of Bombyx mori*. Biochimie. 1979; 61(2): 171-204.
- Petersen TN, Brunak S, von Heijne G, Nielsen H. *SignalP 4.0: discriminating signal peptides from transmembrane regions*. Nat Methods. 2011; 8(10): 785-786.
- Pettersen EF, Goddard TD, Huang CC, Couch GS, Greenblatt DM, Meng EC, Ferrin TE. *UCSF Chimera--a visualization system for exploratory research and analysis*. J Comput Chem. 2004; 25(13): 1605-1612.
- Pierleoni A, Indio V, Savojardo C, Fariselli P, Martelli PL, Casadio R. *MemPype: a pipeline for the annotation of eukaryotic membrane proteins*. Nucleic Acids Res. 2011; 39(Web Server issue): W375-380.
- Poiani SB, da Cruz-Landim C. *Storaged products and presence of acid phosphatase in fat body cells at pre-pupal worker stage of Apis mellifera Linnaeus, 1758 (Hymenoptera, Apidae)*. Micron. 2012; 43(2-3): 475-478.
- Ren J, Gao X, Jin C, Zhu M, Wang X, Shaw A, Wen L, Yao X, Xue Y. *Systematic study of protein sumoylation: Development of a site-specific predictor of SUMOsp 2.0*. Proteomics. 2009; 9(12): 3409-3412.
- Riddiford LM, Hiruma K, Zhou B. *Regulation and role of nuclear receptors during larval molting and metamorphosis of Lepidoptera*. Amer. Zool. 1999; 39: 736-746.

- Riddiford LM, Hiruma K, Zhou X, Nelson CA. *Insights into the molecular basis of the hormonal control of molting and metamorphosis from Manduca sexta and Drosophila melanogaster*. Insect Biochem Mol Biol. 2003; 33(12): 1327-1338. Review.
- Roma GC, Bueno OC, Camargo-Mathias MI. *Morpho-physiological analysis of the insect fat body: a review*. Micron. 2010; 41(5): 395-401.
- Romanelli D, Casati B, Franzetti E, Tettamanti G. *A molecular view of autophagy in Lepidoptera. BioMed Research International*. Review. Under submission
- Rost-Roszkowska M, Chechelska A, Frądczak M, Salitra K. *Ultrastructure of two types of endocrine cells in the midgut epithelium of Spodoptera exiqua hubner, 1808 (Insecta, Lwpidoptera, Noctuidae*). Zoologica Poloniae. 2008; 53(1-4): 27-35.
- Roy A, Kucukural A, Zhang Y. *I-TASSER: a unified platform for automated protein structure and function prediction*. Nat Protoc. 2010; 5(4): 725-738.
- Rusten TE, Lindmo K, Juhász G, Sass M, Seglen PO, Brech A, Stenmark H. *Programmed autophagy in the Drosophila fat body is induced by ecdysone through regulation of the PI3K pathway.* Dev Cell. 2004; 7(2): 179-192.
- Saitou N, Nei M. *The neighbor-joining method — a new method for reconstructing phylogenetic trees*. Mol. Biol. Evol. 1987; 4: 406–425.
- Sakaguchi B. *Gametogenesis, fertilization and embryogenesis of the silkworm*. In: Tazima, Y. (Ed.), The Silkworm: An Important Laboratory Tool. Kodansha, Tokyo. 1978; pp. 5–10.
- Satake S, Kawabe Y, Mizoguchi A. *Carbohydrate metabolism during starvation in the silkworm Bombyx mori*. Arch Insect Biochem Physiol. 2000; 44(2): 90-98.
- Scott RC, Schuldiner O, Neufeld TP. *Role and regulation of starvation-induced autophagy in the Drosophila fat body.* Dev Cell. 2004; 7(2): 167-78.
- Scott RC, Juhász G, Neufeld TP. *Direct induction of autophagy by Atg1 inhibits cell growth and induces apoptotic cell death*. Curr Biol. 2007; 17(1): 1-11.
- Shang L, Wang X. *AMPK and mTOR coordinate the regulation of Ulk1 and mammalian autophagy initiation.* Autophagy. 2011; 7(8): 924-926.
- Sigrist CJ, Cerutti L, Hulo N, Gattiker A, Falquet L, Pagni M, Bairoch A, Bucher P. *PROSITE: a documented database using patterns and profiles as motif descriptors*. Brief Bioinform. 2002; 3(3): 265-274.

- Sigrist CJ, Cerutti L, de Castro E, Langendijk-Genevaux PS, Bulliard V, Bairoch A, Hulo N. *PROSITE, a protein domain database for functional characterization and annotation*. Nucleic Acids Res. 2010; 38(Database issue): D161-D166.
- Sumithra P, Britto CP, Krishnan M. *Modes of cell death in the pupal perivisceral fat body tissue of the silkworm Bombyx mori L*. Cell Tissue Res. 2010; 339(2): 349-358.
- Suzuki K, Kirisako T, Kamada Y, Mizushima N, Noda T, Ohsumi Y. *The preautophagosomal structure organized by concerted functions of APG genes is essential for autophagosome formation.* EMBO J. 2001; 20: 5971–5981.
- Suzuki K, Ohsumi Y. *Molecular machinery of autophagosome formation in yeast, Saccharomyces cerevisiae*. FEBS Lett. 2007; 581(11): 2156-21561. Review.
- Takeshige K, Baba M, Tsuboi S, Noda T, Ohsumi Y. *Autophagy in yeast demonstrated with proteinase-deficient mutants and conditions for its induction*. J Cell Biol. 1992; 119(2): 301-311.
- Tamura K, Dudley J, Nei M, Kumar S. *MEGA4: Molecular Evolutionary Genetics Analysis (MEGA) software version 4.0*. Mol. Biol. Evol 2007; 24: 1596–1599.
- Tang S, Xiao Y, Chen L, Cheke RA. *Integrated pest management models and their dynamical behaviour.* Bull Math Biol. 2005; 67(1): 115-115.
- Tang S, Xiao Y, Cheke RA. *Multiple attractors of host-parasitoid models with integrated pest management strategies: eradication, persistence and outbreak*. Theor Popul Biol. 2008; 73(2): 181-197.
- Terashima J, Yasuhara N, Iwami M, Sakurai S, Sakurai S. *Programmed cell death triggered by insect steroid hormone, 20-hydroxyecdysone, in the anterior silk gland of the silkworm, Bombyx mori.* Dev Genes Evol. 2000; 210(11): 545-558.
- Terra WR. *The origin and functions of the insect peritrophic membrane and peritrophic gel*. Arch Insect Biochem Physiol. 2001; 47(2): 47-61. Review.
- Terra WR, Ferreira C. *Biochemistry of digestion*. In: Gilbert LI, Iatrou K, Gill SS (Eds), Comprehensive Molecular Insect Science, Oxford. 2005; Elsevier 4: 171– 224.
- Terra WR, Costa RH, Ferreira C. *Plasma membranes from insect midgut cells*. An. Acad. Bras. Ciênc. 2006; 78(2): 255-269.
- Tettamanti G, Grimaldi A, Casartelli M, Ambrosetti E, Ponti B, Congiu T, Ferrarese R, Rivas-Pena ML, Pennacchio F, de Eguileor M. *Programmed cell death and stem cell differentiation*

are responsible for midgut replacement in Heliothis virescens during prepupal instar. Cell Tissue Res. 2007a; 330(2): 345-359.

- Tettamanti G, Grimaldi A, Pennacchio F, de Eguileor M. Lepidopteran larval midgut during prepupal instar: digestion or self-digestion? Autophagy. 2007b; 3(6): 630-631.
- Tettamanti G, Cao Y, Feng Q, Grimaldi A, de Eguileor M. *Autophagy in Lepidoptera: more than old wine in new bottle*. ISJ 2011; 8: 5-14. Review.
- Thompson SN. *Trehalose – The Insect 'Blood' Sugar*. Adv Insect Physiol. 2003; 31: 205–285.
- Tian L, Guo E, Diao Y, Zhou S, Peng Q, Cao Y, Ling E, Li S. *Genome-wide regulation of innate immunity by juvenile hormone and 20-hydroxyecdysone in the Bombyx fat body*. BMC Genomics. 2010; 11: 549-560.
- Tian L, Liu S, Liu H, Li S. *20-hydroxyecdysone upregulates apoptotic genes and induces apoptosis in the Bombyx fat body*. Arch Insect Biochem Physiol. 2012; 79(4-5): 207-219.
- Tian L, Ma L, Guo E, Deng X, Ma S, Xia Q, Cao Y, Li S. *20-hydroxyecdysone upregulates Atg genes to induce autophagy in the Bombyx fat body*. Autophagy. 2013; 9(8): 1172-1187.
- Tomoda T, Bhatt RS, Kuroyanagi H, Shirasawa T, Hatten ME. *A mouse serine/threonine kinase homologous to C. elegans UNC51 functions in parallel fiber formation of cerebellar granule neuron*s. Neuron. 1999; 24(4): 833-846.
- Tsukada M, Ohsumi Y. *Isolation and characterization of autophagy-defective mutants of Saccharomyces cerevisiae*. FEBS Lett. 1993; 333(1-2): 169-174.
- Ulukaya E, Acilan C, Yilmaz Y. *Apoptosis: why and how does it occur in biology*? Cell Biochem Funct. 2011; 29(6): 468-480. Review.
- Uwo MF, Ui-Tei K, Park P, Takeda M. *Replacement of midgut epithelium in the greater wax moth, Galleria mellonela, during larval-pupal moult*. Cell Tissue Res. 2002; 308(2): 319-331.
- Vandenborre G, Smagghe G, Ghesquière B, Menschaert G, Nagender Rao R, Gevaert K, Van Damme EJ. *Diversity in protein glycosylation among insect species*. PLoS One. 2011; 6(2): e16682.
- Vanishree V,Nirmala X, Arul E, krishnan M. *Differential sequestration of storage proteins by various fat body tissues during post-larval development in silkworm*, *Bombyx mori* L. Invertebr. Reprod. Dev. 2005; 48(1-3): 81-88.

- Wang CW, Klionsky DJ. *The molecular mechanism of autophagy*. Mol Med. 2003; 9(3-4): 65-76. Review.
- Wang J, Xia Q, He X, Dai M, Ruan J, Chen J, Yu G, Yuan H, Hu Y, Li R, Feng T, Ye C, Lu C, Wang J, Li S, Wong GK, Yang H, Wang J, Xiang Z, Zhou Z, Yu J. *SilkDB: a knowledgebase for silkworm biology and genomics.* Nucleic Acids Res. 2005; 33(Database issue): D399-D402.
- Wang Z, Haunerland NH. *Fate of differentiaites fat body tissues during metamorphosis of Helicoverpa zea*. J Insect Physiol. 1992; 38(3): 199-209, 211-213.
- Wieczorek H, Grber G, Harvey WR, Huss M, Merzendorfer H, Zeiske W. *Structure and regulation of insect plasma membrane H(+)V-ATPase*. J Exp Biol. 2000; 203(Pt 1): 127-135. Review.
- Wigglesworth VB. *Digestion and nutrition*. In: The principles of insect physiology. Chapman & Hall (London). 1972; 476-552.
- Wu W, Wei W, Ablimit M, Ma Y, Fu T, Liu K, Peng J, Li Y, Hong H. *Responses of two insect cell lines to starvation: autophagy prevents them from undergoing apoptosis and necrosis, respectively*. J Insect Physiol. 2011; 57(6): 723-734.
- Xia Q, Li S, Feng Q. *Advances in Silkworm Studies Accelerated by the Genome Sequencing of Bombyx mori*. Annu Rev Entomol. 2014; 59: 513-536.
- Xie Z, Klionsky DJ. *Autophagosome formation: core machinery and adaptations*. Nat Cell Biol. 2007; 9(10): 1102-1109. Review.
- Yan J, Kuroyanagi H, Kuroiwa A, Matsuda Y, Tokumitsu H, Tomoda T, Shirasawa T, Muramatsu M. *Identification of mouse ULK1, a novel protein kinase structurally related to C. elegans UNC-51*. Biochem Biophys Res Commun. 1998; 246(1): 222-227.
- Yeh YY, Wrasman K, Herman PK. *Autophosphorylation within the Atg1 activation loop is required for both kinase activity and the induction of autophagy in Saccharomyces cerevisiae*. Genetics. 2010; 185(3): 871-882.
- Yeh YY, Shah KH, Chou CC, Hsiao HH, Wrasman KM, Stephan JS, Stamatakos D, Khoo KH, Herman PK. *The identification and analysis of phosphorylation sites on the Atg1 protein kinase*. Autophagy. 2011; 7(7): 716-726.
- Zanuncio TV, Zanuncio JC, de Freitas FA, Pratissoli D, Sediyama CA, Maffia VP. *Main lepidopteran pest species from an eucalyptus plantation in Minas Gerais, Brazil*. Rev Biol Trop. 2006; 54(2): 553-560.

- Zhang Y. *Template-based modeling and free modeling by I-TASSER in CASP7*. Proteins. 2007; 69 Suppl 8: 108-117.
- Zhang Y. *I-TASSER server for protein 3D structure prediction*. BMC Bioinformatics. 2008; 9: 40.
- Zhang X, Hu ZY, Li WF, Li QR, Deng XJ, Yang WY, Cao Y, Zhou CZ. *Systematic cloning and analysis of autophagy-related genes from the silkworm Bombyx mori*. BMC Mol Biol. 2009; 10:50.
- Zhou Z, Yang H, Zhong B. *From genome to proteome: great progress in the domesticated silkworm (Bombyx mori L.)*. Acta Biochim Biophys Sin (Shanghai). 2008; 40(7): 601-611. Review.
- Zhou S, Zhou Q, Liu Y, Wang S, Wen D, He Q, Wang W, Bendena WG, Li S. *Two Tor genes in the silkworm Bombyx mori*. Insect Mol Biol. 2010; 19(6): 727-735.
- Ziegler R. Ch*anges in lipid and carbohydrate metabolism during starvation in adult Manduca sexta*. J Comp Physiol B. 1991; 161(2): 125-131.

FIGURES AND TABLES

Figure 1. Structure of midgut epithelium

A-C. Midgut epithelium under physiological conditions. During fifth larval instar (**A**), *B. mori* midgut consists of a monolayered epithelium in which columnar (C) and goblet (G) cells are identifiable. Columnar cells have a luminal brush border (arrowhead), while goblet cells present an intracellular cavity lined by microvilli. Few stem cells are interspersed near the base of mature cells (arrow). During spinning phase (**B**, **C**), stem cells proliferate forming a continuous cell layer which separates the larval epithelium (e) from the basement membrane. At SD1 (**B**), larval epithelial cells (e) are still in close contact with the new cell layer (bracket). At SD2 (**C**), larval epithelium (yb) detaches from the new pupal epithelium (bracket).

D-F. Midgut epithelium under starvation. Larval midgut epithelium (**D**) retains its typical structure up to wandering stage. At SD1 (**E**) yellow body (yb) detaches from the new pupal epithelium (bracket). At SD2 (**F**) a new pupal epithelium is formed and yellow body (yb) is clearly visible in the gut lumen (L). Bar: 100 µm

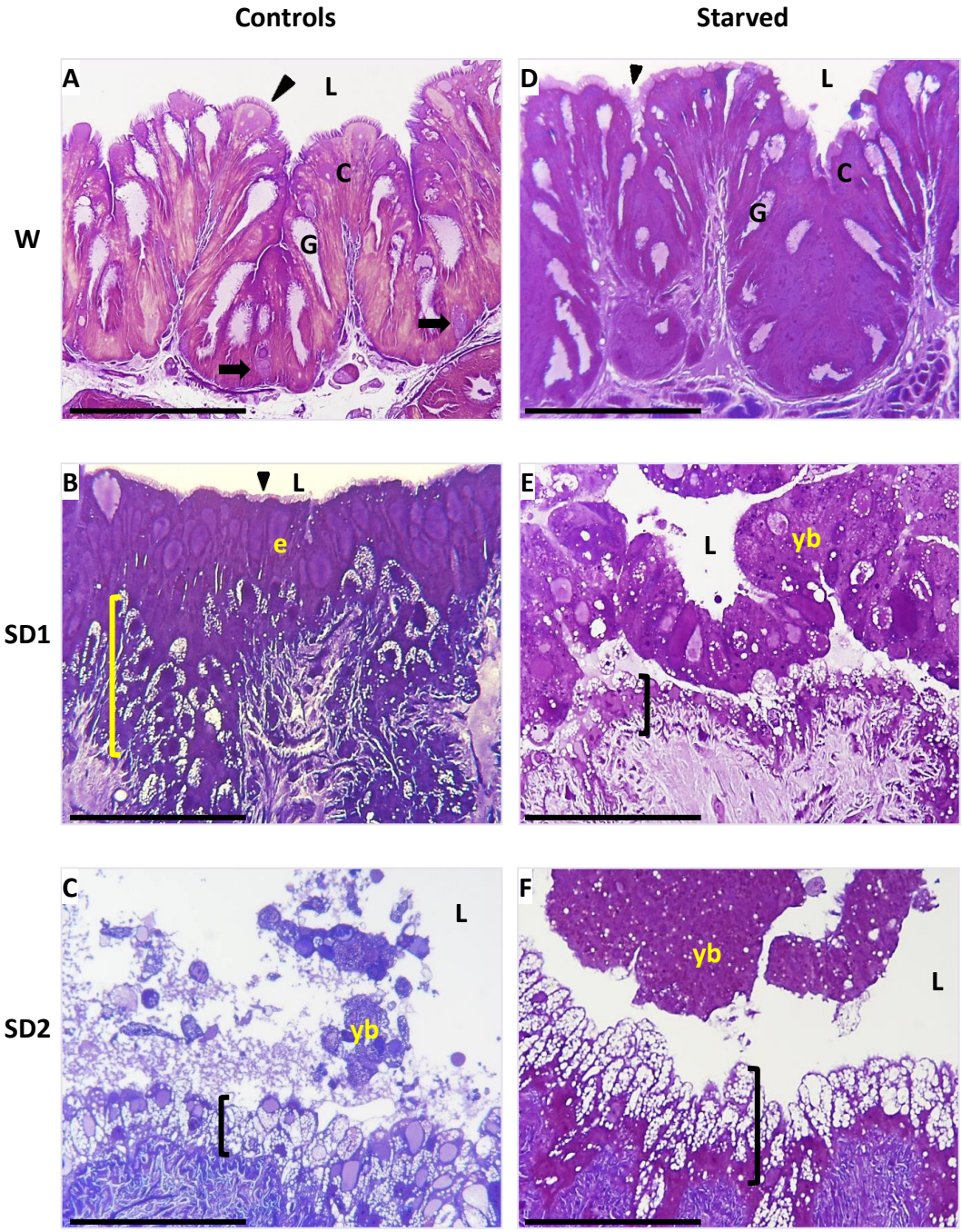
Controls
Starved
W
SD1
SD2
A
L
C
G
D
L
C
G
B
L
e
E
L
yb
C
L
yb
F
yb
L

Figure 2. Histochemical characterization of midgut epithelium: P.A.S.

During fifth larval instar, glycogen granules are present in larval midgut epithelium (**A**, **B**), while during the spinning phase (**C**, **D**) they are found only in the new pupal epithelium (bracket)**.** Under starvation, glycogen granules disappear from larval epithelium as soon as 6 hours after food deprivation (**E**, **F**) and are not present in the new pupal layer (**G**, **H**).

L, gut lumen. Bar: 10 µm

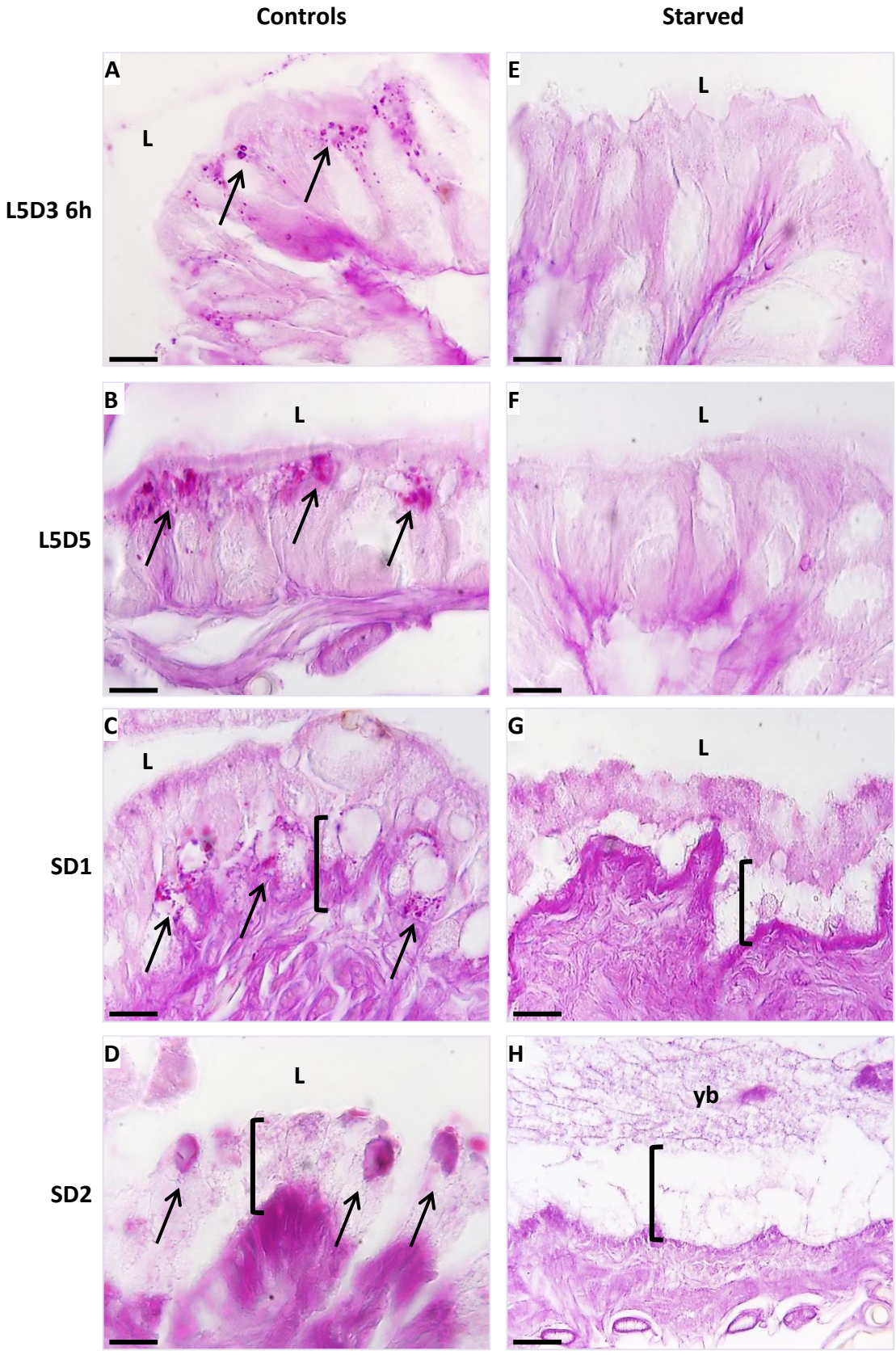
Controls
Starved
L5D3 6h
L5D5
SD1
SD2
A
B
C
D
E
F
G
H
L
yb

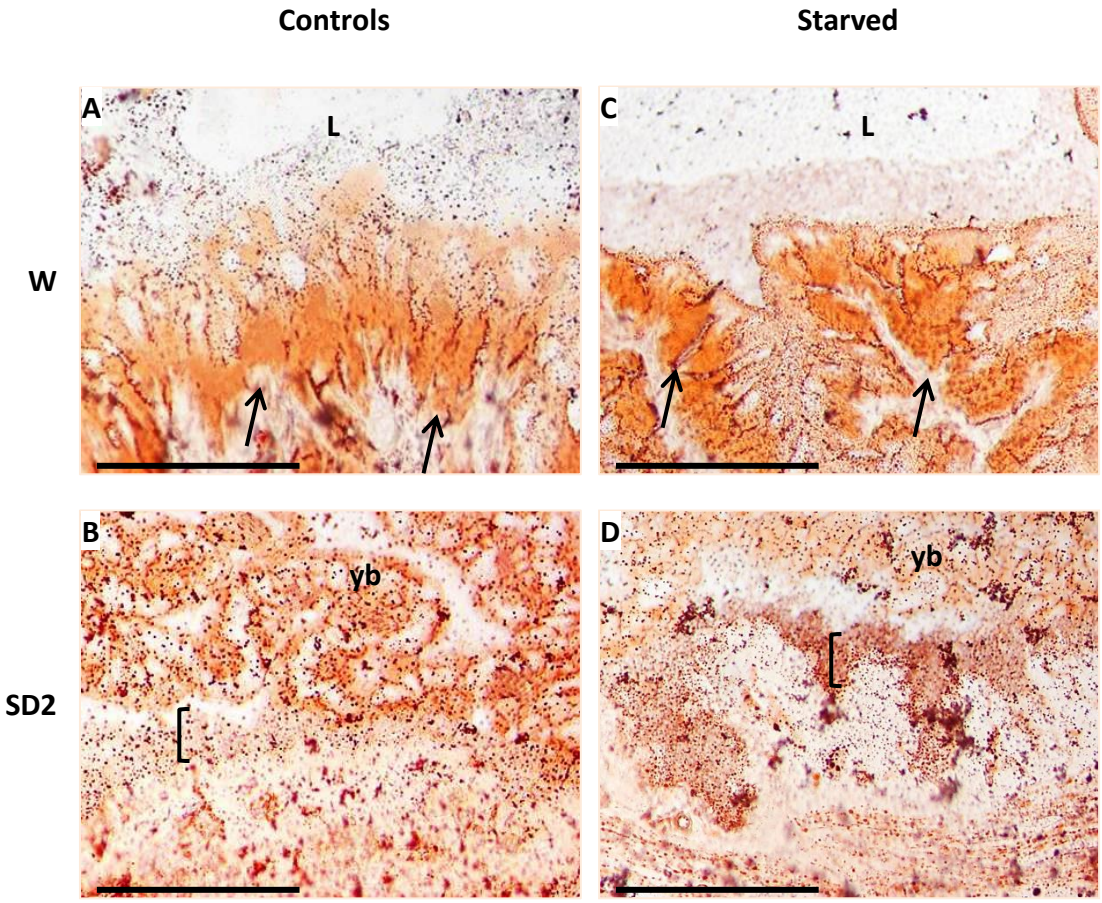

Figure 3. Histochemical characterization of midgut epithelium: O.R.O

According to O.R.O reaction (arrows), fatty acids are present in midgut of both fed (**A**) and starved (**C**) larvae. At the end of spinning period, O.R.O positivity is detected in the yellow body as well as in the new pupal epithelium (bracket) of control (**B**) and unfed (**D**) animals.

L, gut lumen. Bar: 100 µm

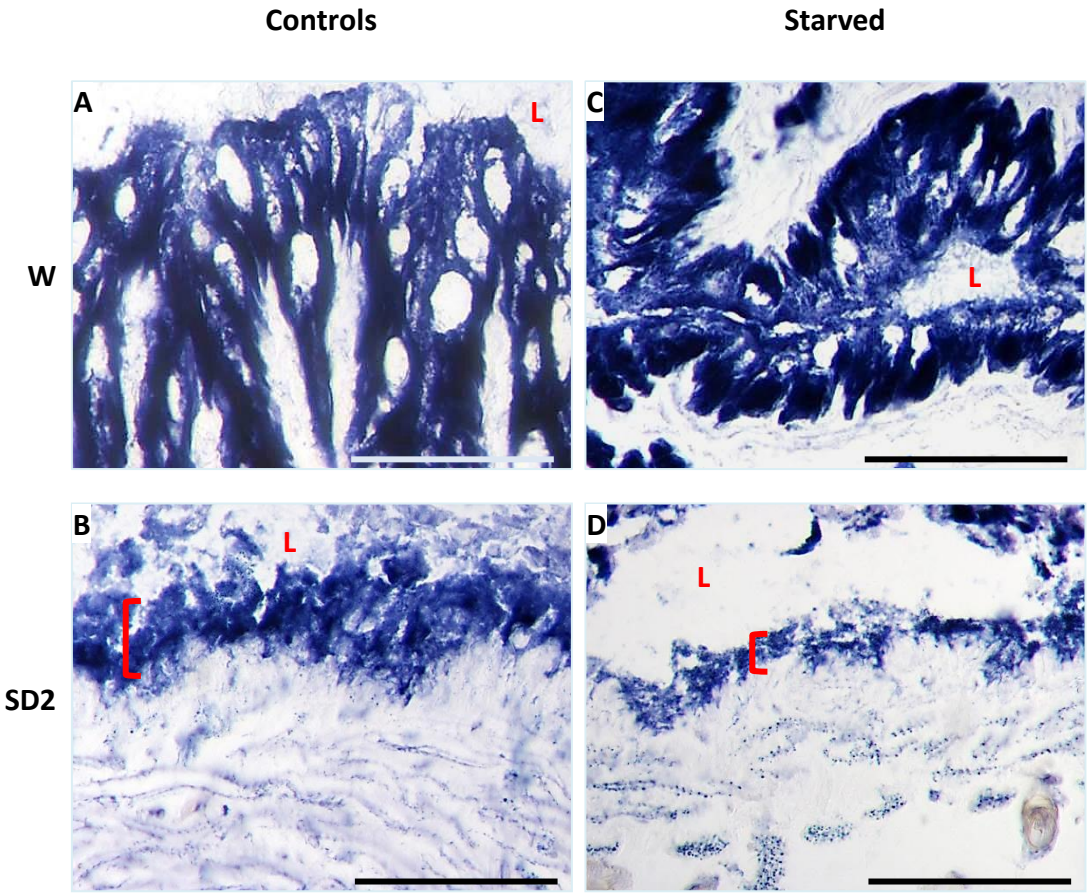

Figure 4. Histochemical characterization of midgut epithelium:
NADH diaphorase

The signal associated with NADH diaphorase (dark blue staining) is strong in epithelial cells of both fed (**A**) and starved (**C**) larvae. During the spinning phase, the positivity is present in the new layer (bracket) that is forming in both controls (**B**) and unfed (**D**) animals.

L, gut lumen. Bar: 100 µm

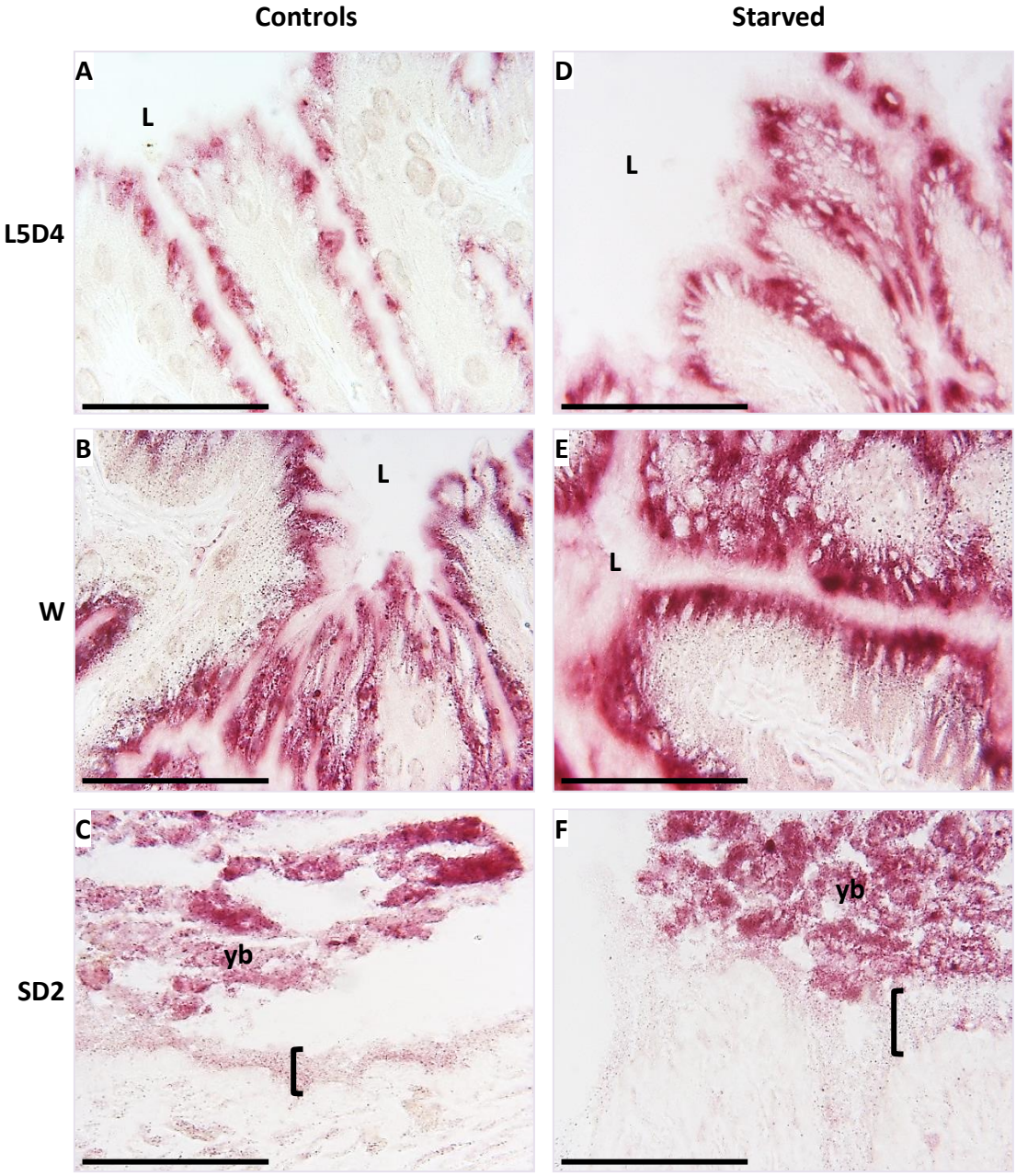

Figure 5. Histochemical characterization of midgut epithelium:
Acid phosphatase

The histochemical staining shows that enzyme activity (red staining) is restricted to larval midgut epithelium in both control (**A-C**) and starved (**D-F**) larvae. Accordingly, at the end of spinning phase (**C**, **F**), the positivity is restricted to the yellow body (yb) and absent in the new pupal epithelium (bracket).

L, gut lumen. Bar: 100 µm

Figure 6. Histochemical characterization of midgut epithelium:

Alkaline phosphatase

The signal associated with alkaline phosphatase is present on the brush border and in the goblet cavity of control epithelial cells up to the wandering stage (**A**, **B**)**.** During the spinning phase, the signal is confined in the larval goblet cells cavity (**C**) and then found only in the yellow body (**D**). In starved larvae, enzyme reactivity is observed on both brush border and cell cavities up to L5D5 (**E**), while at wandering alkaline phosphatase activity is observed only in the goblet cells (**F**). During spinning phase, only yellow body is positive for the histochemical staining (**H**).

New pupal epithelial cells (bracket) are negative for the enzymatic assay in both groups (**D**, **G**, **H**).

L, gut lumen. Bar: 100 µm

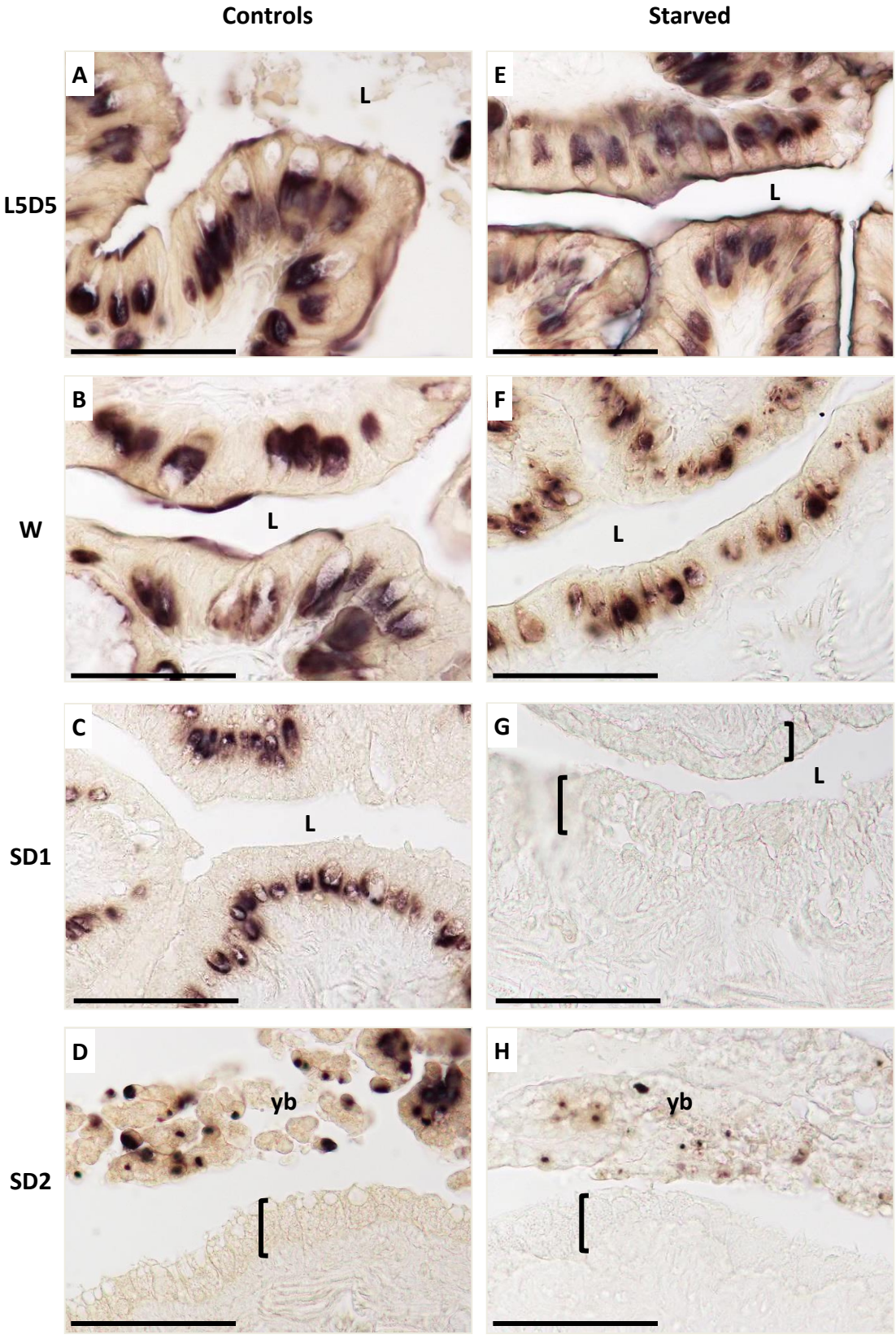
Controls
Starved
L5D5
W
SD1
SD2
A
B
C
D
E
F
G
H
L
yb

Figure 7. Morphology of silkworm fat body

Complete food deprivation induces a significant reduction of tissue volume from wandering stage. In control samples (**A-D**), cell morphology is well defined, cells dimension increases at wandering (**B**) and SD1 (**C**), and lipids are identifiable as white droplets in the cytoplasm. In starved larvae (**E-H**), even though lipid droplets are still present, single adipocytes are less clearly identifiable.

Bar: 100 µm

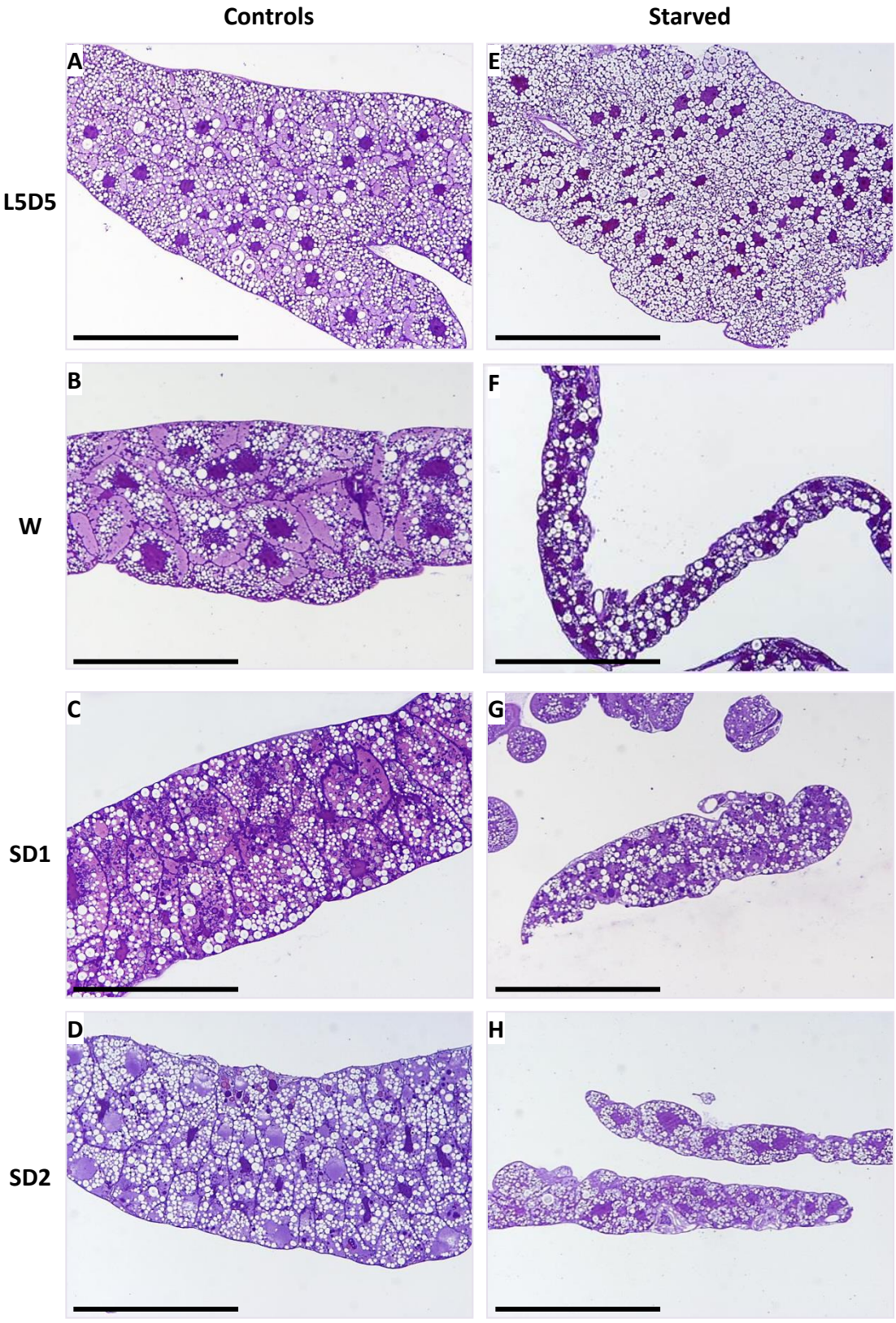
Controls
Starved
L5D5
W
SD1
SD2
A
B
C
D
E
F
G
H

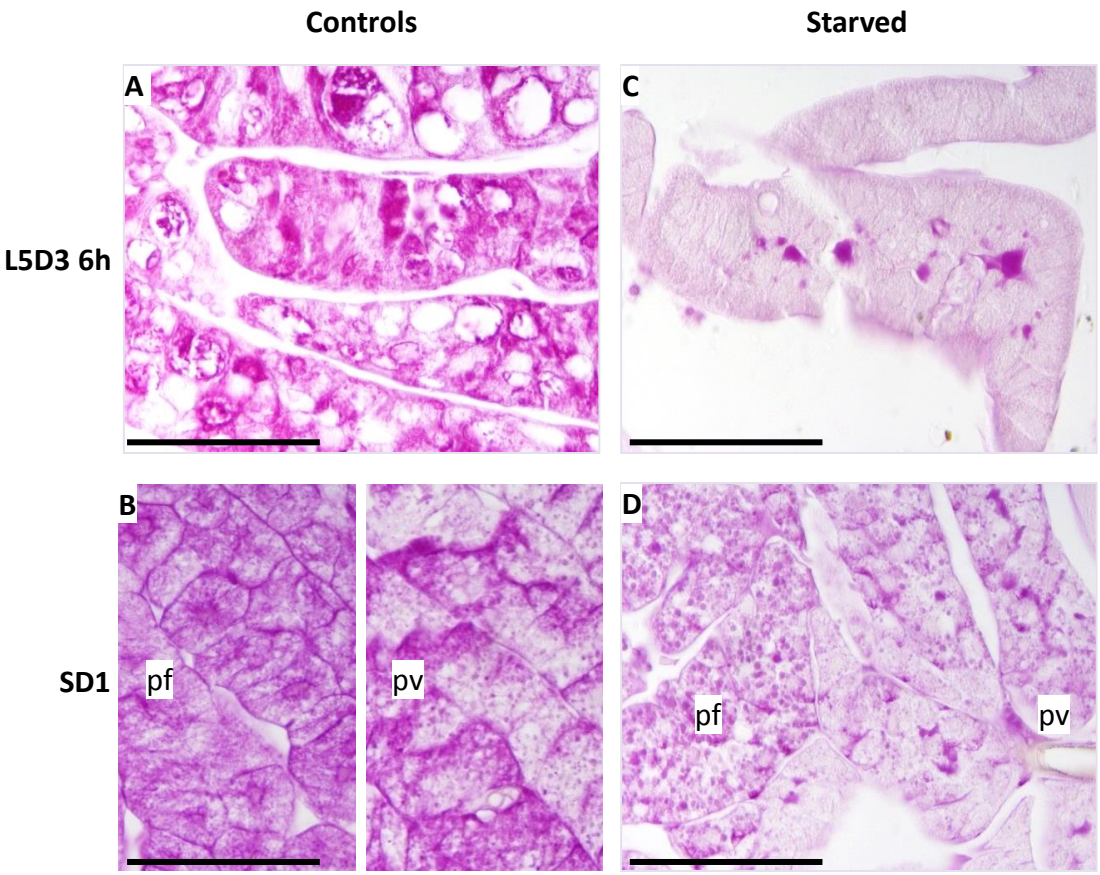

Figure 8. Histochemical characterization of fat body: P.A.S.

Glycogen stores are abundant in control fat body (**A**, **B**). In starved larvae, the presence of glycogen stores decreases as early as 6 hours after food deprivation (**C**). Different P.A.S. positivity in peripheral (pf) and perivisceral (pv) fat body is observed mainly in starved larvae (**D**), and in part in fed animals (**B**), with the major intensity detected in the peripheral fat body.

Bar: 100 µm

Figure 9. Histochemical characterization of fat body:

Controls **Starved**

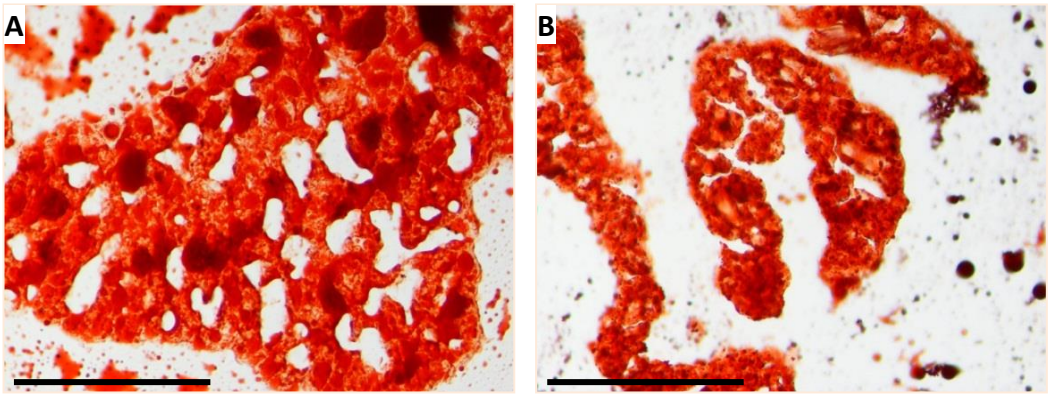

O.R.O

Both fed (**A**) and unfed (**B**) larvae accumulate fatty acids in their fat body cells (red staining) for the whole period under analysis. Here reported SD1 stage as representative of non-feeding period in both animal groups.

Bar: 100 µm

Controls **Starved**

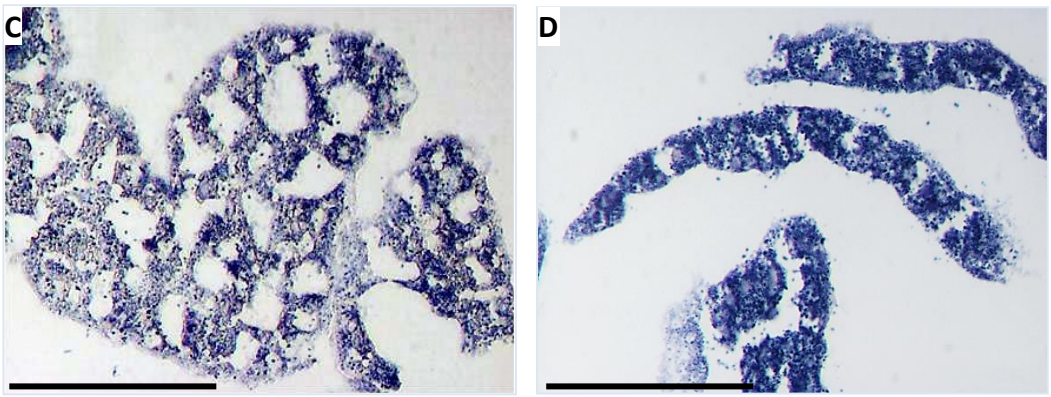

NADH diaphorase

According to NADH diaphorase activity distribution (dark blue staining), fat body cells retain a good mitochondrial activity for the whole period in both control (**C**) and starved (**D**) larvae. Here reported SD1 stage as an example.

Bar: 100 µm

Figure 10. Histochemical characterization of fat body: Acid phosphatase

In fed larvae (**A-D**), fat body cells show an intense lysosomal activity (red staining) at the end of feeding period (**A**) and wandering stage (**B**) as well as in pre-pupal samples (**D**), with a decrease during the spinning phase (**C**). In starved larvae (**E-H**), an increase in acid phosphatase activity is registered at the end of spinning phase (**G**) and pre-pupal period (**H**).

Bar: 100 µm

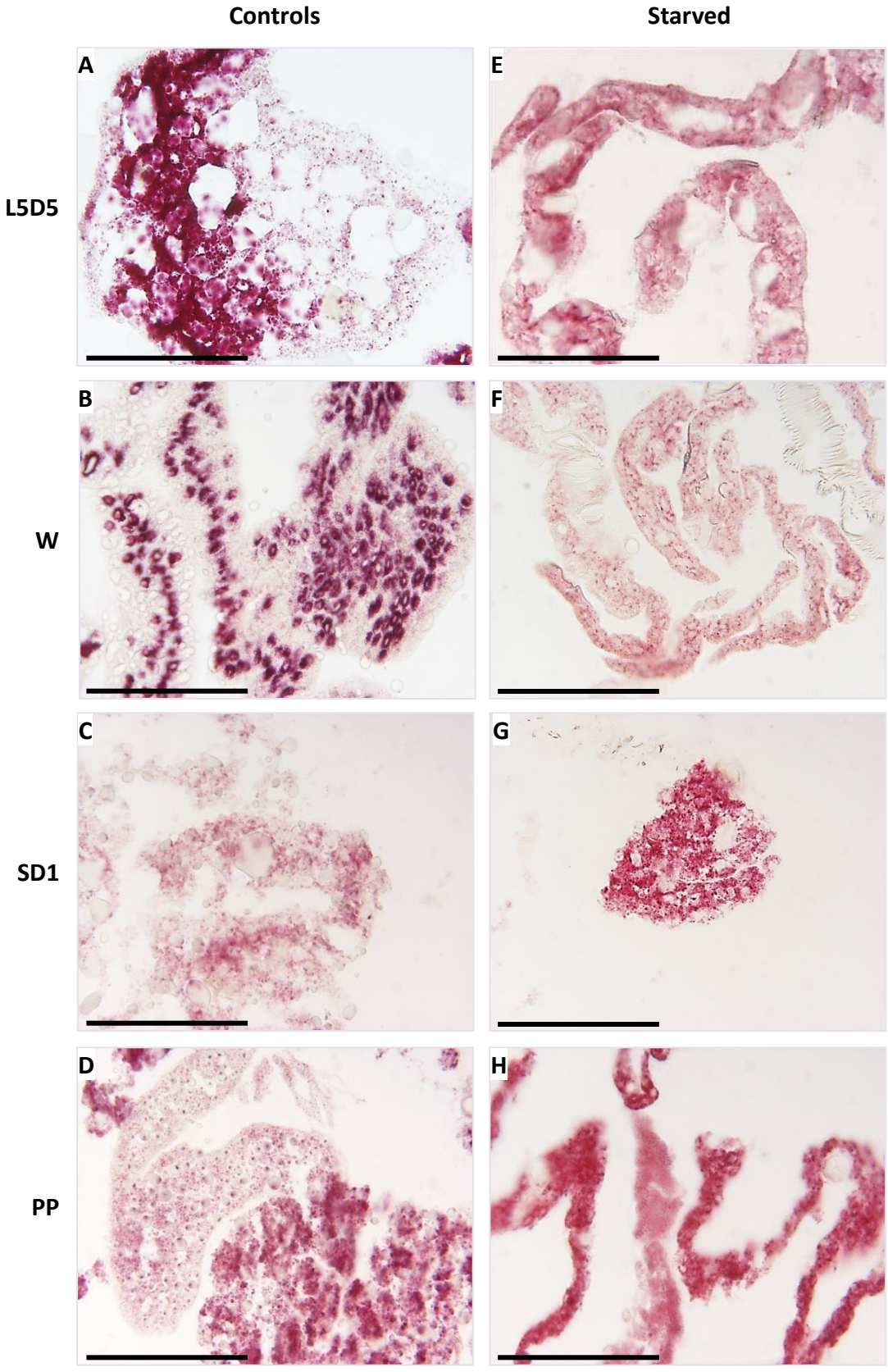
Controls
Starved
L5D5
W
SD1
PP
A
B
C
D
E
F
G
H

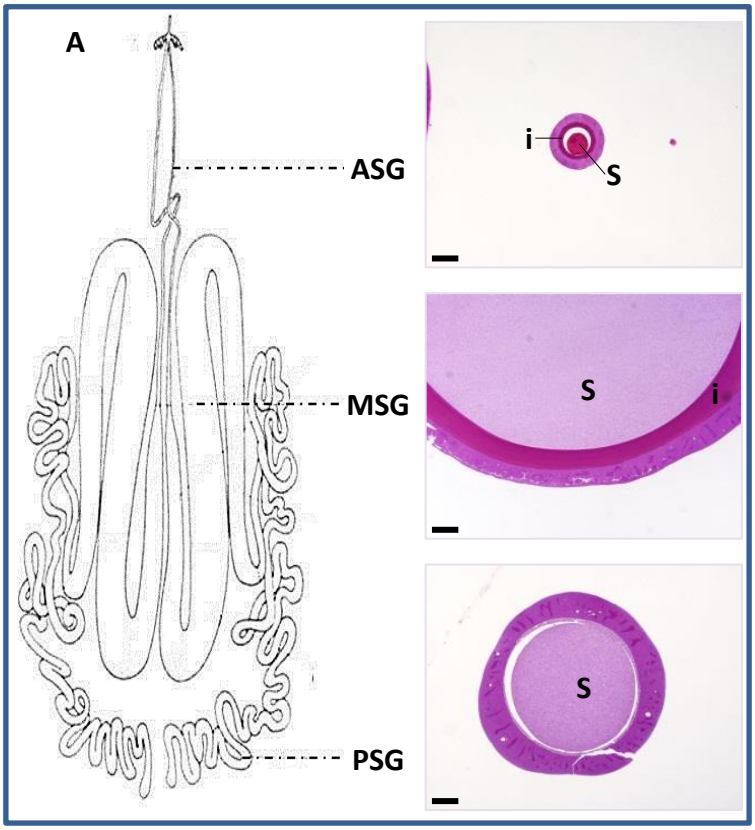

Figure 11. Morphology of silk gland compartments

A. Morphology during last larval instar

Schematic representation of *Bombyx mori* silk gland (Akai, 1983) accompanied by light microscopy images obtained from fifth instar larvae, to compare their sizes.

S, silk. i, cuticula intima. Bar: 100 μm

Figure 11. Morphology of silk gland compartments

B-M. **Morphological comparison of silk gland compartments**

During fifth instar and wandering stage, the diameter of silk gland compartments is comparable among control and starved larvae (data not shown). ASG diameter is still comparable during spinning phase and pre-pupal stage (**B-E**) and a sensible reduction in PSG diameter (**J-M**) is registered in starved PP samples (**M**). On the contrary, MSG retaines a greater diameter in starved (**H**, **I**) than in control animals (**F, G**).

S, silk. i, cuticula intima. Bar: 100 μm

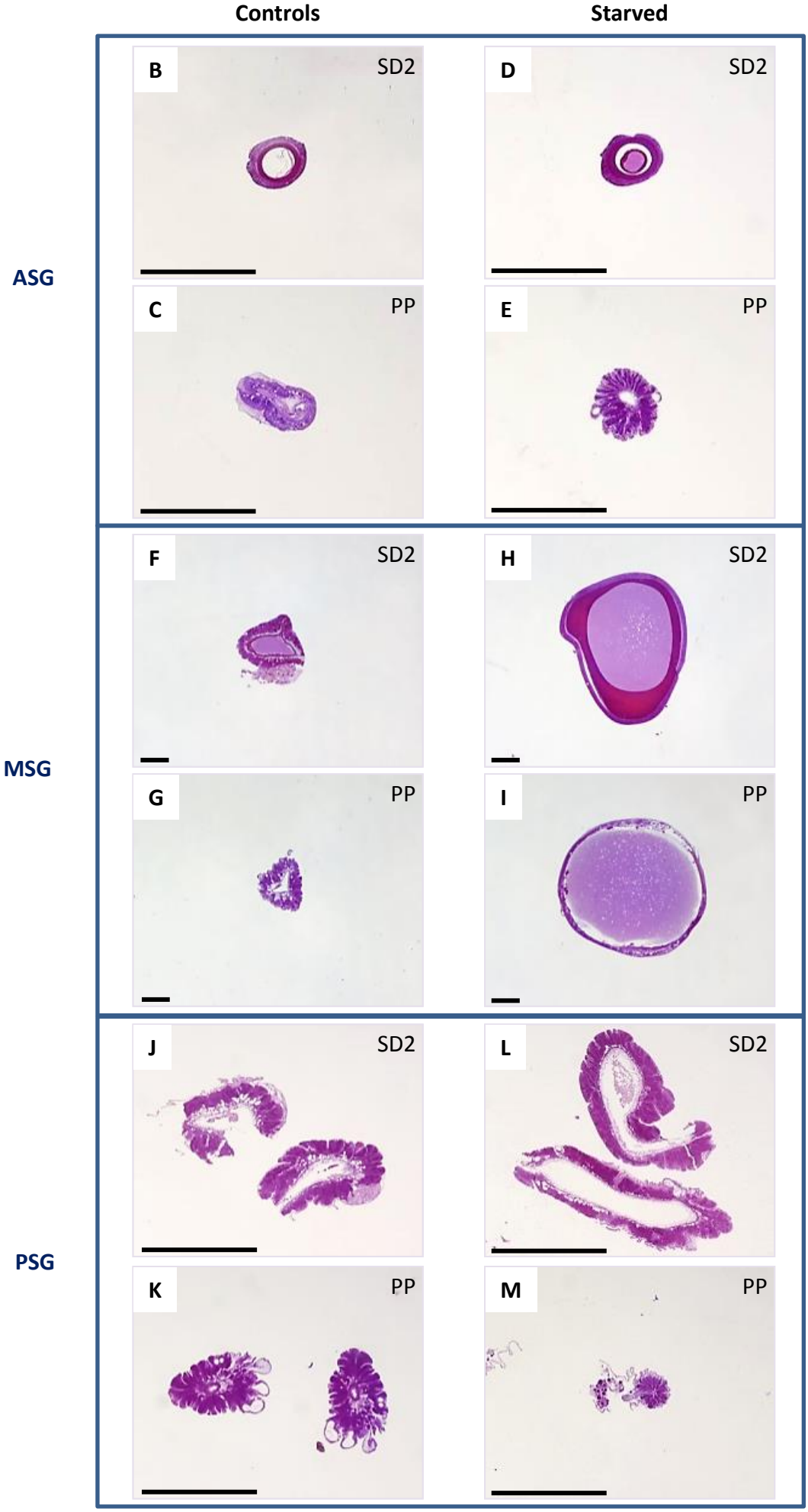
Controls
Starved
ASG
MSG
PSG
B
SD2
D
SD2
C
PP
E
PP
F
SD2
H
SD2
G
PP
I
PP
J
SD2
L
SD2
K
PP
M
PP

Figure 12. Morphological changes in silk gland compartments

A-F. Silk gland under physiological conditions MSG (**C**, **D**) and PSG (**E**, **F**) show morphological features of physiological degeneration from SD2. Nuclear condensation (N) and cytoplasmic vacuolization (arrows) appear in pre-pupal ASG (**B**).

G-L. Silk glands of starved larvae After complete food withdrawal, tunica propria (t) invaginations (arrowheads) appear at PP in ASG (**H**) and from SD2 in PSG (**K**, **L**), while they are not observed in MSG (**I**, **J**). Nuclear condensation (N) and cytoplasmic vacuoles appear at PP in ASG (**H**) and MSG (**J**) and from SD2 in PSG (**K**, **L**).

L, silk gland lumen. t, tunica propria. N, nucleus. Arrowheads, tunica propria invagination. Arrows, cytoplasmic vacuoles. i, cuticula intima. tr, tracheae.

Bar: 100 µm

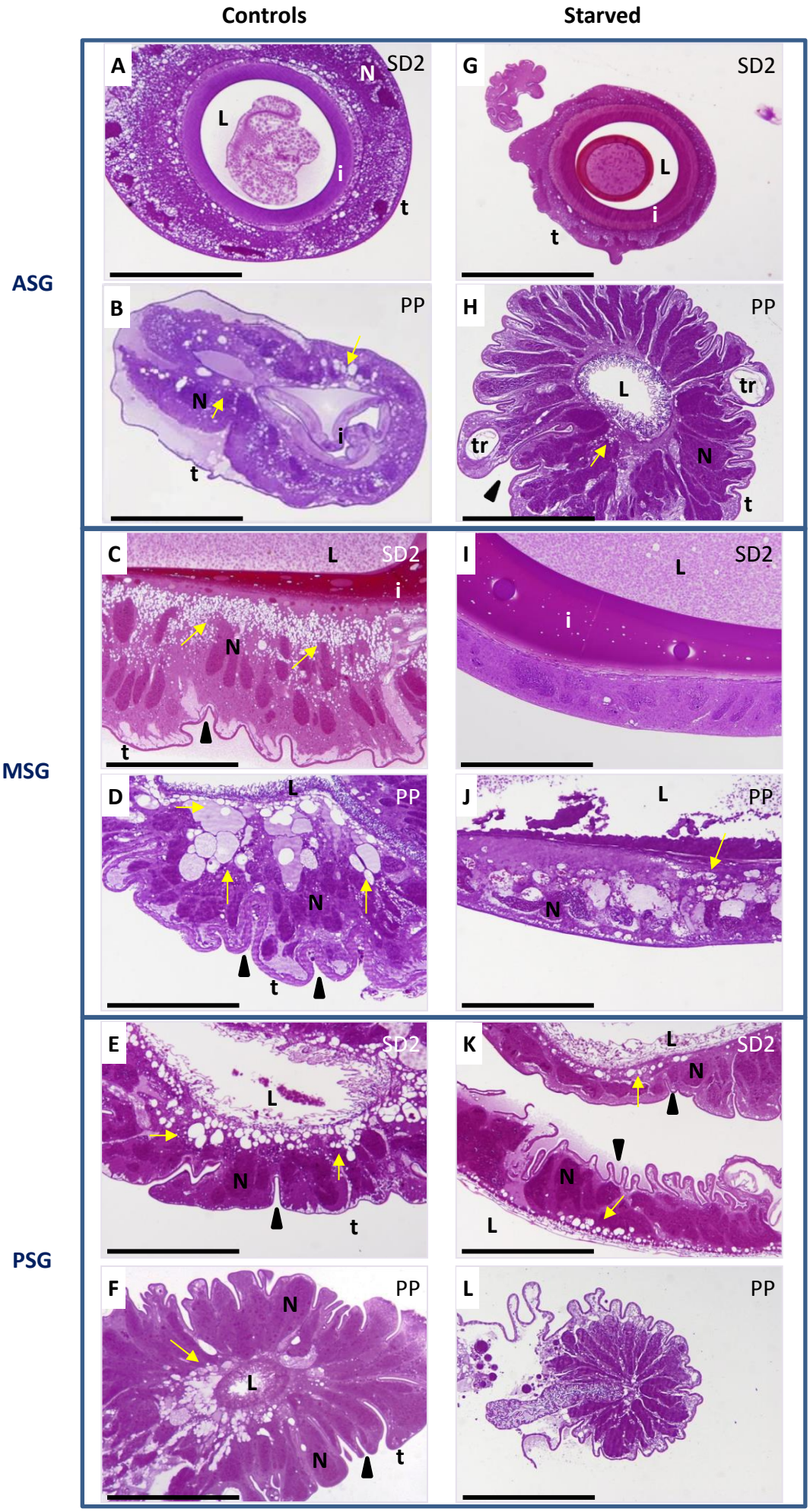
Controls
Starved
ASG
MSG
PSG
A
SD2
N
L
i
t
G
SD2
L
i
t
B
PP
N
i
t
H
PP
L
tr
tr
N
t
C
SD2
L
i
N
t
I
SD2
L
i
D
PP
L
N
t
J
PP
L
N
E
SD2
L
N
t
K
SD2
L
N
N
L
F
PP
N
L
N
t
L
PP

Figure 13. Histochemical characterization of silk gland compartments: P.A.S.
Strong P.A.S. positivity (purple color and arrows) is observed in control samples up to SD2 in ASG (**A**) and PSG (**E**) while it disappears from SD1 in MSG (**D**). Only few spots are present in ASG (**B**) and PSG (**F**) pre-pupal samples. A similar trend is registered in starved samples (**G-L**).
i, cuticula intima. tr, trachea. L, gland lumen. S, silk.
Bars: A, C-G, I-K 100 µm; B, H, L 10 µm.

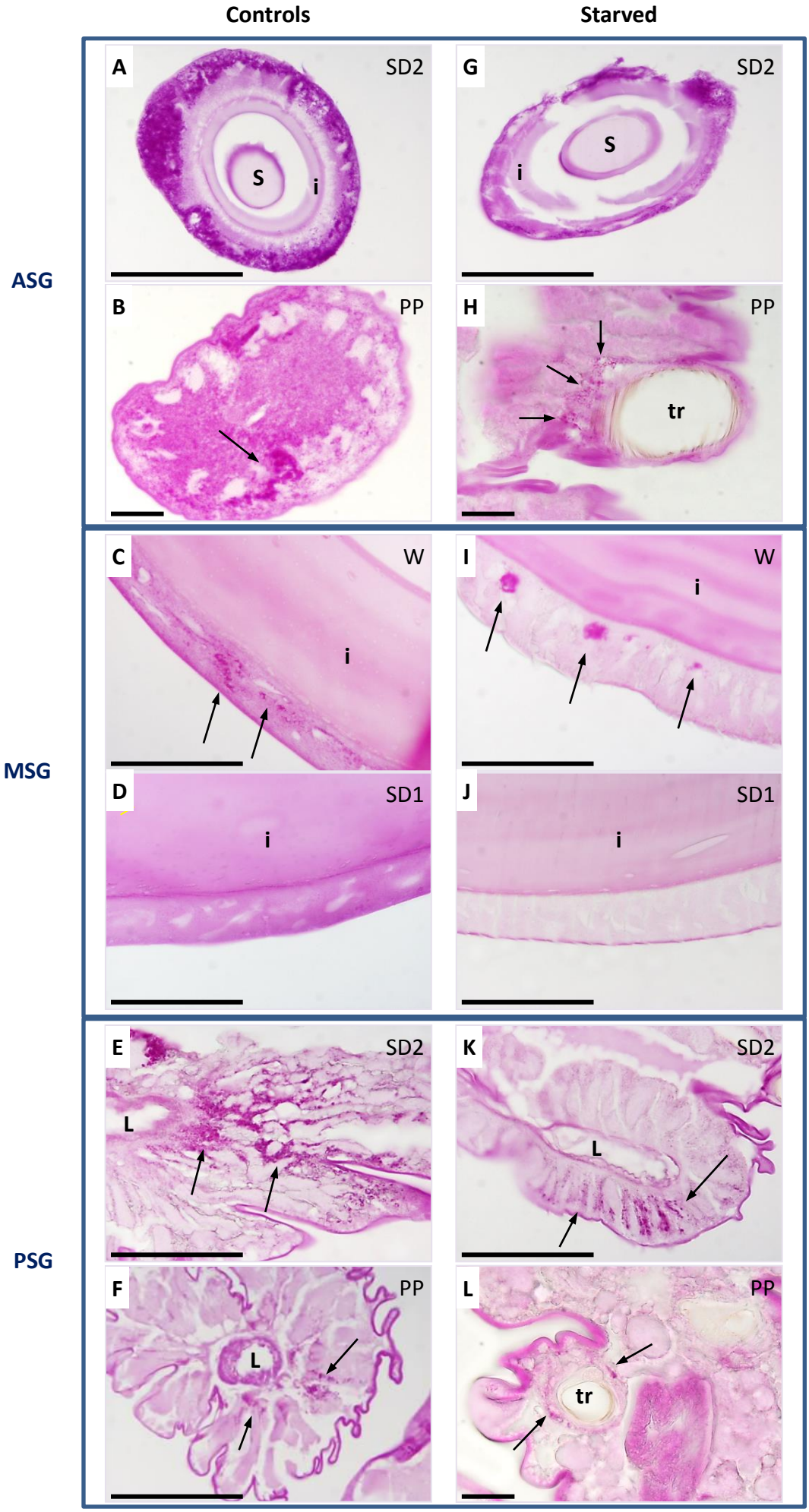
Controls
Starved
ASG
MSG
PSG
A
SD2
S
i
G
SD2
S
i
B
PP
H
PP
tr
C
W
i
I
W
i
D
SD1
i
J
SD1
i
E
SD2
L
K
SD2
L
F
PP
L
L
PP
tr

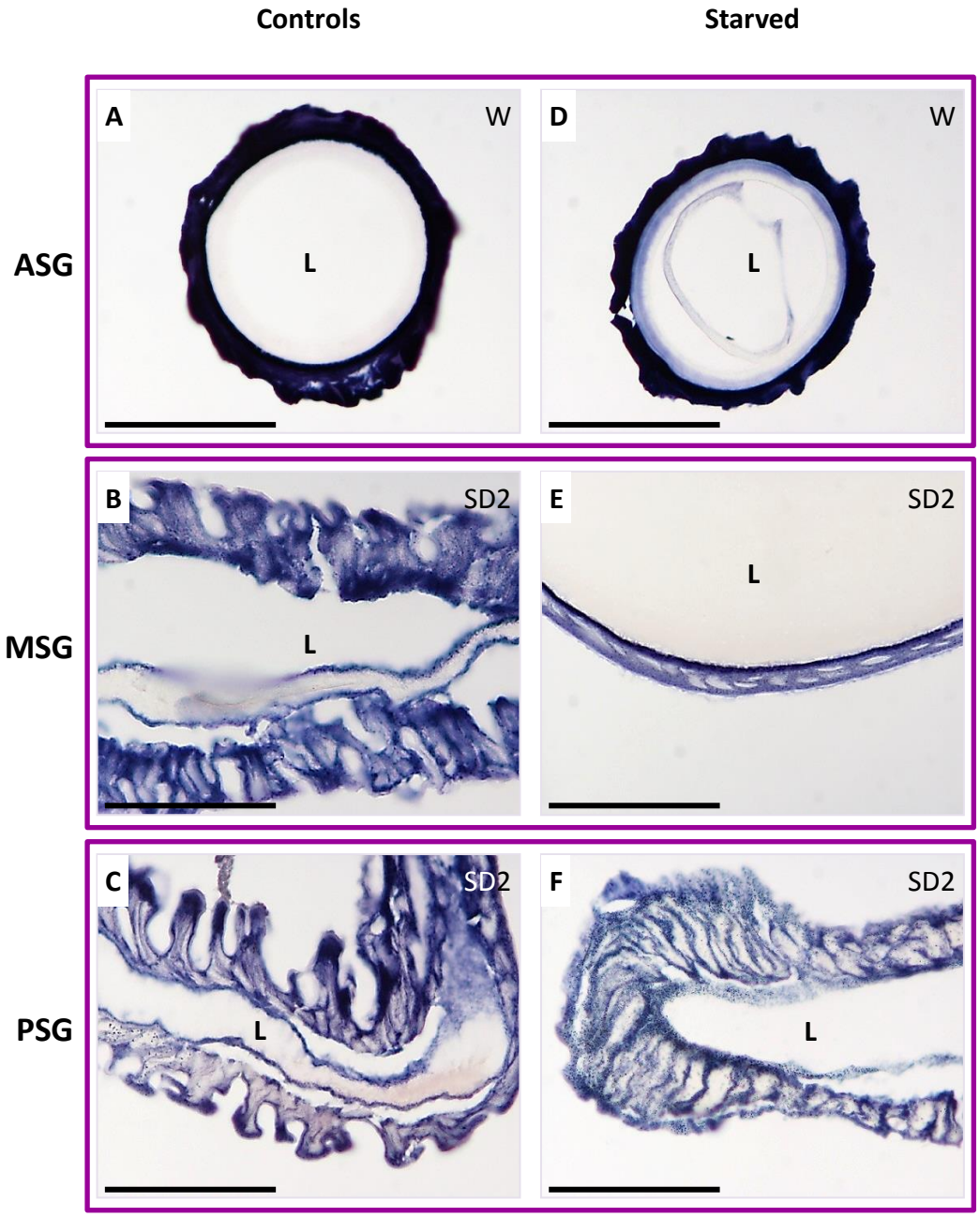

Figure 14. Histochemical characterization of silk gland compartments: NADH diaphorase

According to NADH diaphorase staining (blue color), silk gland cells retain a good mitochondrial activity through the whole period under examination, in all the compartments and in both control (**A-C**) and starved (**D-F**) larvae.

L, silk gland lumen. Bar: 100 µm

Figure 15. Histochemical characterization of silk gland compartments:
Acid phosphatase

Acid phospatase activity increases from W in ASG (**B**), from SD1 in MSG (**D**), and from SD2 in PSG (**F**) of fed larvae, when compared to corresponding larval samples (**A**, **C**, **E**). In starved animals, the staining increases from SD1 in ASG (**H**), from SD2 in PSG (**L**), and slightly from SD1 in MSG (**J**) of unfed larvae, when compared to corresponding larval samples (**G**, **I**, **K**). The intensity of acid phosphatase reaction in MSG of starved animals is less pronounced than in control ones.

L lumen. S, silk. Bars: A-K 100 µm; L 10 µm.

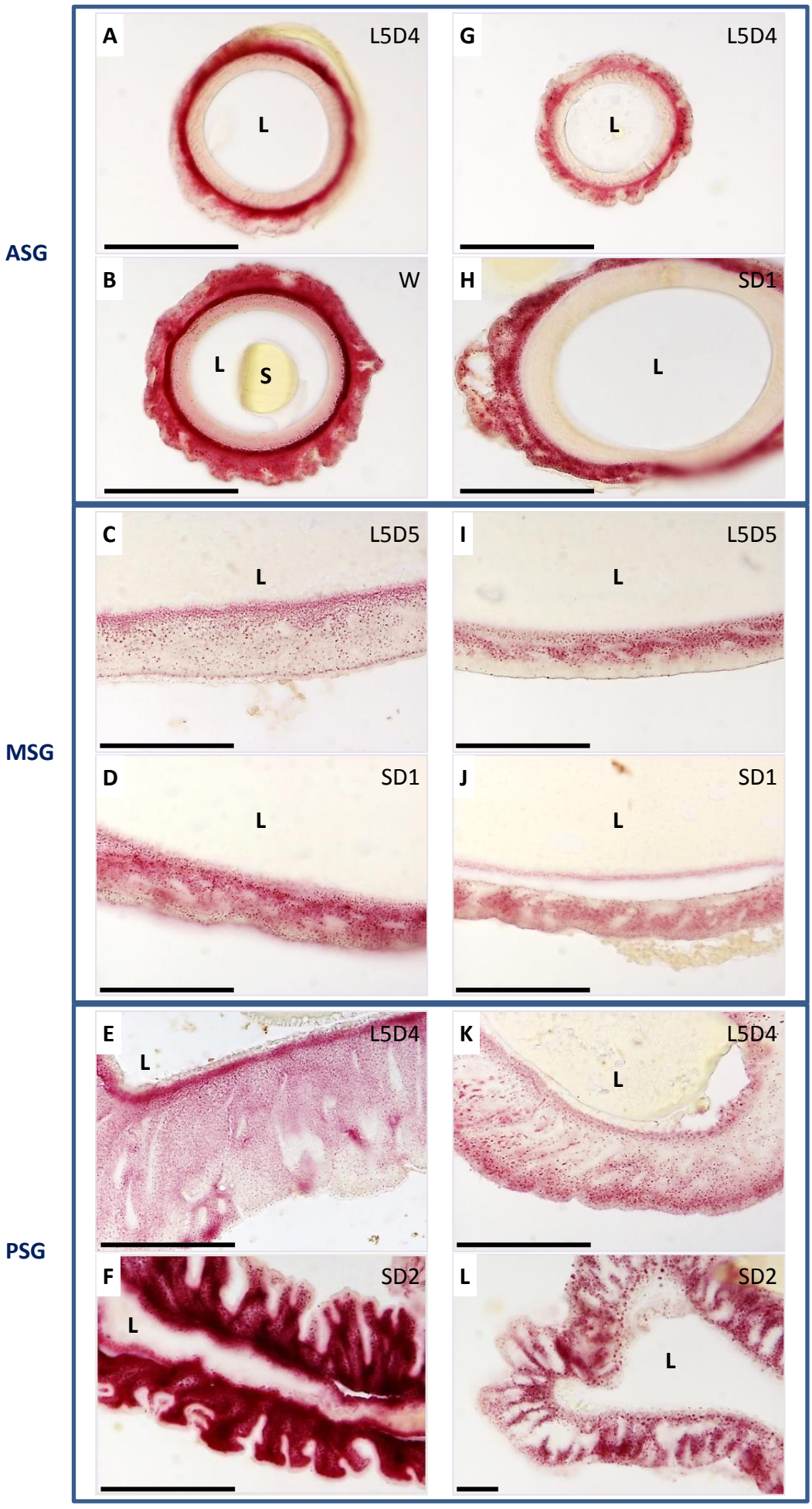
Controls
Starved
ASG
MSG
PSG
A
L5D4
L
G
L5D4
L
B
W
L
S
H
SD1
L
C
L5D5
L
I
L5D5
L
D
SD1
L
J
SD1
L
E
L5D4
L
K
L5D4
L
F
SD2
L
L
SD2
L

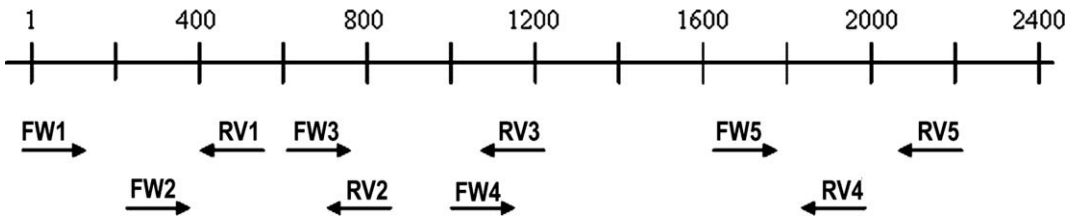

Figure 16. **Schematic representation of primers position in *BmATG1* transcript**. FW, forward primer. RV, reverse primer. Numbers 1-2400 refer to nucleotide length of transcript.

Figure 17. Phylogenetic analysis of *ATG1* sequences. *BmATG1* sequence is compared with those of other invertebrate and vertebrate species. The scale bar refers to evolutionary distances in substitutions per site. The numbers at tree nodes refer to percentage bootstrap values after 1000 replicates.

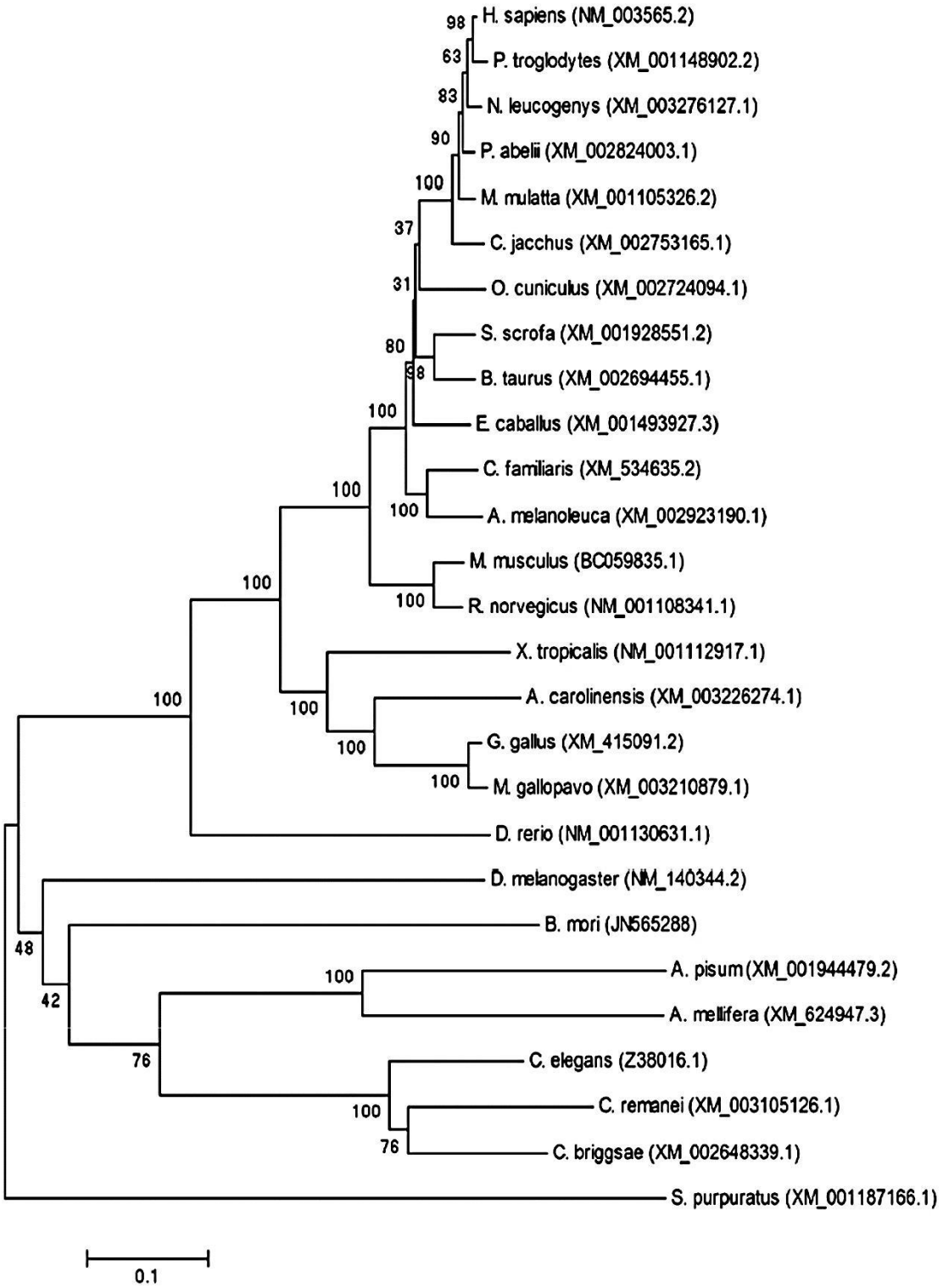
H. sapiens (NM_003565.2)
P. troglodytes (XM_001148902.2)
N. leucogenys (XM_003276127.1)
P. abelii (XM_002824003.1)
M. mulatta (XM_001105326.2)
C. jacchus (XM_002753165.1)
O. cuniculus (XM_002724094.1)
S. scrofa (XM_001928551.2)
B. taurus (XM_002694455.1)
E. caballus (XM_001493927.3)
C. familiaris (XM_534635.2)
A. melanoleuca (XM_002923190.1)
M. musculus (BC059835.1)
R. norvegicus (NM_001108341.1)
X. tropicalis (NM_001112917.1)
A. carolinensis (XM_003226274.1)
G. gallus (XM_415091.2)
M. gallopavo (XM_003210879.1)
D. rerio (NM_001130631.1)
D. melanogaster (NM_140344.2)
B. mori (JN565288)
A. pisum (XM_001944479.2)
A. mellifera (XM_624947.3)
C. elegans (Z38016.1)
C. remanei (XM_003105126.1)
C. briggsae (XM_002648339.1)
S. purpuratus (XM_001187166.1)
98
63
83
90
100
37
31
80
100
100
100
100
100
100
100
100
100
48
42
100
76
100
76
0.1

Figure 18. Subdomains described in catalytic domain of *S. cerevisiae ATG1* (Matsuura et al., 1997). Residues identical in all the orthologs are shown on a black background. Specific phosphorylation sites and ATP-binding sites are shown on a gray background. Black bands hang over Ser/Thr substrate specificity motifs (DLKPQN and GSPMYM) and Mg-binding site (DFG). Conserved residues in all sequences are indicated by an asterisk. Atg1 orthologs are indicated as follows: BmAtg1A and BmAtg1B as *B. mori* transcript variants A and B; DmAtg1 for *D. melanogaster* Atg1; MmUlk1 and HsUlk1 are *M. musculus* and *H*. *sapiens* Atg1 orthologs, respectively; CeUnc51 and ScApg1 are *C. elegans* and *S. cerevisiae* proteins, respectively.

Subdomain I

```
BmAtg1A     27 IGHGAFAMV 35
BmAtg1B     27 IGHGAFAMV 35
DmAtg1      15 LGHGAFAVV 23
MmUlk1      22 IGHGAFAVV 30
HsUlk1      22 IGHGAFAVV 30
CeUnc51     15 LGHGAFAIV 23
ScApg1      30 IGKGSFATV 38
               :*:*:** *
```

Subdomain II

```
BmAtg1A     48 VAVKVV 53
BmAtg1B     48 VAVKVV 53
DmAtg1      35 VAIKCI 40
MmUlk1      43 VAVKCI 48
HsUlk1      43 VAVKCI 48
CeUnc51     36 VAIKAI 41
ScApg1      51 VAIKEV 56
                  **:* :
```

Subdomain III (E), IV (I) and V (GD)

```
BmAtg1A     58 IQKASEILVKEIKILRELTALQHKNLVAMHDCMDSPAYVYVVMEYCNGGDLADYLQTNRL 117
BmAtg1B     58 IQKASEILVKEIKILRELTALQHKNLVAMHDCMDSPAYVYVVMEYCNGGDLADYLQTNRL 117
DmAtg1      45 QLKTQNLLGKEIKILKELTELHHENVVALLDCKESQDCVSLVMEYCNGGDLADYLSVKGT 104
MmUlk1      53 LAKSQTLLGKEIKILKEL---KHENIVALYDFQEMANSVYLVMEYCNGGDLADYLHTMRT 109
HsUlk1      53 LAKSQTLLGKEIKILKEL---KHENIVALYDFQEMANSVYLVMEYCNGGDLADYLHAMRT 109
CeUnc51     46 ISKSKNLLTKEIKILKELSSLKHENLVGLLKCTETPTHVYLVMEFCNGGDLADYLQQKTT 105
ScApg1      60 KLKNKKLLENLEIEIAILKKIKHPHIVGLIDCERTSTDFYLIMEYCALGDLTFLLKRRKE 119
                 * . :* :    :  *   :* ::*.: .       . ::**:*  ***:  *
```

Subdomain VI

```
BmAtg1A     132 AMSAIHAKGIVHRDLKPQN 151
BmAtg1B     132 AMSAIHAKGIVHRDLKPQN 151
DmAtg1      120 AMKALYTKGIVHRDLKPQN 138
MmUlk1      125 AMRLLHSKGIIHRDLKPQN 143
HsUlk1      125 AMRLLHSKGIIHRDLKPQN 143
CeUnc51     121 ALEAINKKGIVHRDLKPQN 139
ScApg1      159 ALKFLRSKNLVHRDIKPQN 177
                *:  :  *.::***:****
```

Subdomain VII and VIII

```
BmAtg1A     173 IADFGFARFLEEGNMAVTLCGSPMYMAPE 201
BmAtg1B     173 IADFGFARFLEEGNMAVTLCGSPMYMAPE 201
DmAtg1      159 IADFGFARFLNEGAMAATLCGSPMYMAPE 187
MmUlk1      163 IADFGFARYLQSNMMAATLCGSPMYMAPE 191
HsUlk1      163 IADFGFARYLQSNMMAATLCGSPMYMAPE 191
CeUnc51     160 LADFGFARFLNDGVMAATLCGSPMYMAPE 188
ScApg1      209 IADFGFARFLPNTSLAETLCGSPLYMAPE 237
                :*******:* .  :* ******:*****
```

Subdomain IX

```
BmAtg1A     213 DLWSLGT 219
BmAtg1B     213 DLWSLGT 219
DmAtg1      199 DLWSLGT 205
MmUlk1      203 DLWSIGT 209
HsUlk1      203 DLWSIGT 209
CeUnc51     200 DLWSIGT 206
ScApg1      249 DLWSVGT 255
                ****:**
```

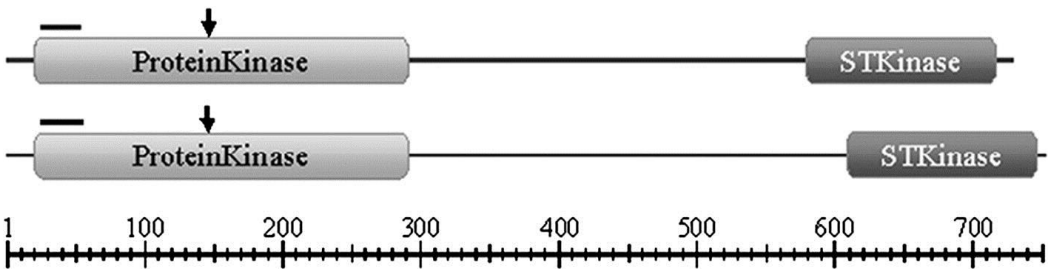

Figure 19. Scheme of the conserved protein kinase domains in the two BmAtg1 isoforms. The domain near the N-terminus is identical in both proteins, extending from position 22–288. The catalytic domain centered on the residue D146 (arrow) and the ATP binding site at K51 (seq: 27–51, the black line) are shown. An additional Ser/Thr kinase near the C-terminus extends between positions 575 and 709 in BmAtg1 isoform A, and between 607 and 741 in BmAtg1 isoform B.

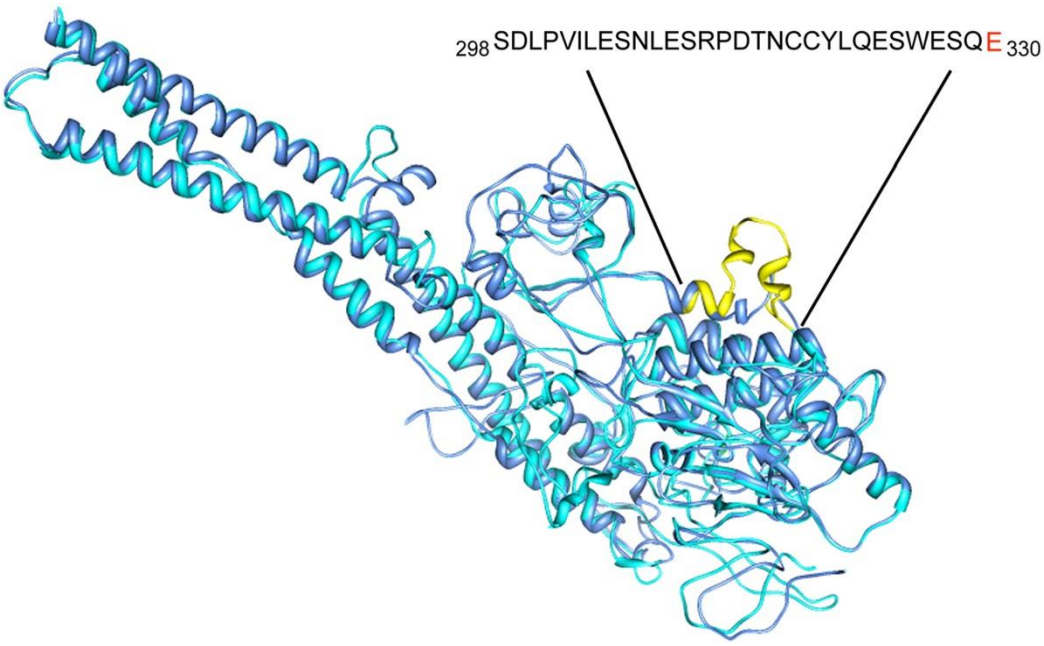

Figure 20. Tertiary structure of the two Atg1 isoforms isolated in *B. mori*. The insert of 33 aa in position 298–330 is shown in yellow, the mutant residue E298K in red. The longer isoform is in light blue and the shorter isoform is in cyan.

Figure 21. *BmATG1* expression profiles

A. Expression levels of *BmATG1* in silkworm tissues measured by real-time PCR at the end of fifth larval instar. Data are represented as mean ± standard deviation.

B. Expression levels of *BmATG1* in the midgut and fat body measured by real-time PCR in the control and starved silkworm. Data are represented as mean ± standard deviation. A significant difference between the starved and control larvae (asterisk), is observed at SD1 in the midgut and from L5D4 to SD1 in the fat body. A significant increase in *BmATG1* expression level, with respect to L5D3 (dots), is observed at SD1 in the midgut and at W and SD1 in the fat body. Statistical analysis is performed by using ANOVA ($p \leq 0.05$).

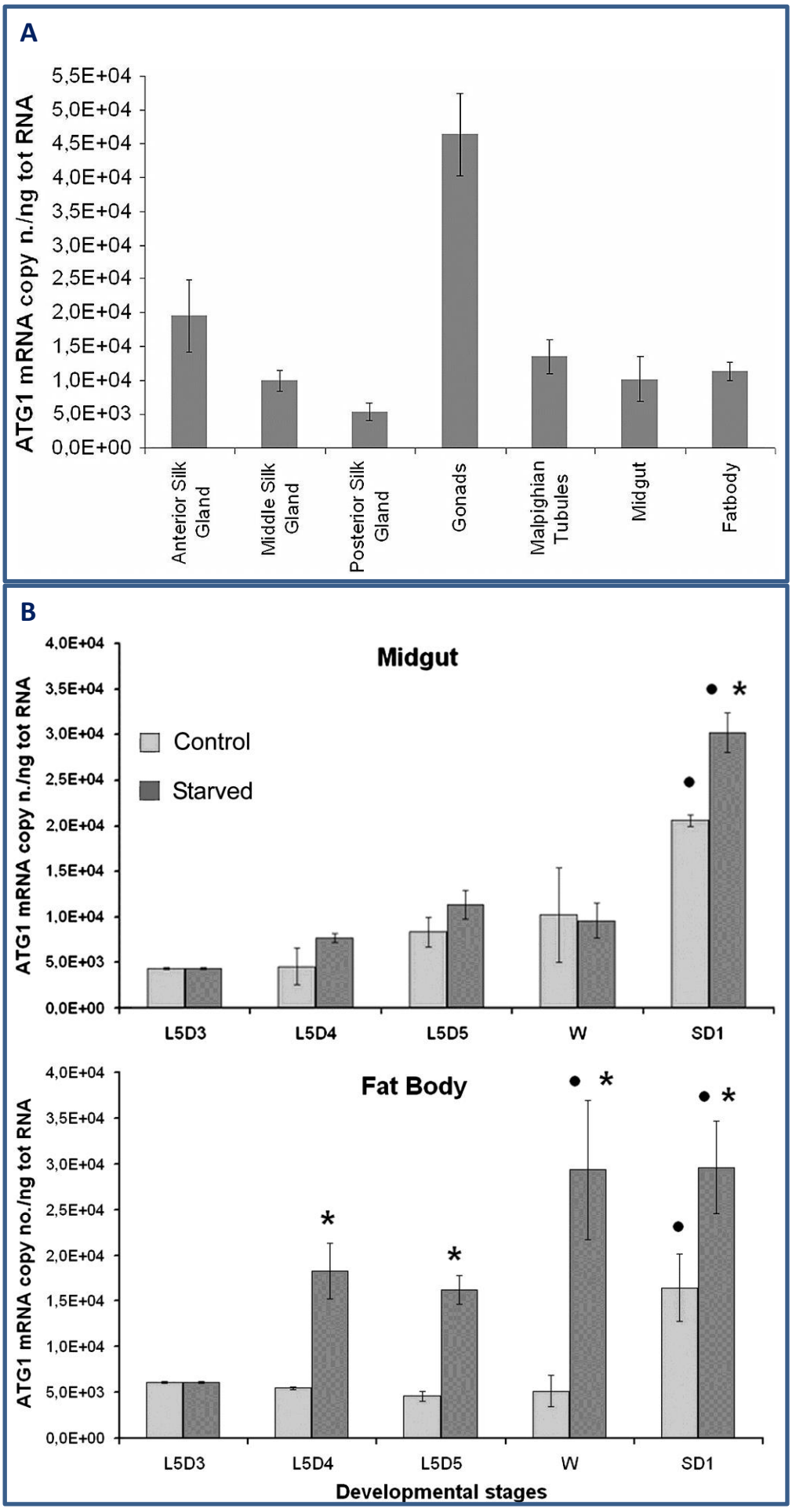
A
ATG1 mRNA copy n./ng tot RNA
5,5E+04
5,0E+04
4,5E+04
4,0E+04
3,5E+04
3,0E+04
2,5E+04
2,0E+04
1,5E+04
1,0E+04
5,0E+03
0,0E+00
Anterior Silk Gland
Middle Silk Gland
Posterior Silk Gland
Gonads
Malpighian Tubules
Midgut
Fatbody
B
Midgut
Control
Starved
ATG1 mRNA copy n./ng tot RNA
4,0E+04
3,5E+04
3,0E+04
2,5E+04
2,0E+04
1,5E+04
1,0E+04
5,0E+03
0,0E+00
L5D3
L5D4
L5D5
W
SD1
Fat Body
ATG1 mRNA copy no./ng tot RNA
4,0E+04
3,5E+04
3,0E+04
2,5E+04
2,0E+04
1,5E+04
1,0E+04
5,0E+03
0,0E+00
L5D3
L5D4
L5D5
W
SD1
Developmental stages

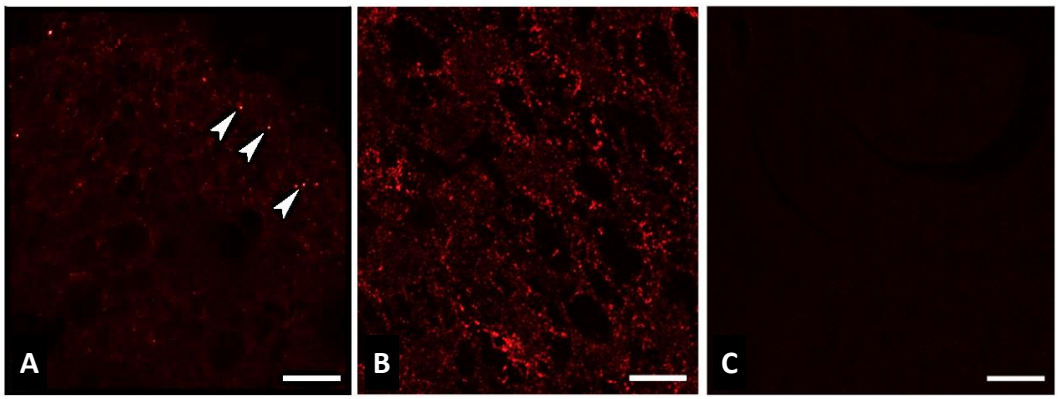

Figure 22. Analysis of BmAtg8 distribution in silkworm fat body. While in L5D5 control larvae the number of Atg8 puncta is scarce (**A**, arrowheads), after starvation the amount of the autophagic compartments greatly increases (**B**, red spots). No staining can be observed in negative controls (**C**).
Bar: 10 µm.

Name	Threonine P	Serine P	Tyrosine P	SUMOylation
BmAtg1, isoform A	114, 163, 170, 190, 235, 257 Post-insert: 294, 318, 329, 336, 405, 418, 419, 441, 445, 565, 595, 601, 693	45, 119, 258, 278, Post-insert: 337, 338, 340, 341, 361, 368, 369, 371, 375, 379, 390, 410, 444, 449, 450, 452, 455, 474, 485, 492, 613	19, 95, 208, Post-insert: 420, 517, 619, 670	10, 70, 207, Post insert: 331, 718
BmAtg1, isoform B	114, 163, 170, 190, 235, 257 Insert: 294, 317 Post-insert: 350, 361, 368, 437, 450, 451, 473, 477, 597, 627, 633, 725	45, 119, 258, 278 Insert: 313, 325, 328 Post-insert: 369, 370, 372, 373, 393, 400, 401, 403, 407, 411, 422, 442, 476, 481, 482, 484, 487, 506, 517, 524, 645	19, 95, 208 Post-insert: 452, 549, 651, 702	10, 70, 207 Post insert: 363, 750

Table 7. In silico predicted sites of T-, S-, Y-phosphorilation and SUMOylation in BmAtg1, isoforms A and B.

Table 8. Predicted glycosylation sites in BmAtg1, isoforms A and B.

Name	O-Glycosylation	ε-Glycosylation	N-Glycosylation	SUMOylation
BmAtg1, isoform A	Post-insert: T318, T395, T466, T635	K5, K7, K10, K37, K56, K140, K228, K240, Post-insert: K331, K618, K620, K709, K713, K718	Post-insert: 404 N(TTV), 423 N(ATN), 467 N(ASP), 571 N(ESV 624 N(ESK)	None
BmAtg1, isoform B	Post-insert: T350, S411, S422, T425, T427, S429, T432, T435, T437, T438, T466, T473, S476, T477, S482, S486, S487, T498, T667	K5, K7, K10, K37, K56, K140, K228, K240, Post-insert: K363, K650, K652, K741, K745, K750	Post-insert: 436 N(TTV), 455 N(ATN), 499 N(ASP), 603 N(ESV), 656 (NESK)	None

Table 9. Accessible N-glycosylation sites and the torsion angle of the N residues in the BmAtg1, isoforms A and B.

Residue position	Torsion angle (0–360°)			
	N_CA_CB_CG	CA_CB_CG_OD1	C1_ND2_CG_CB	O5_C1_ND2_CG
BmAtg1, isoform A				
571	180°	340°	160°	260°
624	180°	340°	160°	260°
BmAtg1, isoform B				
436	300°	340°	160°	260°
455	300°	340°	160°	260°
499	280°	80°	160°	260°
603	200°	340°	160°	260°
656	180°	340°	160°	260°